공학박사학위논문

Development of Knock Prediction Model by Cool Flame Elimination Method Covering NTC Region: Modeling and Experimental Study

NTC 영역을 포함한 엔진 운전에서 냉염 배제법에 의한 노킹 예측모델 개발에 관한 모델링 및 실험적 연구

2017 년 2 월

서울대학교 대학원

기계항공공학부

송 화 섭

Abstract

Development of Knock Prediction Model by Cool Flame Elimination Method Covering NTC Region: Modeling and Experimental Study

Hwasup Song

Department of Mechanical Engineering

The Graduate School

Seoul National University

Livengood-Wu integration model is acknowledged as a relatively simple but fairly accurate autoignition prediction method which has been widely recognized as a methodology predicting knock occurrence of a spark-ignition (SI) engine over years. Fundamental idea of the model is that the chemical reactivity of fuel under a certain thermodynamic state can be represented by a reciprocal of the acquired ignition delay. However, recent studies show that the predictability of the model seems to deteriorate if the tested fuel exhibits negative temperature coefficient (NTC) behavior, which is primarily caused by two-stage ignition characteristics of certain types of fuel with peculiar reaction chemistry. It is convincing that the cool flame exothermicity during the first ignition stage is a major cause that limits the prediction capability of the integration model, therefore a new ignition delay concept based on

cool flame elimination is introduced in order to minimize the thermal effect of the cool flame.

In this dissertation study, knock occurrence of iso-octane fuel in a boosted SI engine simulation is investigated considering the downsizing trend of contemporary SI engines. Iso-octane is selected for its role as a major component of surrogate gasoline, i.e. primary reference fuel (PRF) as well as its NTC behavior relevant to the engine situation, in accordance with its autoignition characteristics by comparing the Livengood-Wu integration results while providing both the cool-flame affected and eliminated ignition delay data. Results show that the predictability of the model is fairly improved by minimizing thermal contribution of the cool flame phenomenon and its validity is also investigated by chemical kinetic analysis. Along with that, cool-flame eliminated ignition delay correlation is newly suggested and tested with both computational and experimental approach, the latter designed and conducted by rapid compression machine (RCM) test to reproduce the thermodynamic history of the engine unburned gas effectively. From experimental results, it is also found that traditional ignition delay correlation is inadequate to utilize for knock prediction in modern downsized and boosted SI engines, whose operating condition is now apart from traditional anti-knock grading methods, thus it is suggested that ignition delay correlation be evaluated considering relevant operating region of modern SI engines and fuel reactivity characteristics as well.

Keywords: Knock, Autoignition, Livengood-Wu model, Cool flame, Iso-octane, Rapid Compression Machine, Chemical kinetics

Student Number: 2013-30201

Table of Contents

Abstract i

Table of Contents iii

List of Figures vi

List of Tables x

Chapter 1. Introduction

1.1 Technical developments and challenges in future spark-ignition (SI) engine 1

1.2 Autoignition of fuel-air mixture and knock 4

1.3 Autoignition prediction method – Livengood-Wu integration model 6

1.4 Literature review 9

1.5 Objectives of this study 14

Chapter 2. Modeling

2.1 SI engine model 16

2.1.1 Modeling details 19

2.1.2 Autoignition of the unburned gas and knock 25

2.2 Ignition delay calculation from constant volume reactor model 28

Chapter 3. Computational results

3.1 SI engine simulation results 32

3.1.1 Unburned gas profiles and inconsistence of Livengood-Wu model 32

3.1.2 Engine operating conditions relevant to cool-flame appearance 39

3.2 Constant volume reactor model results 40

3.2.1 Two-stage ignition behavior in the NTC region 41

3.2.2 Single stage ignition behavior in the post-NTC region 45

3.3 Integration of reaction chemistry and its contribution to the overall reactivity 46

3.3.1 Comparison of original and integrated ignition delay 46

3.3.2 Time reduction by integrated reaction chemistry 48

3.3.3 Reaction pathway of iso-octane oxidation in different temperature range 51

3.4 Cool flame elimination method 53

3.4.1 Accuracy of Livengood-Wu integration for an exemplary non-NTC fuel 53

3.4.2 Cool flame elimination by modulating heat capacity of nitrogen 55

3.4.3 Improvements to Livengood-Wu integration by cool flame elimination 57

3.4.4 Validity of cool flame elimination method 58

3.4.5 Another method from the reaction mechanism perspective 62

Chapter 4. New ignition delay correlation

4.1 Cool flame elimination by heat capacity modulation 64

4.2 Chemical kinetic analysis of cool-flame eliminated ignition delay 68

4.2.1 Reaction pathway analysis 68

4.2.2 Reaction pathways of heat capacity modulated two-stage ignition 69

4.3 Cool flame elimination by empirical correlation 78

4.3.1 RCM modeling details 78

4.3.2 Thermodynamic history of reactant in RCM 80

4.3.3 Empirical correlation by Livengood-Wu integration 82

4.4 Comparison of kinetics-based and correlated ignition delays 87

4.4.1 Traditional ignition delay curves 87

4.4.2 Livengood-Wu integration by each ignition delay 90

Chapter 5. Experimental validation

5.1 Designing appropriate experiment for validation 94

5.2 RCM characteristics 95

5.2.1 Test procedure 95

5.2.2 Data processing 101

5.3 Experimental results and analysis 104

5.3.1 Target test conditions along with the purpose of this study 104

5.3.2 Results from repeated experiments and deriving correlation 107

5.3.3 Comparison with other experimental correlation 110

Chapter 6. Conclusions

6.1 Modeling results 114

6.2 Experimental results 116

6.3 Future works 116

References 118

Abstract (in Korean) 124

List of Figures

Chapter 1

1. Corporate Average Fuel Economy (CAFE) Standards vs. actual fleet fuel economy in the U.S.
2. CO_2 emission regulations of the European Union and China
3. CO_2 emissions and fuel economy target of South Korea by year 2020

Chapter 2

4. A schematic diagram of two-zone SI engine model
5. Combustion duration applied to this study by different engine speed
6. Example of two-zone SI engine model simulation results
7. Predefined mass burn rate by Wiebe correlation and burned fuel mass profile
8. Definition of the ignition delay and other terms

Chapter 3

9. Selected thermodynamic histories of engine unburned gas with various initial intake pressure
10. Unburned gas temperature from the SI engine simulation along with engine crank angle degree
11. Cylinder pressure along with engine crank angle degree
12. Autoignition point prediction by Livengood-Wu integration with cool-flame affected ignition delay
13. Unburned gas temperature with cool-flame appearance in the later burn stage
14. Molar concentration of ·OH radical in the unburned gas prior to autoignition
15. Molar concentration of alkylperoxy radicals in the unburned gas prior to autoignition
16. Cool-flame exhibiting boundary conditions with engine speed and boost pressure
17. Pressure history of original and modulated heat capacity cases for different initial states within the NTC region from Fig. 9

18. Rate of progress of pre-cool flame stage reactions at 7 ms after 700 K, 22 bar initial condition

19. Pressure history of original and modulated heat capacity cases for a post-NTC, single stage ignition region in Fig. 9

20. Comparison of original and integrated ignition delay on the thermodynamic path of the engine unburned gas of 1.0 bar intake pressure

21. Original and integrated ignition delay trend along with corresponding thermodynamic states of the engine unburned gas history

22. Livengood-Wu integration of cool-flame affected ignition delays and their accumulated chemistry

23. Simplified kinetic scheme of iso-octane oxidation for high and low temperature condition

24. Livengood-Wu integration results for various iso-octane-fueled engine simulations along with ethanol-fueled case

25. Extrapolation of heat capacity modulated computation results for cool-flame eliminated first stage ignition delay acquisition

26. Autoignition point prediction with both cool-flame affected (gray) and eliminated (black) ignition delays

27. Instant [·OH] production or consumption rate from constant volume reactor for 700 K, 22 bar initial condition with different level of heat capacity modulation

28. Mean [·OH] change rate of results from Fig. 27 by 0^{th}-order reaction assumption

29. [·OH] change rates in engine unburned gas and 0^{th}-order averaged constant volume reactor cases including heat capacity modulated results

30. Projected ignition delay trends along the engine unburned gas history

Chapter 4

31. Cool-flame affected original ignition delay contours relevant to engine unburned gas history

32. Cool-flame eliminated ignition delay contours by heat capacity modulation

33. Difference between original and heat capacity modulated, cool-flame eliminated ignition delays

34. Application boundary of cool-flame eliminated ignition delay in modern SI engines

35. Major reaction pathways of stoichiometric iso-octane oxidation process in 700 K, 22 bar condition by degree of heat capacity modulation

36. Rate of progress of selected elementary reactions from the major reaction pathway shown in Fig. 42 at 700 K, 22 bar condition

37. Major reaction pathways of stoichiometric iso-octane oxidation process in 750 K, 30 bar condition by degree of heat capacity modulation

38. Rate of progress of selected elementary reactions from the major reaction pathway shown in Fig. 44 at 750 K, 30 bar condition

39. Major reaction pathways of stoichiometric iso-octane oxidation process in 800 K, 41 bar condition by degree of heat capacity modulation

40. Rate of progress of selected elementary reactions from the major reaction pathway shown in Fig. 46 at 800 K, 41 bar condition

41. Examples of RCM test procedure

42. Pressure-temperature histories from the RCM simulation

43. Contour lines of corrected sample standard deviation of RCM simulation histories for pressure and temperature empirical coefficients, assuming Livengood-Wu integration of 1 at the autoignition point

44. Cool-flame eliminated ignition delay contours by empirical correlation

45. Difference between original and empirically correlated, cool-flame eliminated ignition delays

46. Cool-flame affected original ignition delays and their elimination by kinetics-based, heat capacity modulated ones and empirically correlated values

47. Difference of cool-flame eliminated ignition delays by two independent methods

48. Autoignition point prediction with cool-flame eliminated ignition delays computed by heat capacity modulation

49. Autoignition prediction with cool-flame eliminated ignition delays derived from empirical correlation

Chapter 5

50. Temperature calibration curve between the desired and measured values

51. Hydraulic circuit diagram of RCM

52. A full systematic diagram

53. Specific heat ratio curve of stoichiometric iso-octane/air mixture

54. Temperature-pressure history from RCM experiments

55. Contour lines of corrected sample standard deviation of RCM experimental results

with empirical coefficients as both axes, assuming Livengood-Wu integration output of 1 at autoignition point

56. Cool-flame eliminated ignition delay contours evaluated from RCM experimental results

57. Unburned gas histories from SI engine simulation, RON/MON test conditions, and RCM experiments

58. Ignition delay correlations derived from RCM experiment and Douaud-Eyzat coefficients

59. Livengood-Wu prediction by two independent ignition delay correlations

List of Tables

Table 1. Model engine dimensions and operating parameters

Chapter 1. Introduction

1.1 Technical developments and challenges in future spark-ignition (SI) engine

Today's technical challenges in automotive industry are strongly driven by governmental regulations legislating fuel economy and tailpipe emissions towards more efficient and less polluting future for transportation applications. Until now these environmental goals were successfully achieved worldwide as shown in Figs. 1–3 but it looks like stricter regulations are waiting ahead. For example, the U.S. Department of Transportation aims to fulfill the average fuel consumption of fleet by 54.5 miles per gallon until 2025 [1] and the European Union will target the CO_2 emissions level of new passenger cars not to exceed 95-g CO_2/km by 2021 [2] as well. Stringent regulations promote technical advancements in internal combustion engines e.g., boosted downsizing in SI engines, increasing compression ratio, optimum combustion phasing, low temperature combustion strategy, etc., to achieve higher thermal and mechanical efficiency while keeping the engine-out emissions to a lower extent.

Generally, maximum engine work is proportional to the displacement volume in case of naturally aspirated engines, meaning that it wouldn't be really helpful to compare the maximum work rating of any engines with different size if one intends to investigate the engine's "pure" capability to produce work. Instead, engine work per cycle is normalized by its displacement volume and named 'mean effective pressure (MEP)' since this new term has a same unit as pressure, thus higher MEP is an inherent part of extreme operating condition where work is relatively produced more from smaller size. Typical range of maximum MEP for naturally aspirated SI engine

is usually 850–1050 kPa [3]. However, in case of boosted downsizing strategy engine displacement volume is reduced from its naturally aspirated predecessor model, but the output work level is maintained by introducing intake charge boosting technology, usually with the help of turbocharger. As a result, maximum MEP range of turbocharged SI engine was 1250–1700 kPa in the late 80's [3] and now it might be possibly higher. Therefore, downsized engines confront severe operating condition and it may lead to unfavorable combustion phenomena such as engine knock (or knocking) in an SI engine.

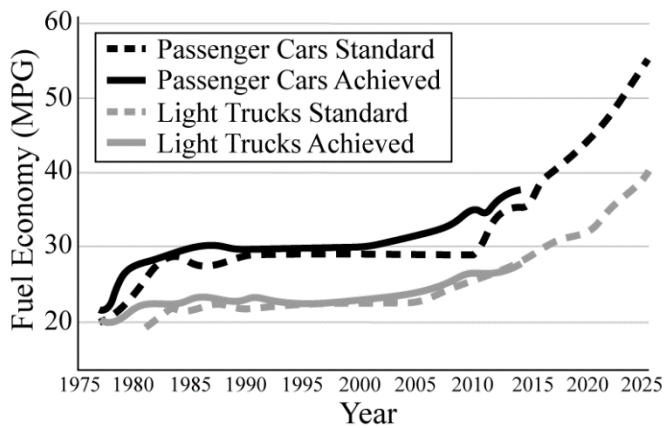

Figure 1. Corporate Average Fuel Economy (CAFE) Standards vs. actual fleet fuel economy in the U.S. [4]

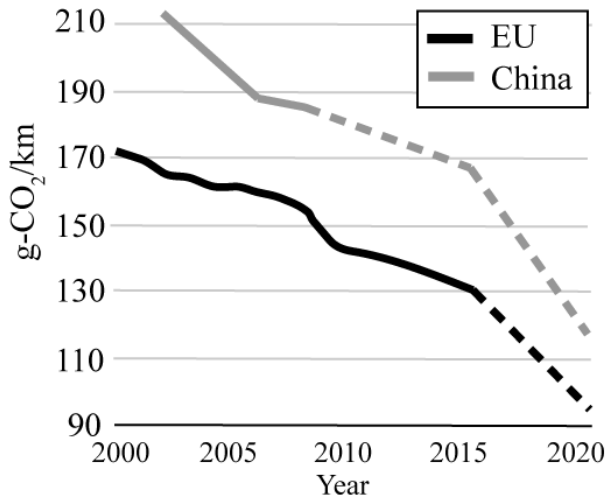

Figure 2. CO_2 emission regulations of the European Union and China [5]

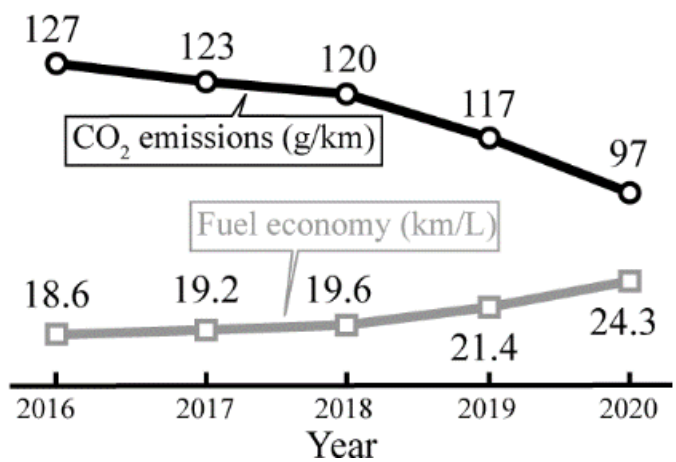

Figure 3. CO_2 emissions and fuel economy target of South Korea by year 2020

1.2 Autoignition of fuel-air mixture and knock

Combustion of fuel-air mixture in an SI engine initiates by a spark plug that forms flame kernel, followed by flame propagation where chemical energy of fuel in the unburned gas is transformed into thermal energy and burned gas remains. In most cases spark timing is well ahead of top dead center (TDC) position in normal 4-stroke SI engine operation, implying that temperature and pressure of the unburned gas continually increases by both the compressive piston motion and flame propagation, as well as the radiative heat transfer from the upcoming flame front. In this manner, increased temperature and pressure stimulate chemical reactions between the molecules inside the unburned gas and may lead to consequent autoignition of the mixture even before the flame front arrival. In case of this "early" autoignition and corresponding instantaneous pressure rise at local region, sudden pressure unbalance across the engine cylinder causes pressure wave and audible "knocking" sound when this wave hits the piston face or the cylinder wall. While engine is running around its maximum MEP range with lower revolutions per minute (RPM), i.e. low speed and high load operation, it leads to knock-prone condition since relatively longer time duration for reaction chemistry progress and dense mixture concentration contribute to easier autoignition onset. Knock intensity is usually proportional to the amplitude of the pressure wave and strong knock may cause damage to the engine components, e.g. piston crack or melt down, piston ring breakage, etc.

Knock outbreak in a contemporary engine depends on number of engine control and design parameters, such as spark timing control logic, compression ratio, exhaust gas recirculation (EGR) strategy and in-cylinder turbulence intensity, to name a few. In-cylinder temperature and pressure of unburned gas varies with engine operating condition and design parameters, however it is usually agreed to behave within a

temperature range of a thousand kelvin and a pressure limit of one hundred bar [6]. Along with that, autoignition behavior of fuel is also a prominent factor which affects knock occurrence dominantly, from the fuel's perspective. Conditions such as temperature, pressure, mixture composition and equivalence ratio determine chemical kinetics and reaction pathway of fuel substance that induce massive radical formation and corresponding autoignition in the end. Reactions between molecules categorize into chain initiation, propagation and branching, and termination process. First, reaction chain is initiated by very first stage collision between fuel and other molecules or unimolecular decomposition of fuel itself to produce radical species, followed by consecutive propagation and branching pathways that break up larger molecules and supply additional radicals. Finally, radicals produced in large quantity stimulate overall reaction rate and induce self-ignition of the mixture without any external ignition source, when enough quantity of radical species is produced.

Hundreds of theoretical modeling and experimental measurements have been conducted and analyzed to build up and validate chemical kinetic reaction mechanism for several fuel components. Basically, calculating the "ab initio" reaction rate between numerous molecules is preceded with some theoretical approaches that are suitable for each kind of species and reaction characteristics, followed by validation with computational means and experiments. During this stage, plenty of data are necessary to improve the reliability of the reaction mechanism on subject. Studies regarding fuels relevant to SI engine application include gasoline [7–9] and its surrogate substances, e.g. iso-octane (2,2,4-trimethylpentane) [10–12], n-heptane [13–15], and blends of multiple components [16–18]. Thanks to those reaction mechanisms and application to the engine simulation model, it is feasible to compute the chemical kinetics of the unburned gas and corresponding onset of autoignition leading to engine knock, nonetheless computing resource and time consumption might become an obstacle when the reaction mechanism is complicated.

For example, detailed reaction mechanism of primary reference fuel (PRF) which consists of iso-octane and n-heptane as a gasoline surrogate contains 1034 species along with 7558 elementary reactions [19] and makes it challenging to solve the kinetics within acceptable time window. Compared to that, the relatively simple gas reaction mechanism including hydrocarbon species up to 3 carbon atoms, i.e. methane, ethane and propane, has only 53 species and 325 reactions [20]. Size of reaction mechanism tends to exponentially grow as the carbon number of base hydrocarbon increases, thus computing the autoignition point in the engine simulation with most of the automotive fuel reaction mechanism is burdensome, especially when the target system is three-dimensional and the carbon number of base fuel components, e.g. n-heptane, iso-octane, toluene, etc., is higher.

1.3 Autoignition prediction method – Livengood-Wu integration model

J.C. Livengood and P.C. Wu suggested a simple autoignition model in 1955 [21] which helps predict the onset of autoignition without massive computation, if appropriate ignition delay data are available. Here, additional considerations had been taken into account before predicting the autoignition of the unburned gas with ignition delay data. Generally, ignition delay of fuel is measured or computed under fixed thermodynamic state, in other words the initial temperature and pressure condition is set and maintained during the test procedure. Compared to this, unburned gas state is continuously changing towards the direction of increasing temperature and pressure by external sources such as zone compression by flame propagation and radiative heat transfer as well as piston motion in an arbitrary SI engine. As a result, autoignition chemistry of fuel initiates and proceeds during the

engine running process which leads to advanced phasing of autoignition chemistry overall. That means, autoignition characteristics of relevant fuel measured in a well-controlled, laboratory-scale environment could not provide appropriate clues which are useful to handle the real engine knock problem.

Livengood-Wu model predicts the moment of autoignition onset by a simple integration where the reciprocals of the ignition delay along the system's thermodynamic profile are integrated to evaluate the reaction chemistry progress quantitatively, leading to autoignition. They assumed that whole reaction chemistry is governed by a zeroth-order global reaction and the onset of autoignition occurs when the concentration of a representative species $[x]$ reaches a critical value $[x]_c$. This can be expressed as

$$\frac{[x]}{[x]_c} = \int_{t_0}^{t_c} \frac{1}{\tau(T, P, \phi, \dots)}\, dt = 1 \qquad \text{(Eq. 1.1)}$$

where autoignition would occur at time t_c as the integration reaches the value of unity. Considering the stoichiometric operation of SI engine in almost all situation, i.e. $\phi = 1$, ignition delay τ is empirically expressed as a function of temperature and pressure. In the same manner, reciprocal of the ignition delay at any thermodynamic state is accepted as an index of instantaneous reactivity at that corresponding moment. For example, if an ignition delay at state A is 1 ms and the other with 10 ms at state B, the instant chemical reactivity at state A is thought to be ten times higher than state B. The onset of autoignition of H_2 and CH_4 fuels was tested in the study of Hernández et al. [22] and it is obvious that the model's predictability is excellent.

However, in the aforementioned study by Hernández et al., it is also revealed that the capability of Livengood-Wu model deteriorates in case of fuels with unique reaction chemistry, i.e. fuels with negative temperature coefficient (NTC)

characteristics. Chemical reactions would speed down as temperature lowers if it follows Arrhenius behavior, thus ignition delay duration becomes longer in normal situation, nevertheless main reaction scheme of NTC-exhibiting fuel is quite distinct in certain temperature range. The reaction mechanism study of iso-octane by Curran et al. [19] revealed that moderate pressure and temperature rise, named 'cool flame' after its relatively mild degree of exothermicity, occurs during the early stage of ignition delay period. Once cool flame appears, succeeding chemical reactions within the reaction chain are spontaneously accelerated by additional contribution of increased temperature and pressure, which may lead to advanced autoignition compared to higher "initial" temperature condition without any cool flame exhibition. Computational approaches have been attempted in other studies [23, 24] to distinguish the thermal effect of cool flame, i.e. relationship between the temperature increment and overall ignition delay, by using different buffer gas components within the reacting mixture to manipulate the extent of temperature increase during the cool-flame stage, but experimental evaluation is limited.

Fundamentals of Livengood-Wu model premises that overall reaction chemistry leading to autoignition can be simplified to a single step global reaction and that the resultant ignition delay is appropriate for representing the instantaneous chemical reactivity at corresponding thermodynamic state. From this point of view, shorter ignition delay stands for higher chemical reactivity with increased reaction rate. On the other hand, this assumption is not applicable to fuels with NTC behavior in which two distinguishable ignition phases of pre- and post-cool flame stage are determined by their respective reaction scheme, implying that it is disputable to claim a single global reaction in this case.

In addition, it is unlikely that the unburned gas state of a contemporary SI engine is largely affected by any cool flame exothermicity, nevertheless its thermodynamic

profile is overlapped on the NTC-exhibiting region of relevant fuels. If we operate two identical engines in different mode, i.e. one with SI and the other with homogeneous charge compression ignition (HCCI), their respective temperature and pressure histories of the unburned mixture are comparably different. There is no external ignition source or flame propagation in HCCI case and thus the sole reason of temperature and pressure increment is the compressive heating from the upward piston motion, compared to an SI engine where there is additional contribution from the unburned zone shrinking by flame propagation as well as the radiative heat transfer from the flame front. Therefore, the unburned gas state in an SI engine would change "faster" than that of an HCCI engine. Along with that, absolute time duration of the unburned gas history within the NTC region is considerably shorter to exhibit the cool flame behavior, implying that the cool flame behavior wouldn't be revealed while the thermodynamic history of the unburned gas of an SI engine is within the NTC region.

Hence, it is controversial to simply insert the reciprocal of 'cool-flame affected ignition delay' into Livengood-Wu integration model to predict the autoignition point of automotive fuel in an SI engine even though the unburned gas' thermodynamic profile is expected to move in the NTC region, at least when no evidence of any cool-flame related exothermicity is perceivable.

1.4 Literature review

Number of studies have been conducted utilizing Livengood-Wu integration to predict knock of an SI engine with various fuels or to locate the start of combustion in advanced internal combustion engine concepts such as an HCCI engine, in which

chemical kinetics of fuel governs combustion process. Selected previous works are as follows:

A.M. Douaud and P. Eyzat compared the knock propensity of commercial gasoline fuels in 1978 [25] and proposed an empirical correlation of ignition delay for fuels with octane number between 80 and 100 which was derived from Livengood-Wu model. They obtained the temperature-pressure histories of the engine unburned gas in different conditions and fitted the data into the Livengood-Wu integral by assuming the value of unity at the end of the integration process within an acceptable error range. They investigated that engine knock is predictable by the integration model, however it is suspicious whether any cool-flame exothermicity appeared in their engine experiments or not. If cool flame appeared, which seems quite probable, their ignition delay correlation and Livengood-Wu integration results are not applicable to modern SI engine situations. This is because their study is based on engine experiments that were conducted at relatively slower engine speed of 600 and 900 RPM, at which standard test method of grading the anti-knock propensity of fuel is prescribed, thus there is sufficient time span available for the cool-flame chemistry to be progressed until the revelation of corresponding exothermicity.

L. Chen et al. [26] utilized the integration model to predict the knock onset along with engine experiments and concluded that multiple effects should be considered for accurate knock prediction in modern engines, e.g. the percentage of EGR and fuel enrichment could be included into the empirical correlation of ignition delay. It seems that cool-flame exothermicity is not observed in their engine experiments under most cases. However, their newly proposed ignition delay correlation with additional parameters is derived from their specific test engine only, implying the lack of validity with other facilities closely related to ignition delay measurement or computation. It is also unknown if the ignition delay correlation of the fuel-air

mixture would be reproducible by the chemical kinetic results if additional terms such as EGR composition and identical air excess ratio are included in the empirical correlation.

Computational work by Hernández et al. [22] applies Livengood-Wu model to handle the strong two-stage ignition fuel, i.e. n-heptane, in an HCCI engine simulation to predict autoignition point. Here, cool flame appears during the compression stroke of engine operation and the integration model predicts the onset of first stage ignition accurately by integrating the reciprocals of only the first stage ignition delay. This stands for the applicability of Livengood-Wu model to the chemical kinetic situation if the governing reaction pathway is mostly dependent on the chemistry itself. On the other hand, the intense main autoignition point could not be predicted satisfactorily if overall ignition delay database including the cool-flame affected two-stage ignition regime are applied to the integration process. They introduced their own modifications to the original Livengood-Wu model to improve predictability; nonetheless, it is curious if their method would fit to the situation where cool flame does not appear until autoignition occurs, i.e. if the engine is running under SI mode, as explained in the previous section.

Another computational study by Pan et al. [27] also investigates the poor performance of Livengood-Wu integration in autoignition prediction of an HCCI engine simulation when fueled with n-heptane or DME (dimethyl ether), thanks to the strong NTC characteristics of those substances relevant to automotive application. They divided the ignition delay curve—which has an “S” shape—into three asymptotes and established an empirical correlation of ignition delay including the NTC behavior, then applied Livengood-Wu integration to predict the accurate point of autoignition within the engine simulation result. Their approach improved the Livengood-Wu predictability in such cases where cool flame revealed during the

compression stroke, however it is not mentioned if their idea could also be applied to other fuels, e.g. iso-octane or other relevant substances which also exhibit NTC behavior, but in relatively higher temperature regime than n-heptane.

An interesting approach of developing the ignition delay correlation for PRF blends from PRF0 (pure n-heptane) to PRF100 (pure iso-octane) was recently presented by DelVescovo et al. [28] whose conclusion claims that the low temperature heat release and relevant low temperature chemistry are negligible in autoignition prediction of HCCI engines based on experiments. From the heat release rate profiles provided in their work, it seems that the order of low temperature chemistry-related exothermicity is significantly smaller than the heat release during the main autoignition phase. This indeed stands for a very limited extent of temperature rise by the cool-flame. However, their experiments were mainly conducted on the low-to-mid load limit of engine operation regime while engine knock tends to occur under high-to-full load situation, including boosted operations. This implies that the average pressure regime of the in-cylinder fuel-air mixture might be considerably apart from that of the end gas of an SI engine. In addition to that, the tested fuel-air mixture was under very lean condition, i.e. equivalence ratio of 0.25–0.30. Though their newly proposed correlation has an empirical term of the mixture strength, it is not fully validated with the stoichiometric fuel-air mixture that is closely related to the SI engine operation.

Beccari et al. [29] also applied Livengood-Wu integration to predict knock during the SI engine experiment with various propane-gasoline blend fuel. They computed the ignition delay under an arbitrary state, i.e. the “mean” temperature and pressure chosen from the continuously varying state of the unburned gas, and compared those results with the integration output for evaluating the performance of the predictive model. Reported accuracy of the model was held between 3–4 CAD (crank angle

degree) under the engine speed of 900 RPM in their study, but the operating condition was somewhat distant from the expected situation in modern SI engines. This implies that the two-stage ignition behavior of gasoline-like fuel components under the temperature and pressure range from their study wouldn't be similar to what is expected in contemporary engines. Therefore, the "mean" temperature and pressure from the engine experiment might have been affected by the cool flame and relevant two-stage ignition behavior as well.

Yates et al. [30] tested various PRF–ethanol blend fuels in an SI engine and applied Livengood-Wu integration with two distinguished ignition regimes. In detail, the time span from the initial state to the onset of cool-flame was measured separately from that of the post cool-flame condition to the main autoignition, followed by combination of those individual numbers into a single integral equation to predict the autoignition point. It was clearly shown that the NTC behavior weakens as the ethanol fraction increases. In addition, the heat release intensity of the cool flame is very limited even with 20 % of n-heptane included in the blend. This is noticeable since n-heptane is widely known with its strong NTC behavior under the temperature range relevant to engine operating conditions. In number of cases, the cool-flame behavior was unrecognizable in the engine experiment results, thus the integration of reciprocals of the first-stage ignition delay are not counted into the prediction in this situation and this does not comply with their predictive model concept.

Kalghatgi et al. [31] also conducted an experimental study with a single cylinder SI engine under various intake pressure values, including a boosted condition. Five different blends of gasoline surrogate fuel were tested. Interestingly, the authors assumed a temperature offset for an in-cylinder local hot spot than the acquired temperature-pressure histories of the unburned gas, and fitted those arbitrarily shifted data with Livengood-Wu integration to give out the desired result. Hot spots usually

exist in realistic situations because of temperature inhomogeneity of the in-cylinder mixture with increased turbulent mixing of modern engines. They estimated the degree of temperature rise at local hot spots about 10–30 K than the mixture temperature.

1.5 Objectives of this study

Upon previous findings, the use of Livengood-Wu model in engine application is summarized as follows:

First, integration of the reciprocals of the ignition delay is adopted to find the moment of autoignition [22, 27, 28] when the corresponding ignition delay database, usually from computational results, is provided. Modifying the original Livengood-Wu concept is also tried in various aspects to handle two-stage ignition fuels, nonetheless it requires significant amount of background data for precise computation and is only applicable to a single thermodynamic history of the system at each. This wouldn't be quite suitable in situations where time consumption becomes a major limiting factor, such as a real-time control problem.

Another way of application is that the integration model can be used to derive an ignition delay expression of the specific fuel for autoignition prediction [25, 26, 29–31] in an arbitrary engine. This approach premises that Livengood-Wu integral reaches unity when autoignition takes place, thus the set of input variables relevant to the empirical correlation formula, e.g. temperature, pressure, equivalence ratio, mole fraction of oxygen, etc., are translated to derive the ignition delay expression. Therefore, the validity of Livengood-Wu model must be resolved in advance to adopt the outputs of those kind of studies.

Major objective of this dissertation study is to investigate the applicability of Livengood-Wu integration model for knock prediction in a modern SI engine fuels exhibiting NTC behavior. An alternative scheme will be proposed to improve the autoignition predictability of Livengood-Wu model via a new ignition delay concept which minimizes the contribution from cool flame exothermicity into the integration process. The findings are based on the chemical kinetic perspectives unlike previous studies, in order to grant a theoretical basis from the fundamental aspects of two-stage ignition characteristics.

In Chapter 2, modeling descriptions of an SI engine and constant volume reactor are provided which gives motivation and adequate method to this study, followed by Chapter 3 where detailed computational results are provided and discussed in various ways, e.g. quantitative comparison of reaction progress and Livengood-Wu integration with different ignition delays is provided. Also in the same subsection a new concept of ignition delay applicable to two-stage ignition fuels under specific situation is proposed by cancelling out thermal contribution of cool-flame with modeling approach. This new ignition delay is also applied to predict the autoignition point with Livengood-Wu integration and their validity is also investigated. Expansion to more general application is made in Chapter 4 by deriving a new ignition delay correlation as well as conducting chemical kinetic analysis to study its applicability. Finally, experimental results are presented and compared to other works in Chapter 5 to validate this new ignition delay concept, followed by concluding remarks and potential future works in Chapter 6.

Chapter 2. Modeling

In this chapter, concepts and details of an SI engine and autoignition modeling as well as constant volume reactor for ignition delay calculation are described. A set of ordinary differential equations is constructed and solved in each cases, respectively.

2.1 SI engine model

There are multiple modeling options to choose from when constructing an SI engine simulation: first of all, the number of in-cylinder zones is decided by main objectives of the study. For example, a three-zone model, which consists of two respective zones of the unburned and burned gases with the flame zone, can be an ideal solution to investigate the effect of in-cylinder flame dynamics. Along with that, the dimensionality of zones is also an important factor which depends on the system characteristics, e.g. 1-D or 2-D assumption may be helpful to focus on the effect of spatial distribution of the temperature field or the temperature gradient inside the cylinder.

In this study, a zero-dimensional two-zone SI engine model by Lumley [32] is adopted to simulate the SI engine operation including combustion process, which is adequate to handle the fuel reactivity characteristics inducing autoignition and corresponding engine knock. Multi-zones and dimensionality may be useful and somewhat closer to the real situation when computing the combustion process by the flame model, which is strongly dependent on the in-cylinder turbulence intensity and decided by system parameters such as engine speed, piston shape, valve flow, etc. On the other hand, it could conceal the fundamental aspects of fuel reactivity leading to autoignition if some engine-specific parameters govern combustion and affect

autoignition phenomena. Hence, the SI engine model applied in this study is constructed to neglect any dimensional factors and focus on the fuel reactivity itself. A schematic diagram of the model is drawn in Fig. 4.

An in-house SI engine code which consists of number of ordinary differential equations with respect to time is developed via MathWorks MATLAB 2015b with Cantera thermochemistry toolbox for chemical kinetics calculation. Engine dimensions are provided in Table 1 whose numbers are adopted from Cooperative Fuels Research (CFR) engine. Representative operating parameters come from the standard test methods [33, 34] which are utilized to grade the anti-knock capability of test fuel by intentionally inducing autoignition of unburned mixture before the end of engine combustion process and reproducing that same knocking behavior, i.e. similar knock intensity measured by an external metering sensor. PRF is a designated gasoline surrogate and the blending ratio of each substance—iso-octane and n-heptane—is adjusted to exhibit the similar knock characteristics of the test fuel. However, operating condition of boosted downsizing SI engines shift towards the opposite direction from that of both octane rating standards, hence it is controversial to cope with knocking trend of modern SI engines by relatively “traditional” test methods in today’s situation.

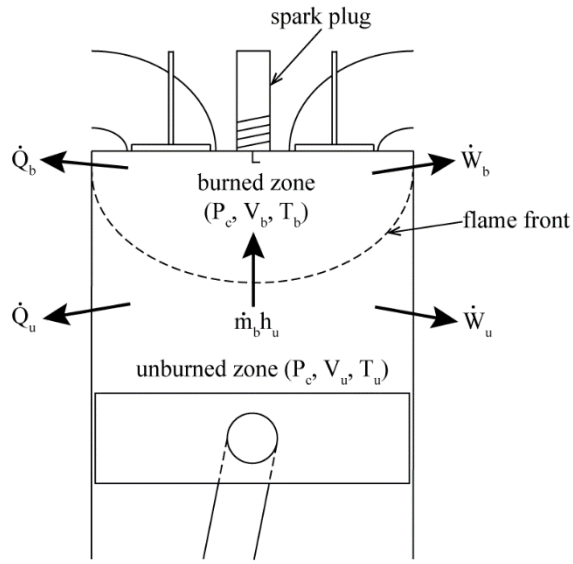

Figure 4. A schematic diagram of two-zone SI engine model

Table 1. Model engine dimensions and operating parameters

Bore	82.6 mm
Stroke	114.3 mm
Displacement volume	612 cc
Inlet air temperature	52°C
Spark timing	13 CAD bTDC
Engine speed	1200, 1500, and 1800 RPM
Intake Valve Close (IVC)	34 CAD aBDC
Equivalence ratio	1.0
Wall temperature	200°C

2.1.1 Modeling details

Simulation begins at IVC timing where temperature, pressure, volume, and mixture composition are given as initial condition and in-cylinder volume being considered a single zone with homogeneous gas properties until the spark timing, followed by zone division where thermodynamic states of two respective zones of unburned and burned gases are decided by mass and energy balance equations. In detail, in-cylinder mass is conserved throughout the whole simulation process and is written as

$$m_u + m_b = m \qquad \text{(Eq. 2.1)}$$

where subscripts u and b denote unburned and burned gases after ignition, respectively. Therefore,

$$\dot{m}_u + \dot{m}_b = 0 \qquad \text{(Eq. 2.2)}$$

and the mass burn rate $\dot{m}_b$ must be known. This is given by Wiebe function [3] in which burned mass fraction at an arbitrary crank angle is determined by predefined parameters such as burning rate and combustion duration. Wiebe function is acknowledged as a simple and robust correlation in modeling engine combustion process [35] which also fits into this study as the relationship between the autoignition propensity of the unburned gas in later burn stage and the fuel reactivity is one of the major objectives. Burned mass fraction x_b at an arbitrary crank angle θ is expressed as

$$x_b = 1 - exp\left[-a\left(\frac{\theta - \theta_0}{\Delta\theta}\right)^{m+1}\right] \qquad \text{(Eq. 2.3)}$$

where $\Delta\theta$ is the combustion duration of corresponding cycle and θ_0 the crank position at start of combustion. Fitting parameters *a* and *m* adjust the overall 'shape'

of burning rate curve, which are set 6 and 2, respectively. In addition to that, combustion duration must be specified which is resultant from in-cylinder turbulence intensity and consequent turbulent flame velocity in real situation, however it is defined as a function of RPM in this study which is an appropriate assumption as faster piston motion would induce larger turbulence intensity and shorter combustion time. Detailed numbers are referred from [3] and plotted in Fig. 5. Therefore, differentiating x_b along with crank angle gives mass burn rate against crank angle degree

$$\frac{dx_b}{d\theta} = \mathrm{a} \cdot \left(\frac{1}{\Delta\theta}\right)^{m+1} \cdot (m+1) \cdot \theta^m \cdot exp\left[-a\left(\frac{\theta}{\Delta\theta}\right)^{m+1}\right] \qquad \text{(Eq. 2.4)}$$

and applying chain rule, it gives the time-basis mass burn rate

$$\dot{m}_b = \frac{dx_b}{dt} = \frac{dx_b}{d\theta} \cdot \frac{d\theta}{dt} \qquad \text{(Eq. 2.5)}$$

if crank angle degree is also written as a function of time.

Energy equations on both the unburned and burned zone can be written as

$$0 = \dot{m}_b h_u + \dot{Q}_u + P_c \frac{dV_u}{dt} + \frac{dU_u}{dt} \qquad \text{(Eq. 2.6)}$$

for the unburned zone and

$$\dot{m}_b h_u = \dot{Q}_b + P_c \frac{dV_b}{dt} + \frac{dU_b}{dt} \qquad \text{(Eq. 2.7)}$$

for the burned zone, where h is the enthalpy; $\dot{Q}$ is the heat transfer to the cylinder walls; P_c is the pressure in the cylinder; V is the volume; and U is the total internal energy of each zones.

Knowing that the sum of the respective volumes of the unburned and burned zone is identical to the total in-cylinder volume at corresponding crank angle position, it may be written as

$$V_c = V_u + V_b = \frac{m_u \bar{R}_u T_u}{P_c} + \frac{m_b \bar{R}_b T_b}{P_c} \qquad \text{(Eq. 2.8)}$$

where $\bar{R}_u$ and $\bar{R}_b$ each stand for the individual gas constant, that is the universal gas constant R divided by the molecular weight of each gas, respectively. In Lumley's model Eq. 2.8 is multiplied by P_c and differentiated, then introducing a new term $\alpha = \bar{R}T$, it becomes

$$\begin{aligned} \frac{dP_c}{dt} V_c + \frac{dV_c}{dt} P_c &= \left(\frac{dm_u}{dt} \bar{R}_u T_u + \frac{d\bar{R}_u}{dt} m_u T_u + \frac{dT_u}{dt} m_u \bar{R}_u \right) \\ &\quad + \left(\frac{dm_b}{dt} \bar{R}_b T_b + \frac{d\bar{R}_b}{dt} m_b T_b + \frac{dT_b}{dt} m_b \bar{R}_b \right) \\ &= \dot{m}_b (\alpha_b - \alpha_u) + m_u \bar{R}_u \frac{dT_u}{dt} + m_b \bar{R}_b \frac{dT_b}{dt} \end{aligned} \qquad \text{(Eq. 2.9)}$$

If Eqs. 2.6 and 2.7 are expressed in terms of total enthalpy, *H=U+PV*, they are rearranged by

$$0 = \dot{m}_b h_u + \dot{Q}_u - V_u \frac{dP_c}{dt} + \frac{dH_u}{dt} \qquad \text{(Eq. 2.10)}$$

and

$$\dot{m}_b h_u = \dot{Q}_b - V_b \frac{dP_c}{dt} + \frac{dH_b}{dt} \qquad \text{(Eq. 2.11)}$$

respectively. Manipulating them with $H = mh$ and from the ideal gas equation of state $dh = c_p dt$, they become

$$m_u c_{p,u} \frac{dT_u}{dt} = V_u \frac{dP_c}{dt} - \dot{Q}_u \qquad \text{(Eq. 2.12)}$$

for the unburned zone and

$$m_b c_{p,b} \frac{dT_b}{dt} = V_b \frac{dP_c}{dt} - \dot{Q}_b + \dot{m}_b (h_u - h_b) \qquad \text{(Eq. 2.13)}$$

for the burned zone. Eqs. 2.12 and 2.13 replace the temperature term in Eq. 2.9 to give

$$\frac{dP_c}{dt}(V_c - \beta_u V_u - \beta_b V_b) = -\frac{dV_c}{dt} P_c + \beta_b \dot{m}_b (h_u - h_b) - \left(\beta_u \dot{Q}_u + \beta_b \dot{Q}_b\right) + \dot{m}_b (\alpha_b - \alpha_u) \qquad \text{(Eq. 2.14)}$$

where $\beta = \bar{R}/c_p$.

Heat transfer rates of two individual zones to the cylinder walls are also necessary to solve these time differential equations which are acquired from the engine heat transfer study by G. Woschni [36]. Convection heat coefficients during the gas exchange process, compression stroke, and combustion and expansion period are calculated by engine dimension parameters as well as gas state variables, i.e. volume, temperature, pressure, cylinder bore, etc. It is summarized as

$$h_c[\mathrm{W/m^2 \cdot K}] = 3.26 \cdot Bore[\mathrm{m}]^{-0.2} \cdot P[\mathrm{kPa}]^{0.8} \cdot T[\mathrm{K}]^{-0.55} \cdot w[m/s]^{0.8} \qquad \text{(Eq. 2.15)}$$

while w is defined by

$$\mathrm{w} = \left[C_1 \bar{S}_p + C_2 \frac{V_d T_r}{P_r V_r}(P - P_m)\right] \qquad \text{(Eq. 2.16)}$$

with coefficients

$C_1 = 6.18, C_2 = 0$ For the gas exchange process

$C_1 = 2.28, C_2 = 0$ For the compression stroke

$C_1 = 2.28, C_2 = 0.00324$ For the combustion and expansion period.

Effective heat transfer area is also derived from instantaneous gas volume. Some preliminary engine simulation results are presented in Fig. 6.

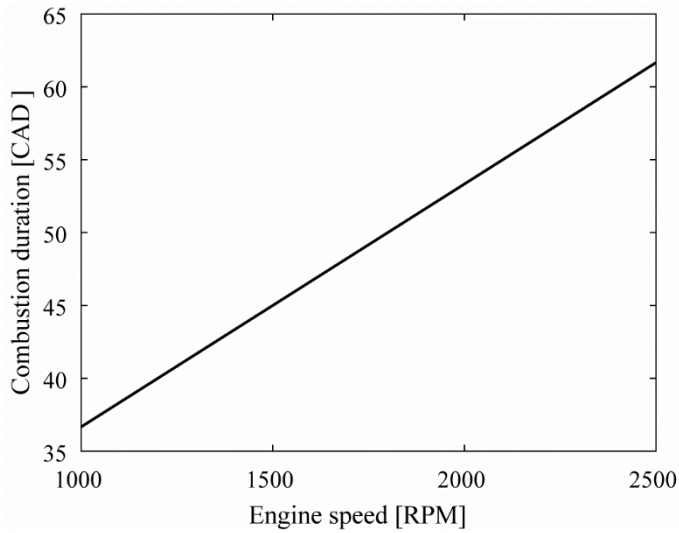

Figure 5. Combustion duration applied to this study by different engine speed

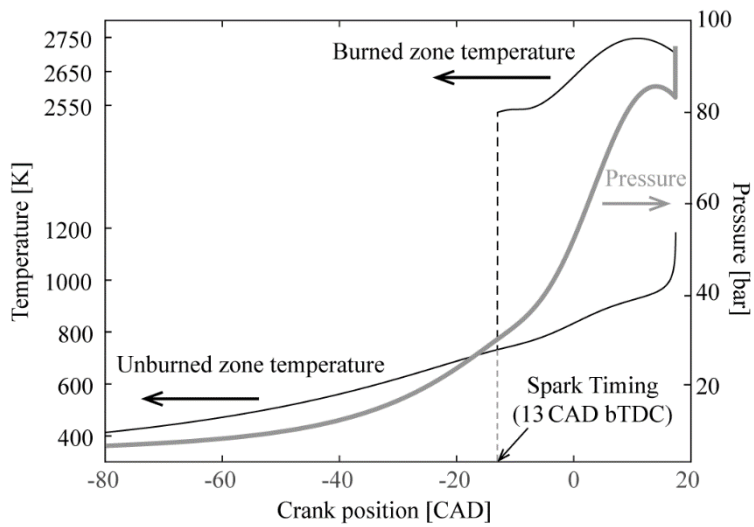

Figure 6. Example of two-zone SI engine model simulation results

2.1.2 Autoignition of the unburned gas and knock

Chemical kinetics of the molecules within fuel-air mixture is considered in the single zone during the compression stroke prior to spark timing as well as the unburned zone after ignition, while the burned gas composition is assumed as complete combustion products, i.e. carbon dioxide, water (as steam), and inert nitrogen. For computational results, up-to-date iso-octane reaction mechanism from Lawrence Livermore National Laboratory is adopted which consists of 874 species and 6864 reactions [10, 37] due to its role as a major component of PRF in grading the anti-knock propensity of fuel. Conducting this, it becomes feasible to check whether the autoignition of the unburned gas takes place or not before the end of combustion period. Autoignition is determined under the following hypothesis; time history of the mass fraction of fuel substances would follow the predefined Wiebe correlation curve while combustion is ongoing. If autoignition would break out it is thought that the mass fraction of initial fuel would decrease faster than the Wiebe profile since larger molecules are expected to break into smaller intermediate species to produce massive amount of radicals as the reactivity of the mixture is stimulated. This strongly implies that the unburned mass fraction of in-cylinder gas, which follows the predefined Wiebe curve, tends to be larger than the unburned 'fuel' fraction at the autoignition point in many cases. Therefore, it is assumed an autoignition outbreak if the mass fraction of the fuel substance reaches 3% of the initial amount of fuel at that moment, followed by immediate knocking. Graphical explanation is also provided in Fig. 7 for clarity.

It seems that there might be a certain connection between the knock intensity and the unburned mass fraction at autoignition point, for example Mehl et al. [38] assumed that the more the unburned mass remaining, the stronger the knock intensity, i.e. autoignition at the point of 30 % unburned mass is defined heavy knock. However,

it is still controversial to designate such relationship as other studies [39] claim that the knock intensity is inversely proportional to the amount of unburned gas leftover. In this study, the proportionality assumption between the unburned mass fraction and the knock intensity is accepted.

On the other hand, not all the autoignition develops into engine knock. That is, if autoignition of the unburned gas occurs considerably later in the combustion period or its intensity is almost negligible, it wouldn't be developed into "measurable" knock. For instance, it may be referred from [38] that the smallest measurable knock is recorded in the CFR engine experiment with approximate compression ratio of 7.9 when fueled with iso-octane. That compression ratio gave out the unburned mass fraction circa 5 % in our engine simulation when autoignition occurred. Therefore, when unburned mass fraction is less than 5 % of total in-cylinder gas at the autoignition point, it is not considered as a knock, nevertheless autoignition has occurred.

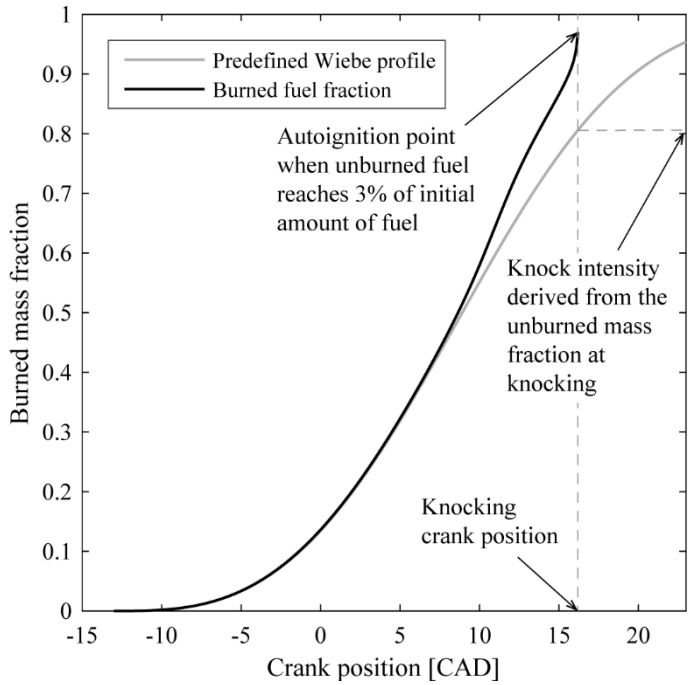

Figure 7. Predefined mass burn rate by Wiebe correlation and burned fuel mass profile

2.2 Ignition delay calculation from constant volume reactor model

Ignition delay data is necessary to evaluate Livengood-Wu integration along with the unburned gas profile acquired from an engine simulation, and the data set is obtained from an ideal constant volume reactor model. From the first law of thermodynamics, it is obvious that any heat addition to the control volume of the reactor by molecular reactions results in temperature and pressure increase while there is no expansion work. Along with that, thermodynamic states are homogeneous inside the reactor and elementary reactions occur uniformly within the gas volume. In detail, the first law is written for a fixed mass as

$$\dot{Q} = \dot{U} = m\frac{du}{dt} \qquad \text{(Eq. 2.17)}$$

and internal energy of the gas is given by

$$u = \frac{U}{m} = \frac{1}{m}\sum_{i=1}^{N} N_i \overline{u_i} \qquad \text{(Eq. 2.18)}$$

where N_i and $\overline{u_i}$ stands for number of moles and molar internal energy of any i-th species, respectively. Differentiating Eq. 2.18 with time gives

$$\frac{du}{dt} = \frac{1}{m}\left[\sum_{i=1}^{N}\left(\overline{u_i}\frac{dN_i}{dt}\right) + \sum_{i=1}^{N}\left(N_i\frac{d\overline{u_i}}{dt}\right)\right] \qquad \text{(Eq. 2.19)}$$

The number of moles of i-th species is $N_i = V[X_i]$. Hence, for a constant volume reactor,

$$\frac{dN_i}{dt} = V\frac{d[X_i]}{dt} \equiv V\dot{\omega}_i \qquad \text{(Eq. 2.20)}$$

where $\dot{\omega}_i$ is the concentration change of i-th species only by chemical reactions.

Applying chain rule to the internal energy term in Eq. 2.19 it transforms into a combination of constant volume specific heat and temperature change rate, in detail

$$\frac{d\overline{u_\iota}}{dt} = \frac{d\overline{u_\iota}}{dT}\frac{dT}{dt} = \overline{c_{v,\iota}}\frac{dT}{dt} \qquad \text{(Eq. 2.21)}$$

For example, the temperature change rate is derived by replacing the terms in Eq. 2.19 as

$$\begin{aligned}\frac{\dot{Q}}{m} = \frac{du}{dt} &= \frac{1}{m}\left[\sum_{i=1}^{N}(\overline{u_\iota}V\dot{\omega}_i) + \sum_{i=1}^{N}\left(N_i\overline{c_{v,\iota}}\frac{dT}{dt}\right)\right] \\ &= \frac{1}{m}\left[\sum_{i=1}^{N}(\overline{u_\iota}V\dot{\omega}_i) + \sum_{i=1}^{N}\left(V[X_i]\overline{c_{v,\iota}}\frac{dT}{dt}\right)\right] \\ &= \frac{V}{m}\left[\sum_{i=1}^{N}(\overline{u_\iota}\dot{\omega}_i) + \sum_{i=1}^{N}\left([X_i]\overline{c_{v,\iota}}\frac{dT}{dt}\right)\right] \\ \therefore\ \frac{dT}{dt} &= \frac{\left(\dot{Q}/V\right) - \sum_{i=1}^{N}(\overline{u_\iota}\dot{\omega}_i)}{\sum_{i=1}^{N}\left([X_i]\overline{c_{v,\iota}}\right)} \qquad \text{(Eq. 2.22)}\end{aligned}$$

and other parameters of interest, such as pressure change rate, are also obtainable to determine the thermodynamic states of the system at every time step, including chemical reactions.

Time duration from the initial state to the point of maximum pressure rise rate is defined as the ignition delay of fuel-air mixture at the given corresponding state, as plotted in Fig. 8. Maximum [·OH] change rate is also applicable instead of maximum pressure rise rate, since these two different definitions would provide almost identical results when the massive formation of reactive hydroxyl radical occurs along with autoignition and pressure rise. Usually, [·OH] rate is favored within the test apparatus with optical measurement while the pressure-time history is easier to handle in most experimental facilities. Two-stage ignition behavior by cool flame

appearance is also shown in the same figure. There are two individual ignition delays, i.e. cool-flame ignition delay τ_{cf} and second-stage main ignition delay τ_{2nd}, while the pressure rise by the cool flame ΔP_{cf} is evaluated at the local minima of pressure rise rate within the first ignition stage.

While the reason would be clearer in Chapter 3, the heat capacity of nitrogen included in the reaction mechanism is intentionally multiplied by a factor of 2–5 in order to suppress cool flame exothermicity and quantify its thermal contribution in stimulating the overall reactivity of two-stage ignition fuels. With this approach, the relationship between ΔP_{cf} and τ_{cf} can be established and expanded to the limit where cool flame is fully "eliminated" as ΔP_{cf} approximates zero. Along with that, second stage ignition delay τ_{2nd} is assumed to follow Arrhenius behavior, i.e. post cool-flame pressure and temperature determines τ_{2nd}. Finally, cool-flame eliminated ignition delay is obtained and it is thought to become a better representative of instantaneous chemical reactivity of the engine unburned gas from Livengood-Wu model perspective, especially when there is no clear sign of cool-flame exothermicity perceived during the compression stroke and combustion process of the engine operation with NTC-exhibiting fuels.

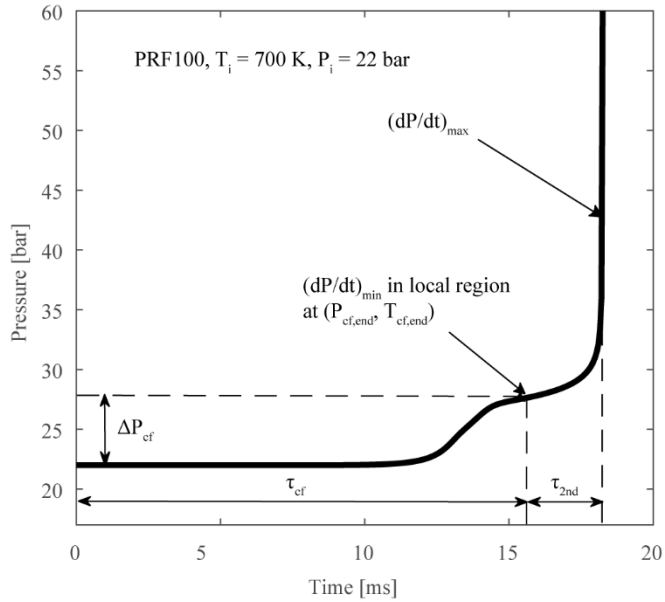

Figure 8. Definition of the ignition delay and other terms

Chapter 3. Computational results

In this chapter, simulation results from both the SI engine model and the constant volume reactor model are presented and analyzed to promote the necessity of improved knock prediction model for modern SI engines.

3.1 SI engine simulation results

3.1.1 Unburned gas profiles and inconsistence of Livengood-Wu model

Thermodynamic profiles of the unburned gas under knocking situation are depicted in Fig. 9 with various intake pressure conditions assuming turbocharged operation of a contemporary engine fueled with iso-octane. In the figure legend, '1.0 bar' stands for an atmospheric intake pressure, i.e. wide open throttle under naturally aspirated operation. Total ignition delay values are also shown as the background contours on a natural log scale. It is clear that the downsized boosting strategy shifts the major thermodynamic operation regime towards low temperature and high pressure region where the NTC characteristic of fuel is dominant. Similar temperature-pressure trajectory curves from both the computational [38] and experimental [11] studies are also found. However, it does not guarantee the cool-flame appearance during the engine operation in above cases, nonetheless most of them are overlapped on the NTC-exhibiting region. For example, cool-flame exothermicity during the process is only measured at the highest overall pressure condition (i.e. extreme boost pressure) in the iso-octane study of Scott Goldsborough [11].

For example, Figs. 10 and 11 present temperature- and pressure-CAD history of the unburned gas for compression ratio of 12.6 and 1500 RPM engine speed with 1.4 bar initial pressure condition, i.e. boost pressure of 0.4 bar, from Fig. 9. Dashed curves in each figure indicate that the chemical kinetics of the unburned gas species is deactivated, thus it is useful to distinguish the cool-flame exothermicity from the reacting profile by overlaying two independent curves on a same plot, as there wouldn't be any composition change by chemical reactions in the deactivated case. In Figs. 10 and 11, there isn't any mild pressure or temperature jump revealed which are relevant to cool-flame exothermicity, nevertheless most of its temperature and pressure conditions are under the NTC region of Fig. 9 before reaching the main autoignition point. Such behavior is also reported in the work by M. Perumal and G. Floweday [40] with the same CFR engine simulation results fueled with iso-octane.

When no cool flame appears in various engine simulation results until the autoignition point, it is quite controversial to apply Livengood-Wu integration along the unburned gas profile with the reciprocal of corresponding cool-flame affected ignition delay in the NTC region, since it is not relevant to autoignition prediction because of lack of cool flame revealed in the unburned gas profile. That is, cool-flame affected ignition delays of any given initial condition are inappropriate to represent the instantaneous chemical reactivity of the unburned gas when its thermodynamic states are almost identical to the cool-flame affected ignition delay case, because there hasn't been any cool flame appeared regardless of the same thermodynamic state at that corresponding moment. Therefore, the accuracy of autoignition predictability deteriorates when the reciprocal of those cool-flame affected ignition delays are applied to Livengood-Wu model in such cases, as presented in Fig.12 in which the grey-colored diagonal line stands for a perfect agreement between the computed knocking point from the engine simulation and the predicted knocking position by Livengood-Wu integration. It is found out that

Livengood-Wu integration overestimates the autoignition point with the cool-flame affected ignition delays due to the exaggerated contribution of ignition delay reciprocals to the integration process while the unburned gas profiles are overlapped on the NTC region.

On the other hand, cool-flame exothermicity appears at somewhere during the combustion process if the unburned gas states shift towards even lower temperature and higher pressure region. For comparison, higher boost level of 2.5 bar initial pressure condition is selected and the simulation results are presented in Fig. 13 in which temperature rise by cool-flame exothermicity is visible. This is more clearly shown in Figs. 14 and 15 if the representative species history is tracked and compared with other cases that doesn't show any meaningful cool-flame behavior during the combustion stage. In the figures molar concentration of both ·OH and alkylperoxy radicals (i.e. $\alpha, \beta, \gamma, \text{and } \delta - C_8H_{17}O_2$) in the engine unburned gas are plotted with various intake pressure condition. It is obvious that cool flame appearance is deservingly comparable depending on the chemical kinetic behavior of the unburned gas, as found in the figures. Iso-octane molecules would break up and follow their own reaction pathway as the unburned gas states change towards increasing temperature and pressure in the later burn stage, and if their own governing reaction scheme were distinct to each other, i.e. one with cool-flame appearance and the other not, radical species history should be distinguishable thanks to different reaction rates and corresponding chemical progress. In the iso-octane study by Scott Goldsborough [11], similar behavior of the cool flame chemistry was reported in which cool flame only appeared in rapid compression machine (RCM) experiments with higher pressure condition.

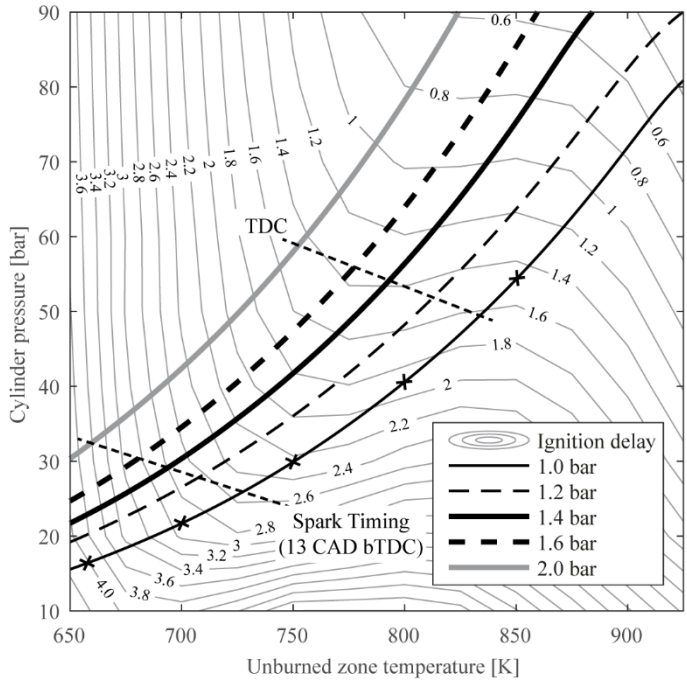

Figure 9. Selected thermodynamic histories of engine unburned gas with various initial intake pressure.

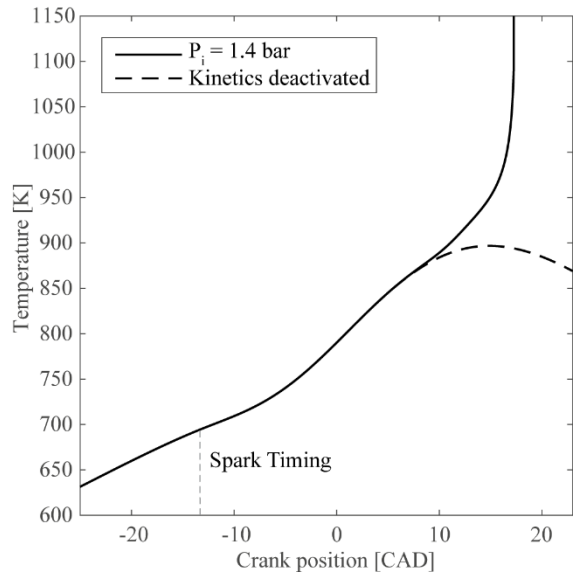

Figure 10. Unburned gas temperature from the SI engine simulation along with engine crank angle degree.

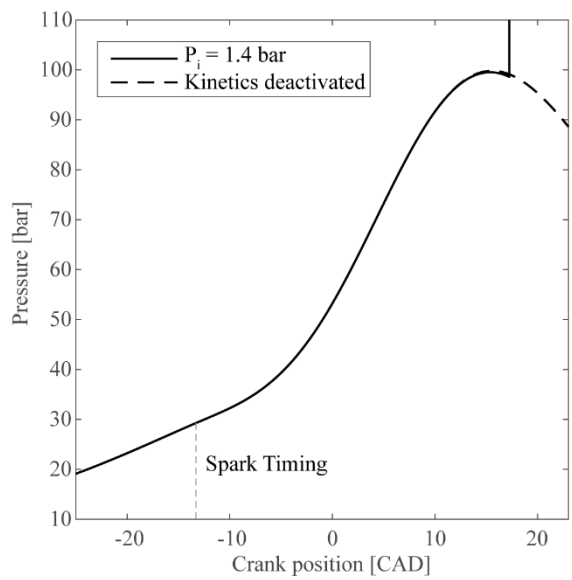

Figure 11. Cylinder pressure along with engine crank angle degree.

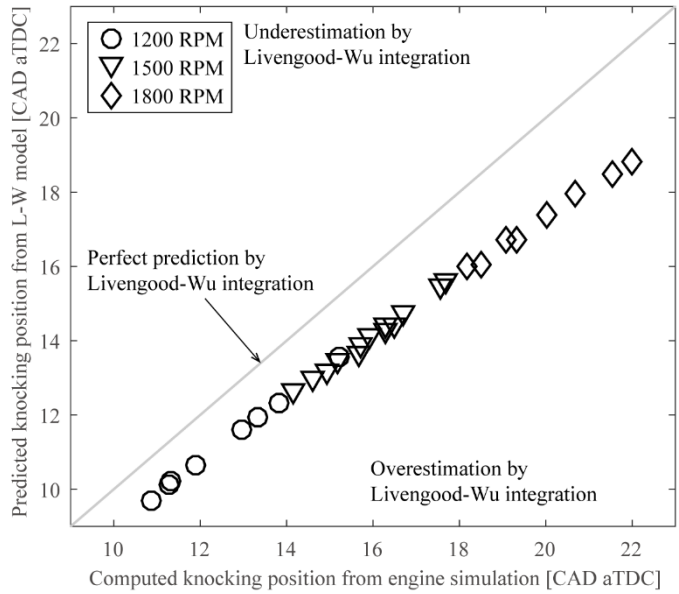

Figure 12. Autoignition point prediction by Livengood-Wu integration with cool-flame affected ignition delay

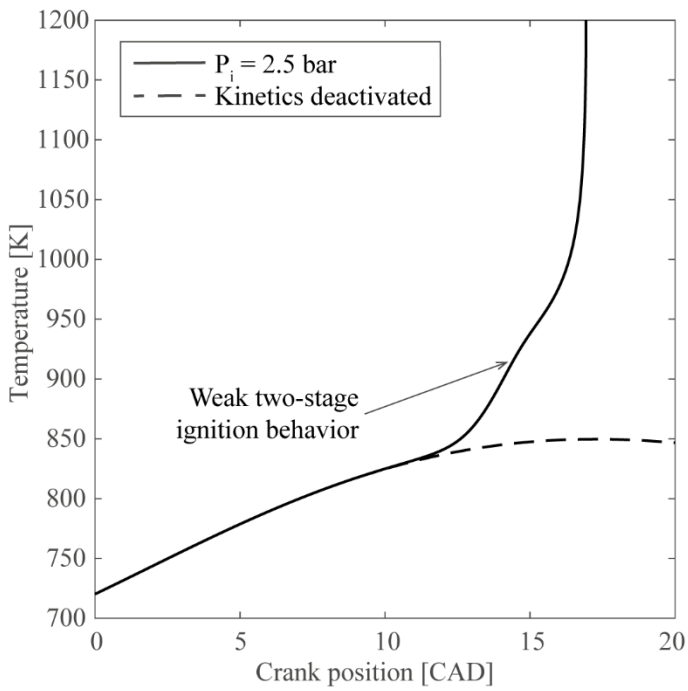

Figure 13. Unburned gas temperature with cool-flame appearance in the later burn stage

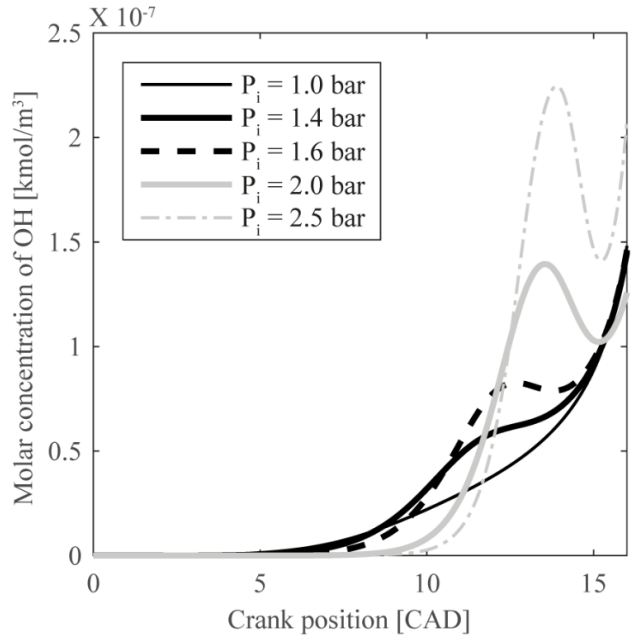

Figure 14. Molar concentration of ·OH radical in the unburned gas prior to autoignition

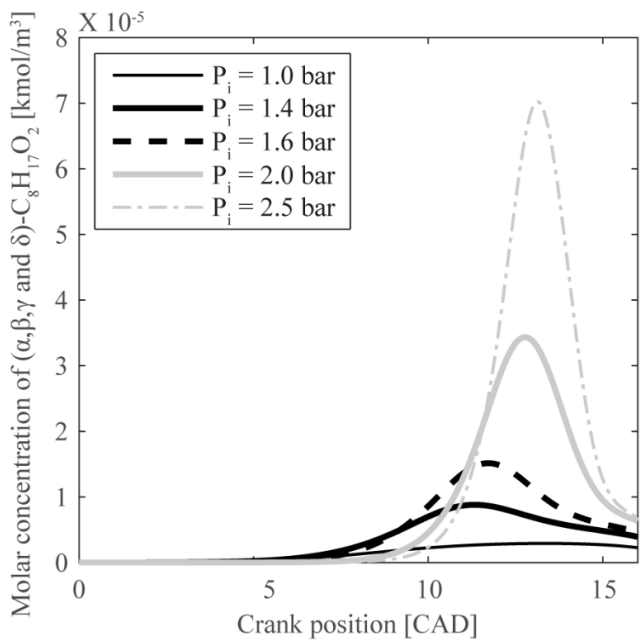

Figure 15. Molar concentration of alkylperoxy radical in the unburned gas prior to autoignition

3.1.2 Engine operating conditions relevant to cool-flame appearance

Based on computation results and literature surveys, it may be concluded that there exists certain "threshold" which suppresses the cool-flame and corresponding exothermicity appearance within the unburned gas states of any SI engine during the combustion process. While there are many parameters affecting in-cylinder combustion in zero-dimensional model, e.g. initial temperature and pressure, spark timing, EGR ratio, RPM, type of fuel, etc., potential boundary condition of cool-flameless unburned gas history of this study is presented in Fig. 16 whose knock predictability by cool-flame affected ignition delay values is at most mediocre. Hence, it is worth investigating the alternate way to improve the prediction capability of Livengood-Wu model in those cases, as the next-generation SI engines with higher boosting strategy are directly related to these operating conditions.

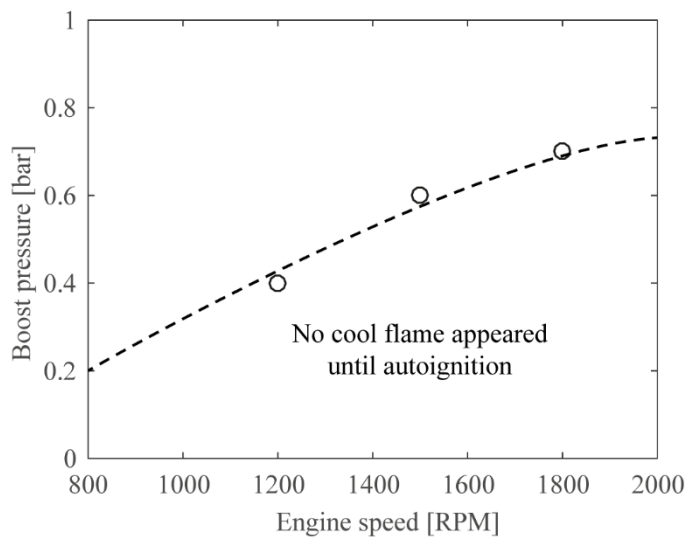

Figure 16. Cool-flame exhibiting boundary conditions with engine speed and boost pressure

3.2 Constant volume reactor model results

As aforementioned, original ignition delay is calculated by detailed iso-octane reaction mechanism with multiple cases of heat capacity modulation of nitrogen to absorb exothermic heat of cool flame. In case of the chemical kinetic mechanism based on NASA thermodynamic properties table [41], constant pressure heat capacity of any substance over the gas constant R is given as a 4^{th} order polynomial of temperature, thus multiplying those polynomial coefficients would result in increased heat capacity value. While the autoignition process is computed with the reaction mechanism adopted in this study, there is no single elementary reaction that handles nitrogen both as a reactant or product. Therefore, altering the thermodynamic property of nitrogen doesn't affect the oxidation process from the chemistry perspective, compared to the thermal effect relevant to the change in temperature increment by cool flame phenomenon which are acquirable with this methodology. In reality, the oxidation of nitrogen to produce NOx would occur, but that is comparably negligible to the main oxidation pathways of fuel, hence it is not considered in this study.

Other components that consist of the engine intake mixture (e.g. carbon dioxide and steam as the in-cylinder residual gas from the previous cycle) were once considered to play the same role of nitrogen as they have larger specific heat values, but they are final combustion products of hydrocarbon oxidation and thus modifications to the thermodynamic property would result in chemical equilibrium to be changed, meaning that additional chemistry effect may appear and becoming more complex to analyze. This is because the entropy term in the mechanism is also the polynomial equation of temperature and multiplying those polynomial coefficients should modulate the entropy value.

Here, initial mixture composition is identical to the engine intake mixture and for comparison, five different sets of temperature and pressure are chosen and marked by ‘X’ symbol in Fig. 9 whose two-stage ignition behavior are contrary to one another. Along with that, “integrated” ignition delays at the same ‘X’ points are also computed by reflecting the unburned mixture composition change during the compression stroke and combustion process of an engine cycle, in detail the mixture composition at temperature and pressure of ‘X’ from the engine simulation result is brought to the constant volume reactor model. Comparison of original and integrated ignition delay at every thermodynamic state thus provides insight to quantify the progress of reaction chemistry along with time.

3.2.1 Two-stage ignition behavior in the NTC region

Number of independent pressure-time histories by heat capacity modulation of nitrogen and corresponding original ignition delays are plotted in Fig. 17 with initial thermodynamic states of the first four ‘X’ points within the NTC region of Fig. 9. Intense cool flame and two-stage ignition behavior is observed in 660–750 K condition while the intensity weakens as temperature increases. Also, it is clear that suppressing the thermal contribution of cool flame by absorbing more exothermic heat with the help of “modulated” nitrogen leads to retarded end of first stage ignition and resultant longer overall ignition delay regardless of initial temperature.

However, there seems no discernible change to the initiating point of first stage ignition by heat capacity modulation which suggests that the major reaction pathway inducing cool flame behavior depends largely upon the mixture composition. Chemical kinetics studies [19, 42] mentioned that the oxidation of alkyl radical,

$$C_nH_{2n+1} + O_2 \rightleftharpoons C_nH_{2n+1}O_2$$

is a predominant reaction causing cool-flame in the two-stage ignition region. Thus, heat capacity modulation of nitrogen would affect the initiation of cool flame phenomenon within very limited extent, leading to the similar starting point of cool flame shown in Fig. 17.

Supporting this hypothesis, rate of progress of most reactive elementary reactions at the cool-flame initiation point with different heat capacity values at an arbitrary representative initial condition of 700 K and 22 bar are also compared in Fig. 18, showing that the cool flame chemistry is almost not affected by modulation. Similar behavior is also observed other than this specific initial condition within the NTC region.

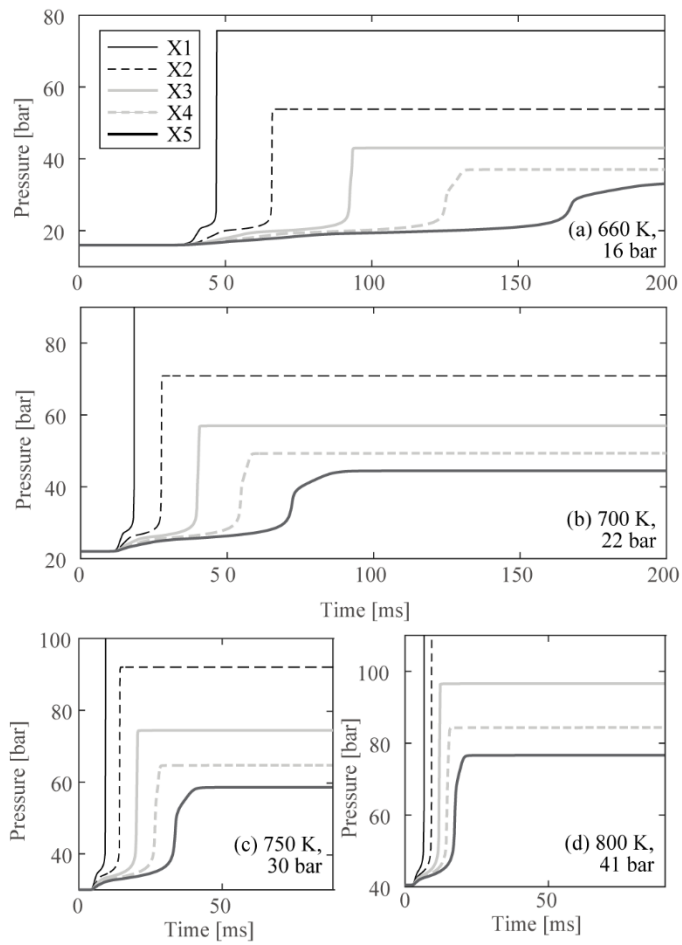

Figure 17. Pressure history of original and modulated heat capacity cases for different initial states within the NTC region from Fig. 9.

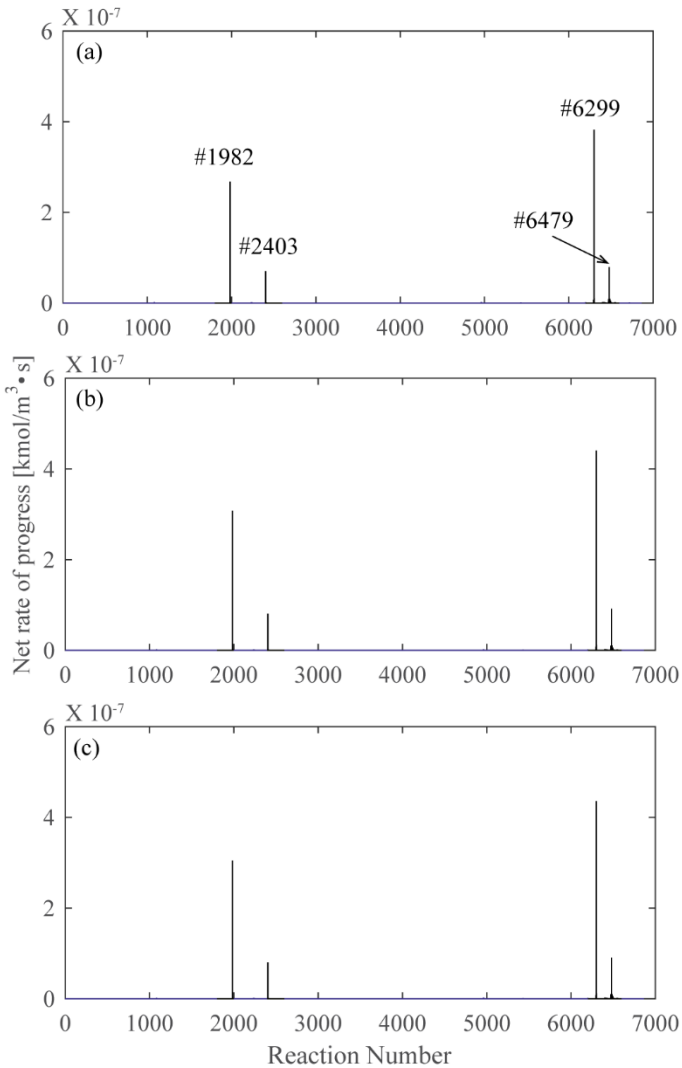

Figure 18. Rate of progress of pre-cool flame stage reactions at 7 ms after 700 K, 22 bar initial condition, (a) X1, (b) X2, and (c) X3 cases.

3.2.2 Single stage ignition behavior in the post-NTC region

Figure 19 depicts the pressure-time history and original ignition delay with initial condition of 850 K and 54 bar in which two-stage ignition behavior diminishes. Nonetheless, it is noted that number of preceding chemistry in the intermediate-to-high temperature oxidation scheme of iso-octane are known as exothermic [43], implying that the relatively slight pressure and temperature rise before autoignition is also affected by modulating the heat capacity of nitrogen regardless of cool flame chemistry. Indeed, it is expected that there would be only slight extension of the ignition delay by heat capacity modulation in the post-NTC, single stage ignition region.

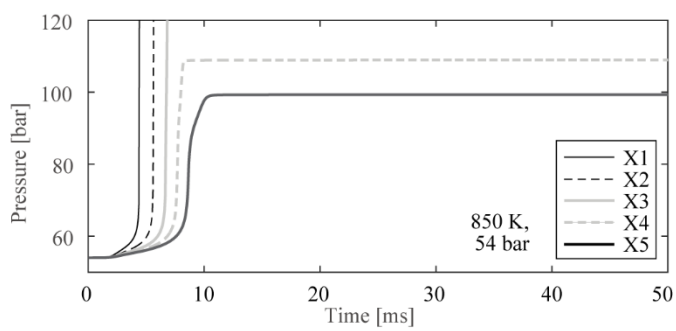

Figure 19. Pressure history of original and modulated heat capacity cases for a post-NTC, single stage ignition region from Fig. 9

3.3 Integration of reaction chemistry and its contribution to the overall reactivity

3.3.1 Comparison of original and integrated ignition delay

Figure 20 presents the computed results of original and integrated ignition delays that were explained previously while following the thermodynamic history of the engine unburned gas of 1.0 bar intake pressure condition, and it is seen that the reduction in integrated ignition delay is kept less than a millisecond order while the conditions are within the NTC region where the engine unburned gas passes through. This reduction in overall ignition delay should have been resulted from the integrated progress of cool flame chemistry during the engine process until the moment of interest. However, it is important that main autoignition chemistry is hardly affected since the time shift between two delays is kept almost constant until autoignition point, e.g. gap between the positions where 50 % of cool flame pressure rise occurs are very similar to that of autoignition points. As the unburned gas states are being progressed and the integrated preceding chemistry accumulates, time shift (in advancing direction, definitely) also increases along the unburned gas history until autoignition, which is found in the following section.

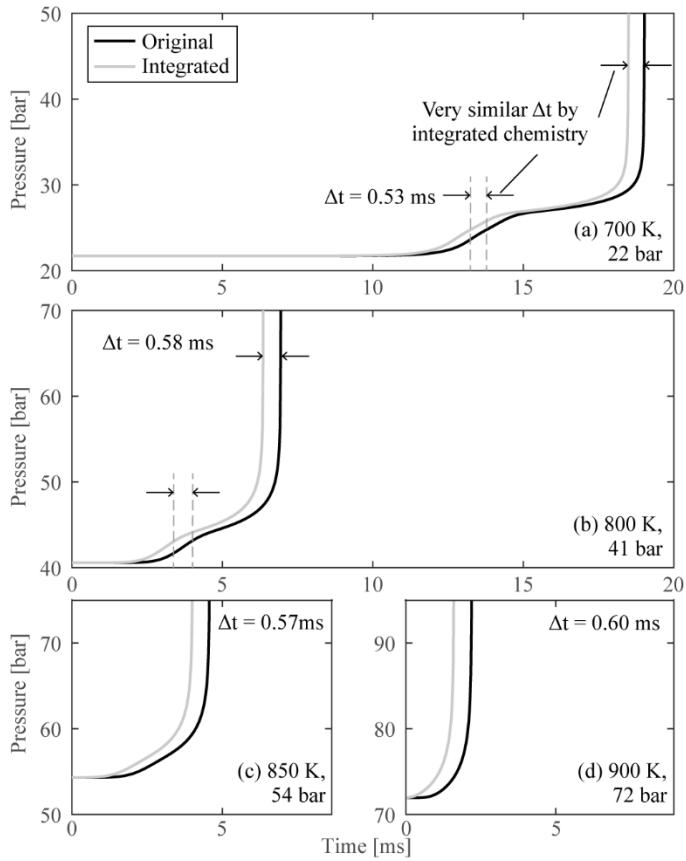

Figure 20. Comparison of original and integrated ignition delay on the thermodynamic path of the engine unburned gas of 1.0 bar intake pressure

3.3.2 Time reduction by integrated reaction chemistry

The degree of accumulated reaction chemistry could be quantitatively reviewed by adopting the basic idea of Livengood-Wu integration model as follows; first, the relationship between original and integrated ignition delay can be established as

$$\int_{t_0=0}^{\tau_{integrated}} \frac{1}{\tau_{original}} dt = \frac{\tau_{integrated}}{\tau_{original}} \qquad \text{(Eq. 3.1)}$$

and since every integrated delay is always shorter than the original ones under their same thermodynamic conditions and reduced relatively more along with the increment in degree of accumulated reaction chemistry, it is certain that the outcome of Eq. 3.1 should always be less than 1. Therefore, the difference between unity, i.e. an ideal result from the Livengood-Wu model perspective at autoignition point, and the calculation from Eq. 3.1 is obtained along with the unburned gas history and this value can be accepted as an index of integrated reaction chemistry. Figure 21 presents the trend of integrated reaction chemistry of the engine unburned gas along with the crank position, and it is seen that the difference between two delays is somewhat indistinct while the unburned gas state remains within the NTC region, implying that the effect of integrated chemistry in overall reactivity is very limited in this case. On the other hand, the integration effect to the mixture reactivity is comparably noticeable in the post-NTC region in which integrated delay shortens relatively more as the unburned gas history proceeds.

The role of cool-flame affected ignition delay leading to overestimating trend of Livengood-Wu integration was briefly discussed in Chapter 3.1.1, and now it becomes clear that cool-flame affected ignition delay is inappropriate to represent the instantaneous reactivity if no cool flame appeared within the engine situation. The reactivity integration by Livengood-Wu model and the accumulated chemistry

progress which was described in Fig. 21 are depicted together in Fig. 22 and it is obvious that the reciprocals of cool-flame affected ignition delay exaggerates the role of integrated chemistry advancing the overall autoignition phase. Much of this discrepancy seems to come from the thermal contribution of cool flame in cool-flame affected ignition delay, which is unnecessarily considered in the integration process. Hence, it is concluded that when two-stage ignition fuel is of interest and no cool flame is revealed within the thermodynamic history of the engine unburned gas, considerations must be preceded to exclude the thermal effect of cool flame from the cool-flame affected ignition delay.

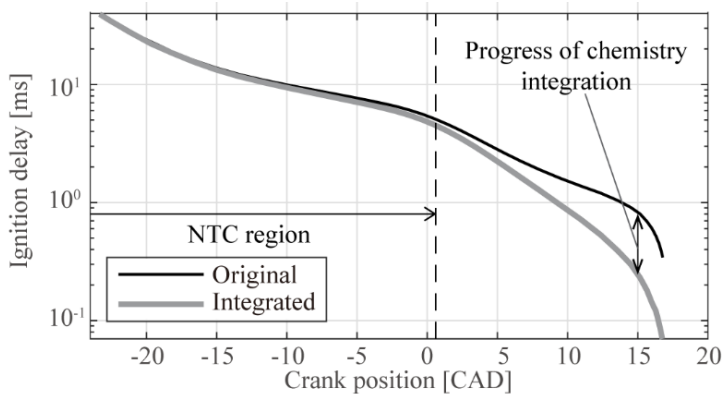

Figure 21. Original and integrated ignition delay trend along with corresponding thermodynamic states of the engine unburned gas history

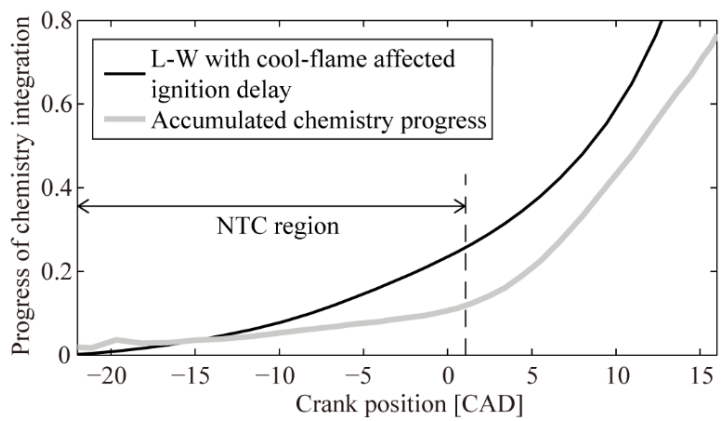

Figure 22. Livengood-Wu integration of cool-flame affected ignition delays and their accumulated chemistry

3.3.3 Reaction pathway of iso-octane oxidation in different temperature range

Basically, integration of cool flame chemistry would naturally affect the main autoignition point to the advancing direction when the unburned gas states continuously change and escape from the NTC region to enter the single stage ignition domain. In the meantime, major reaction pathway of iso-octane is also in transition thus the change in mixture composition by integrated chemistry is now governed by high temperature reaction scheme until autoignition. That means, reactive radicals in small quantity from accumulated low temperature chemistry before cool flame would contribute to chain propagation and branching of high temperature chemistry.

Detailed reaction mechanism study of iso-octane by Curran et al. [19] explains the different reaction pathway by temperature range as follows;

1. In higher temperature condition about T > 1000 K, initial fuel molecule is split into smaller alkyl radicals by unimolecular decomposition pathway which leads to faster chain propagation and branching as the radical product moles are bigger than the parent fuel. Some of fuel molecules would become a C_8 alkyl radical by H-abstraction, and those alkyl radicals also decompose to produce olefin (C_nH_{2n}) and additional smaller alkyl radicals by β-scission.

2. In low-to-intermediate temperature conditions, the governing reaction pathway is oxidation of C_8 alkyl radicals to produce alkylperoxy radicals, whose forward and reverse reaction characteristics are mentioned previously in Chapter 3.2.1. This leads to direct isomerization of alkylperoxy radicals to QOOH species where Q denotes olefinic species, followed by different pathways which includes the production of ·OH and HO_2 radicals as well as oxidation of QOOH and further progress to smaller

species. Within this reaction scheme, both ·OH and $\cdot HO_2$ are known as the most prevalent radicals at low and intermediate temperatures.

Simplified kinetic scheme for iso-octane oxidation is presented in Fig. 23.

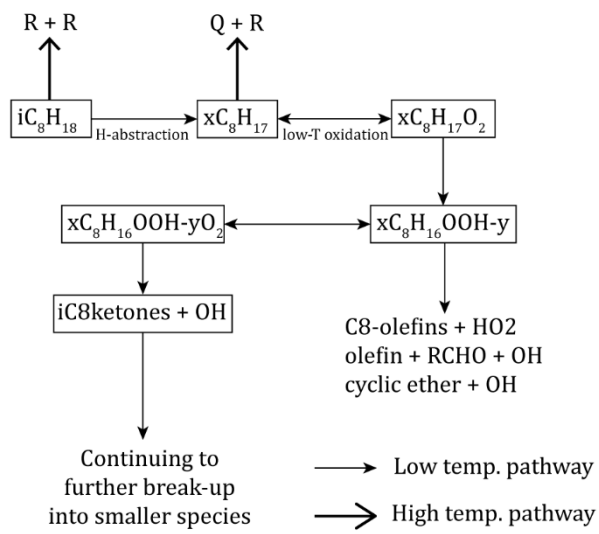

Figure 23. Simplified kinetic scheme of iso-octane oxidation for high and low temperature condition [19]

3.4 Cool flame elimination method

Constant volume reactor model results from Chapter 3.2 showed that sufficient time duration is a prerequisite for low temperature chemistry initiation and corresponding cool flame exhibition when initial thermodynamic states are relevant to the engine unburned gas history. However, it is against the unburned gas behavior as explained in Chapter 3.1.1 since the unburned gas history is changing much faster than the first stage ignition delay under the NTC region before any cool flame exothermicity is revealed. Also provided is the fact that integration of cool flame chemistry during the unburned gas history under the NTC region should affect the post-NTC, single stage autoignition by advancing the autoignition point. In accordance with above discussions and arguments, an alternative approach is proposed here which minimizes and finally eliminates the thermal contribution of cool flame in stimulating the overall reactivity.

3.4.1 Accuracy of Livengood-Wu integration for an exemplary non-NTC fuel

The accuracy of Livengood-Wu integration model for non-NTC fuels is already proved by numerous previous studies, for example hydrogen and methane fuels are investigated in [22]. In the same manner, ethanol is acknowledged as a non-NTC automotive fuel whose strong anti-knock behavior is also well-known [44, 45], thus Livengood-Wu integration for ethanol-fueled engine simulation is conducted and results are shown in Fig. 24 along with the iso-octane case. Terminating points of each curve indicate the autoignition point computed by engine simulation while the crank locations intercepting y-axis at y=1 are predicted knocking position by Livengood-Wu integral. It is clearly shown that there is an overestimation found in the predictive results which is caused by cool-flame affected ignition delays,

compared to the case of ethanol-fueled simulation as the knock predictability of Livengood-Wu integration is fairly acceptable.

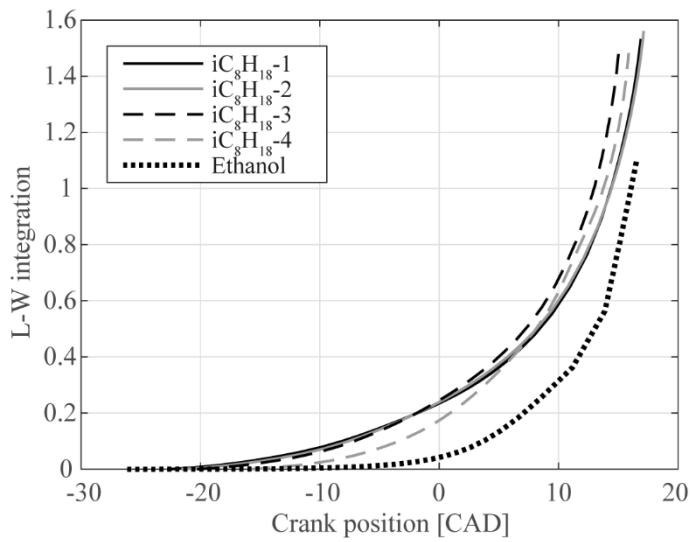

Figure 24. Livengood-Wu integration results for various iso-octane-fueled engine simulations along with ethanol-fueled case.

3.4.2 Cool flame elimination by modulating heat capacity of nitrogen

Cool-flame eliminated ignition delay is proposed to improve the knock predictability of Livengood-Wu integration model when handling NTC-exhibiting fuels. In detail, thermal contribution of cool flame is excluded by computational approach which stimulates consecutive reactions during the cool-flame period of two-stage ignition fuels, thereby only the chemical part remains and it seems more appropriate to the basis of Livengood-Wu model.

An apparent relationship between ΔP_{cf} and τ_{cf}, which are previously defined in Fig. 8, is established by modulating the heat capacity of nitrogen in different level and fitting into a quadratic correlation. Extrapolating ΔP_{cf} to zero leads to the ultimate location of $\tau_{cf,elmntd}$ assuming that cool flame is fully eliminated as pointed out in Fig. 25. Along with that, τ_{2nd} is evaluated with $P_{cf,end}$ and $T_{cf,end}$ by adopting Arrhenius behavior, in detail it may be expressed as

$$\tau_{2nd} = \mathrm{A} \cdot P_{cf,end}^{-n} \cdot \exp\left(\frac{B}{T_{cf,end}}\right) \qquad \text{(Eq. 3.2)}$$

while the coefficients A, n, and B are derived from the logarithmic linear combination of at least three sets of τ_{2nd}, $P_{cf,end}$, and $T_{cf,end}$ values acquired from computational results. Therefore, assuming that cool flame is fully eliminated, $P_{cf,end}$ and $T_{cf,end}$ are identical to the initial pressure and temperature at t = 0 and inserting into Eq. 3.2 gives the value $\tau_{2nd,elmntd}$, which is summed together with $\tau_{cf,elmntd}$ to obtain the cool-flame eliminated ignition delay of given initial condition. This replaces the cool-flame affected original ignition delay and applied to Livengood-Wu integration while the engine unburned gas history is under the NTC region but without any cool-flame appearance; it could be somewhat controversial to distinguish between the two-stage and single stage ignition region

clearly, thus in our calculation the criterion is that if there were no local minima of pressure rise rate until main autoignition, i.e. second derivative of pressure history is always positive, it is conceded a single stage ignition.

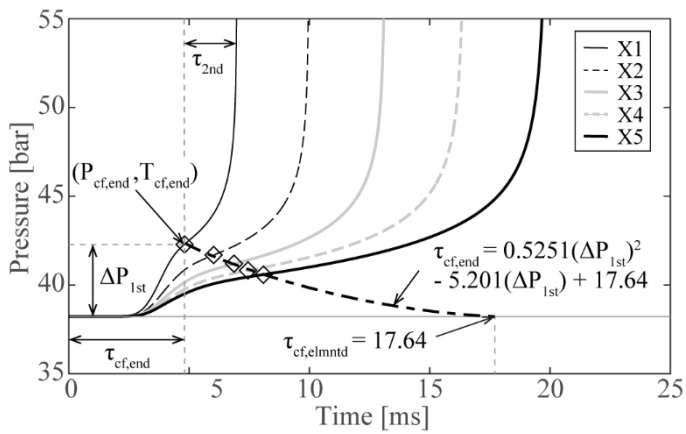

Figure 25. Extrapolation of heat capacity modulated computation results for cool-flame eliminated first stage ignition delay acquisition

3.4.3 Improvements to Livengood-Wu integration by cool flame elimination

Knock prediction results of Livengood-Wu integration by substituting cool-flame eliminated ignition delay for cool-flame affected one are presented in Fig. 26 which shows good agreement between the knocking positions from the engine simulation results and the predicted points by the integration model. Obviously, reciprocals of the cool-flame eliminated ignition delay contribute only to a limited extent from the integration perspective, leading to an improved autoignition prediction over all engine speed range computed.

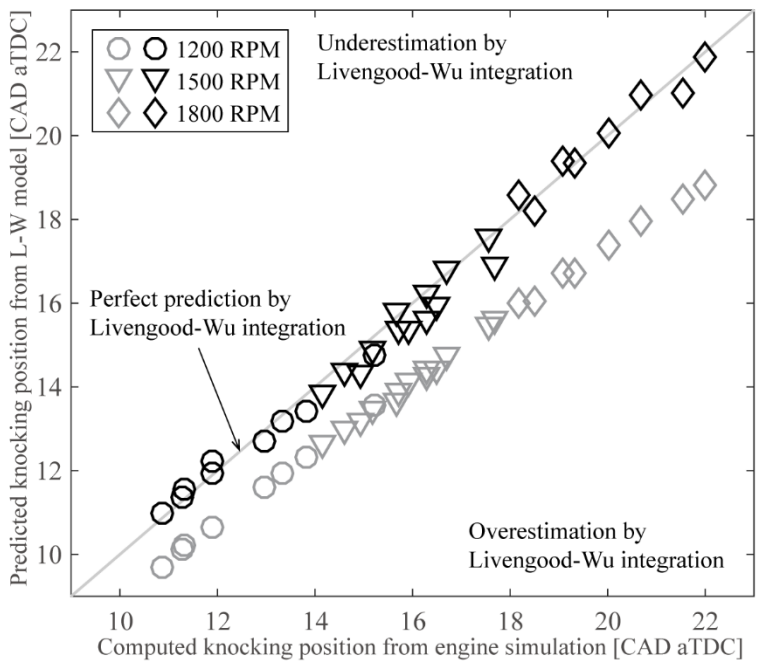

Figure 26. Autoignition point prediction with both cool-flame affected (gray) and eliminated (black) ignition delays

3.4.4 Validity of cool flame elimination method

Basic idea of Livengood-Wu integration model expects that when autoignition is about to occur, it reaches the critical concentration of a representative species by accumulated chemistry. In that context, ·OH radical is a reasonable choice based on its major role as a reaction chain carrier in oxidation chemistry of alkane fuels, regardless of temperature range. However, it is not directly applicable to the engine unburned gas profile with the time-·OH history from the constant volume reactor model, since Livengood-Wu model assumes a zeroth-order global reaction governing the autoignition chemistry which may disagree with a realistic combustion process of an arbitrary n-th order reaction. This discordance is recently resolved by Pan et al. [27] in which "averaged" reaction rate of any n-th order could be applicable instead of zeroth-order assumption to a certain extent, thus following validation is also admitted.

Molar concentration change rate of ·OH radical—d[·OH]/dt—is selected as an index of an instantaneous reactivity of a system, since any rate of progress of chemical reaction depends on the molar concentration of reactants and products from a net rate basis. Figure 27 presents the example of rate of [·OH] change derived from the constant volume reactor model under same initial condition, but different heat capacity of nitrogen. Area under each curve thus stands for the accumulated [·OH] quantity (in positive-y side) until the autoignition points of each case. Taking this into a zeroth-order reaction assumption results in mean [·OH] change rate as depicted in Fig. 28 where the hatched areas are identical to the corresponding colored area of Fig. 27.

Following this hypothesis, averaged [·OH] change rates along with the thermodynamic history of the engine unburned gas are acquirable and plotted together in Fig. 29 with the "real" d[·OH]/dt of the unburned gas which is derived

from the SI engine simulation result. It is obvious that the constant volume reactor model-derived values with original heat capacity of nitrogen, noted X1 in the figure, are inadequate to reflect the "chemical" reactivity of the unburned gas under the NTC region in engine situation. On the other hand, increasing the heat capacity of nitrogen and suppressing thermal contribution of the cool flame allows the averaged values to approach closer to the engine unburned gas situation, nonetheless there still remains orders of difference between the values. This strongly implies the possible good agreement between the cool-flame eliminated values and the engine-derived d[·OH]/dt curve, due to the fact that averaged [·OH] change rates decrease with longer overall ignition delay. Along with that, the discrepancy diminishes as the cool-flame exothermicity and corresponding NTC behavior weakens while the engine combustion proceeds and the thermodynamic states of the unburned gas changes continuously to the direction of post-NTC region.

The concept of mean [·OH] change rate as a representative of instantaneous chemical reactivity, i.e. d[·OH]/dt curve, becomes more convincing in higher temperature, single stage ignition region. Symbols which stand for a mean [·OH] change rate assuming 0^{th} order global reaction deserve to represent the instantaneous reactivity as their values are closely plotted to the curve until autoignition. Therefore, reciprocals of corresponding ignition delay within this single stage ignition region are adequate to play their role as a reactivity representative, in that Livengood-Wu integration model premises a critical concentration of the representative species at the autoignition moment.

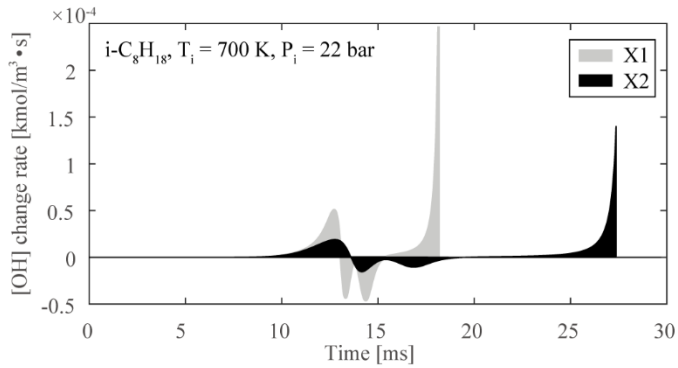

Figure 27. Instant [·OH] production or consumption rate from constant volume reactor for 700 K, 22 bar initial condition with different level of heat capacity modulation

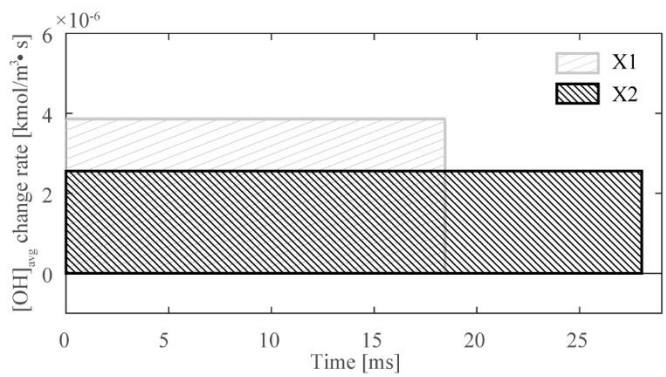

Figure 28. Mean [·OH] change rate of results from Fig. 27 by 0^{th}-order reaction assumption

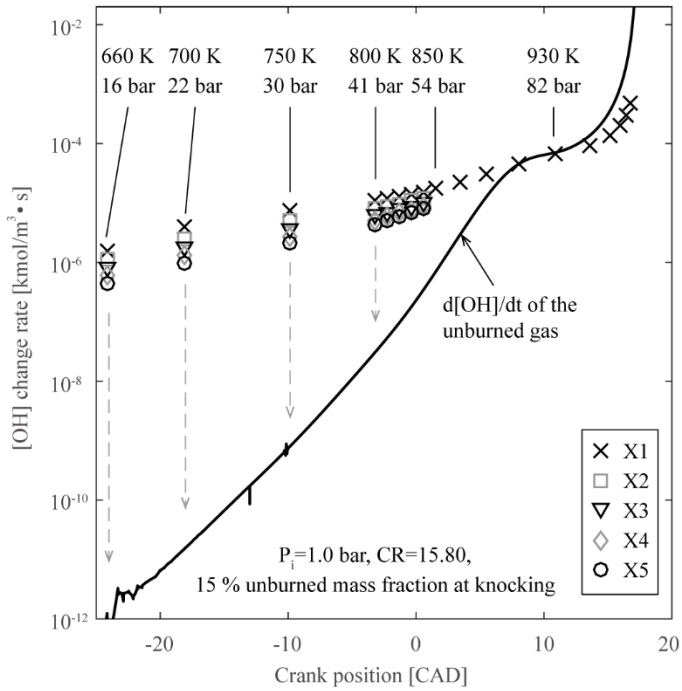

Figure 29. [·OH] change rates in engine unburned gas and 0th-order averaged constant volume reactor cases including heat capacity modulated results

3.4.5 Another method from the reaction mechanism perspective

An alternative method is also applicable to eliminate cool-flame exothermicity by modifying the reaction mechanism itself. For example, it is discussed in Chapters 3.2.1 and 3.3.2 that the major reaction pathway relevant to cool-flame exothermicity is the oxidation of alkyl radical. Hence, inhibiting these specific reactions by decreasing their reaction rates close to zero is also an alternative approach for eliminating the cool-flame behavior, and the example case is plotted in Fig. 30 where the overall behavior of newly derived ignition delay seems quite similar to the heat capacity modulation method. Modifying the reaction rate itself means that both the chemical and thermal aspects of cool-flame are eliminated, thus when compared to the heat capacity modulated calculations the contribution of composition change by the reaction chemistry is qualitatively measurable, which is expected as being shown with the difference between the heat capacity modulated curve and reaction rate modified one. It seems that the chemistry contribution is relatively small, however this could be critical in engine simulation process since modifying the major reaction pathway would not allow any reactive radicals be produced, implying that overall chemistry cannot be "triggered," considering that the order of reaction is usually non-zero, thus affected by reactant concentration. Therefore, it is not suggested if one desires to eliminate only the thermal contribution of cool flame but maintaining its own chemistry.

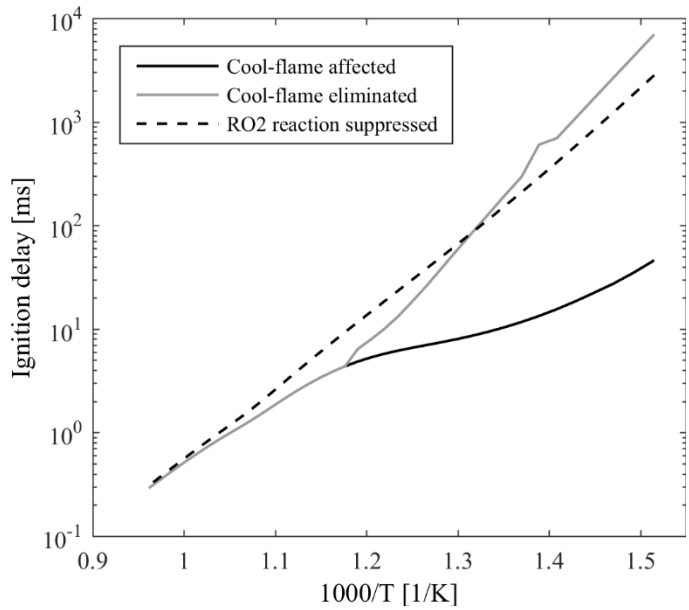

Figure 30. Projected ignition delay trends along the engine unburned gas history

Chapter 4. New ignition delay correlation

Until now, it has been discussed that cool-flame affected ignition delay is not suitable for representing the instant chemical reactivity of gas in most cases, regarding possible operating conditions expected in modern SI engines. It is also concluded that the thermal effect of cool flame, which stimulates overall reactivity of the mixture, needs to be excluded when accounting for the integration of chemistry progress in the NTC region without cool-flame appearance, thus autoignition predictability could be improved, at least for the specific test conditions conducted with the engine simulation. Now in this section, cool-flame elimination method is applied to the broad range of temperature and pressure conditions and evaluated to accommodate any thermodynamic history of mixture that is relevant to the NTC region without any cool-flame appearance.

4.1 Cool flame elimination by heat capacity modulation

First of all, cool-flame affected original ignition delay contours are depicted in Fig. 31 over the thermodynamic states relevant to the engine unburned gas history. Numbers on each contour line indicates the natural logarithmic ignition delays. Strong NTC behavior is found in lower temperature region around 700 K–800 K in low pressure and about 700–850 K in high pressure conditions, respectively. Compared to this, Fig. 32 presents the contours of cool-flame eliminated ignition delay derived from the same methodology explained in Chapter 3.4.2, in detail their values are extrapolated from the heat capacity modulation results within the NTC region while maintaining the original delays in the single stage ignition domain. It is shown that the distance between any two neighboring contour lines are closer in this

newly-derived, cool-flame eliminated region than the original ones, implying that the chemical reactivity of iso-octane without the thermal contribution of cool-flame decreases rapidly as temperature lowers. Therefore, when the thermodynamic history of any mixture including iso-octane sweeps over this region, the contribution of this integrated chemistry in autoignition phasing is considerably small by Livengood-Wu integration, which is also concluded from the comparison of original and integrated ignition delays in Chapter 3.3.

The difference between original and cool-flame eliminated ignition delay is graphically expressed in Fig. 33 which provides the degree of reactivity change by cool-flame elimination quantitatively within the NTC region. For example, it can be interpreted as follows; In Chapter 3.4.4 and Fig. 29 the relationship between mean and instantaneous reactivity was discussed by introducing the molar concentration change rate of ·OH radical in which the mean reactivity of cool-flame affected two-stage ignition was exaggerated than the "real" instantaneous reactivity of the unburned gas under the NTC region and the gap reduced while moving towards non-NTC region. Similar behavior is also found in Fig. 33 by following the unburned gas thermodynamic history along the contours and it is obvious that the ignition delay difference is continuously reducing towards non-NTC region and finally reaches zero.

Based on this result, Fig. 16 which gives the potential applicable boundary of cool-flame eliminated ignition delay model for autoignition prediction may be supported by Fig. 34 at which the boundary of non-zero difference between two ignition delays is drawn. Therefore, when the unburned gas history is acquirable and overlapped on Fig. 32, the boundary of non-zero difference may be referenced for use where cool-flame eliminated ignition delay allows more accurate autoignition prediction.

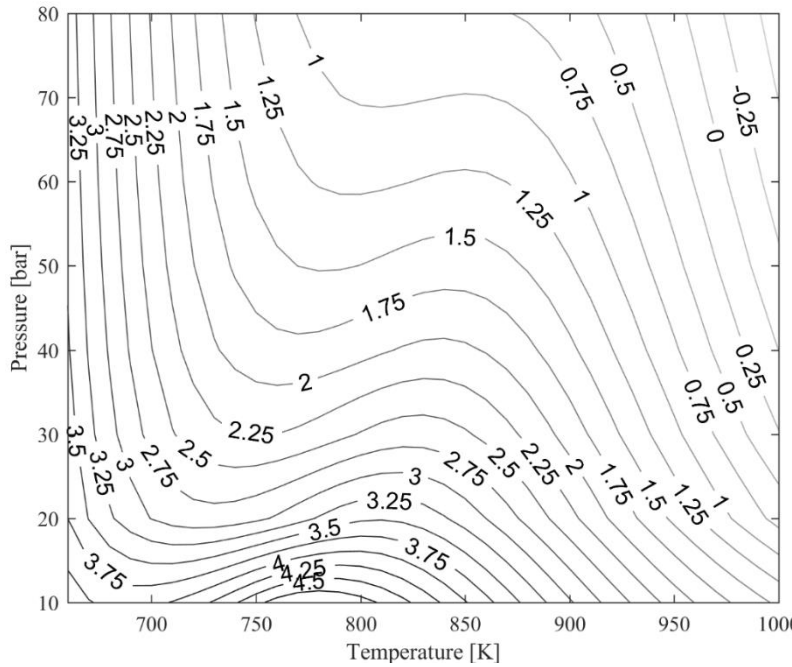

Figure 31. Cool-flame affected original ignition delay contours relevant to engine unburned gas history

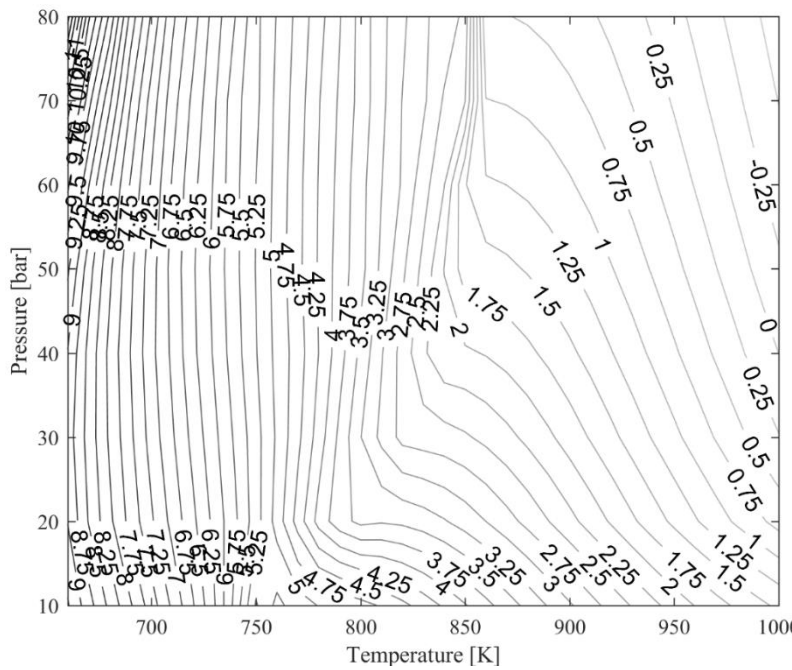

Figure 32. Cool-flame eliminated ignition delay contours by heat capacity modulation

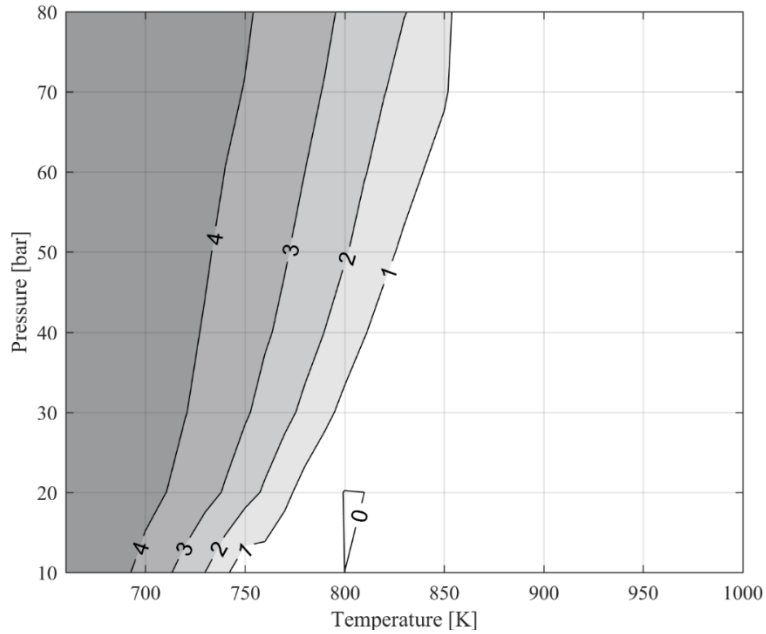

Figure 33. Difference between original and heat capacity modulated, cool-flame eliminated ignition delays on a natural logarithm basis

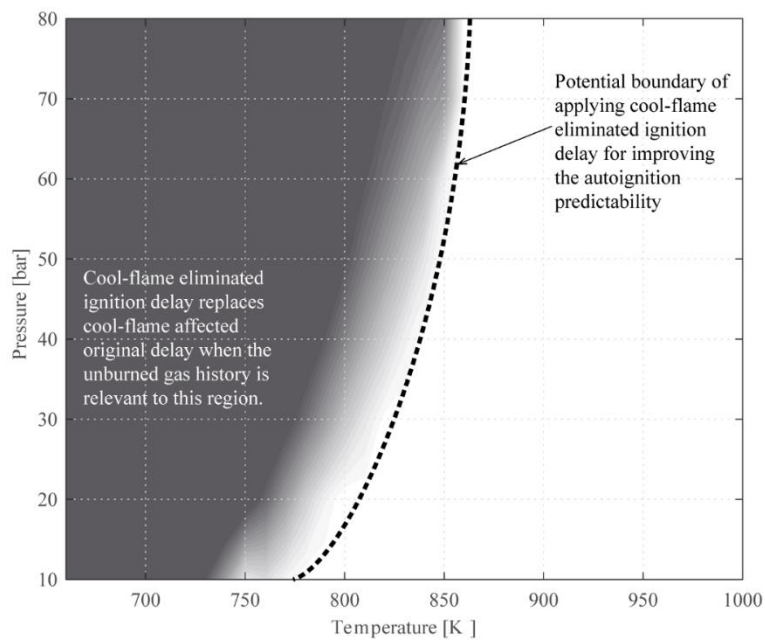

Figure 34. Application boundary of cool-flame eliminated ignition delay in modern SI engines

4.2 Chemical kinetic analysis of cool-flame eliminated ignition delay

4.2.1 Reaction pathway analysis

The reactivity change of cool-flame elimination by heat capacity modulation was discussed in Chapter 3.4.4 by introducing the rate of molar concentration change of a representative species, ·OH, as a reactivity index. It was concluded that the mean overall reactivity of cool-flame affected autoignition is considerably exaggerated when compared to the instantaneous reactivity of the engine unburned gas. In this part, the effect of cool flame elimination by suppressing temperature and pressure rise is analyzed with the reaction pathway change of cool-flame eliminated cases.

Reaction pathway analysis is widely applied in numerous fields of research, and in case of chemical kinetics study it is a powerful tool for visualizing the main reaction pathway with which the parent species should follow under given thermodynamic condition [46]. Both the instantaneous as well as time-integrated fluxes are generally used by one's own objectives and will be briefly explained here.

According to Androulakis et al. [47], the instantaneous chemical flux of atom A from species *j* to species *k* through reaction *i* is defined as

$$\dot{A}_{ijk} = q_i \frac{n_{A,j} n_{A,k}}{N_{A,i}} \qquad \text{(Eq. 4.6)}$$

where q_i is the net production rate of reaction *i*, $n_{A,j}$ is the number of A atoms in species *j*, $n_{A,k}$ is the number of A atoms in species *k*, and $N_{A,i}$ is the total number of atoms of element A in reaction *i*. Atomic fluxes through the reaction *i* is distributed between the different species of the reaction by Eq. 4.6. Thus, the total transferred amount of element mass A for any related species by their participation within all

reactions of the reaction mechanism regardless of reactants or products, with time *t*, is defined as

$$\bar{A}_{FROM,TO}(t) = \sum_{i=1}^{N_{rxns}} A_{i,FROM,TO}(t) \qquad \text{(Eq. 4.7)}$$

It is useful to look into the instantaneous reaction pathway of species at a given instant *t*, nevertheless it may be difficult to see the global information with this approach.

On the other hand, the time-integrated flux is established to provide helpful insights of reaction chemistry from a global point of view. In the same study, time-integrated flux is defined as

$$\hat{A}_{FROM,TO} = \frac{\int_{t=0}^{\tau} \bar{A}_{FROM,TO}(t)dt}{max \int_{t=0}^{\tau} \bar{A}_{FROM,TO}(t)dt} \qquad \text{(Eq. 4.8)}$$

as a normalized term. In this way, the entire reaction trajectory is taken into account for a given time span. It is also stated that this time-integrated flux approach is useful to "characterize the main transformations that take place during the reaction period. The analysis reveals key pathways in terms of source–sink relationships." [47] Based on the global point of view, reaction pathways of cool-flame affected original ignition and heat capacity modulated cases within the NTC region of engine-relevant conditions will be revisited in a subsequent section.

4.2.2 Reaction pathways of heat capacity modulated two-stage ignition

First of all, time-integrated reaction pathway of iso-octane from the initial state to the end of first ignition stage under selected conditions within the NTC region, i.e. τ_{cf} in Fig. 8, is derived and compared with the heat capacity modulated cases in

order to visualize the “chemical” effect of cool-flame elimination method qualitatively, in that any changes to the major reaction pathway could be detected if it happens.

For example, Fig. 35 presents the pathway flow of stoichiometric iso-octane in constant volume reactor under 700 K, 22 bar initial condition with heat capacity modulation level of X1, X3, and X5 cases until the end of first ignition stage, respectively. For simplicity, pathways possessing more than 1 % of total rate of progress are drawn only, in other words the cutoff threshold for visualization is 0.01, thus it avoids drawing all pathways of 874 species of the detailed reaction mechanism and making it too complexed to explore. As seen on the figure, it is obvious that the low temperature reaction channel of iso-octane oxidation is dominant regardless of the level of heat capacity modulation, implying that suppressing cool-flame exothermicity by heat capacity modulation hardly affects the main chemistry of fuel oxidation channel. Based on this, it is reasonable to conclude that the longer total ignition delay and reduced overall reactivity by heat capacity modulation in the two-stage ignition region is mostly caused by limiting the thermal contribution of cool flame while major chemistry is conserved. Therefore, this thermal effect of cool-flame exothermicity must be excluded from integrating the chemistry progress of two-stage ignition fuels, especially when there were no cool-flame related exothermicity found while the thermodynamic history of mixture being overlapped on its NTC-exhibiting region, just like the unburned gas histories of iso-octane-fueled SI engine.

Along with that, reaction pathways of two other heat capacity modulation cases than X1 show the propagation of carbon oxidation channel until CO, which is just ahead of the final combustion product—CO2—being appeared. Because of relatively longer time span until the end of first stage ignition in modulated situation, some

portion of carbon atom reaches its almost-final stage of combustion process, nonetheless both [CO] and the rate of progress of elementary reactions producing CO are almost negligible whose values are near the projection threshold.

Rate of progress of major reactions are also compared in Fig. 36 to support previous statement that the limited degree of temperature increment of cool-flame exothermicity by heat capacity modulation is responsible for the reduced reactivity, in that the rates are decreasing against the heat capacity modulation. Therefore, the physical meaning of cool flame elimination method is proved that it is an effective way of handling only the chemical reactivity of two-stage ignition fuels within the NTC region when necessary.

Additional reaction pathway analyses for 750 K, 30 bar and 800 K, 41 bar initial condition are also shown in Figs. 37–40. All cases show similar trend of maintaining the major reaction pathway with reduced overall rate of progress by heat capacity modulation when their thermodynamic states are under the influence of NTC region of iso-octane.

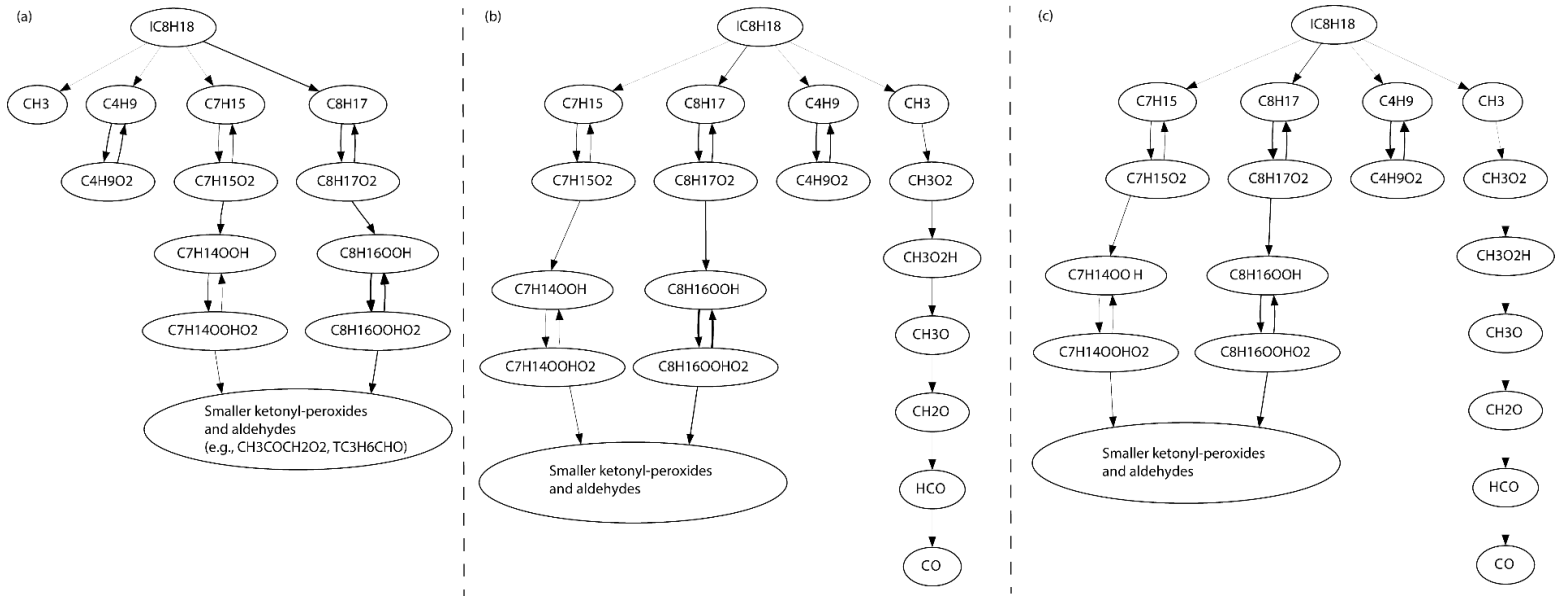

Figure 35. Major reaction pathways of stoichiometric iso-octane oxidation process in 700 K, 22 bar condition by degree of heat capacity modulation, in which (a) original heat capacity of nitrogen maintained, (b) tripled, and (c) quintupled

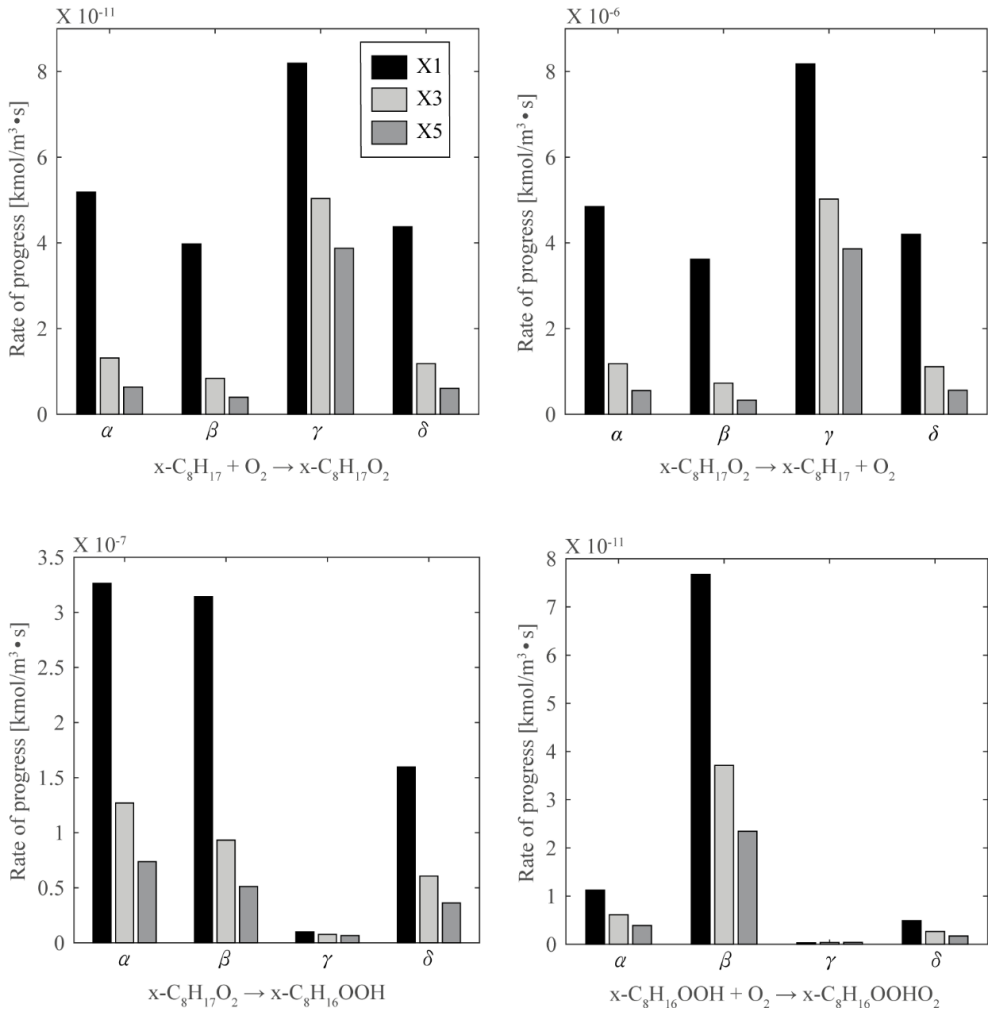

Figure 36. Rate of progress of selected elementary reactions from the major reaction pathway shown in Fig. 35 at 700 K, 22 bar condition.

α, β, γ, and δ signs denote the radical site of iso-octane molecule.

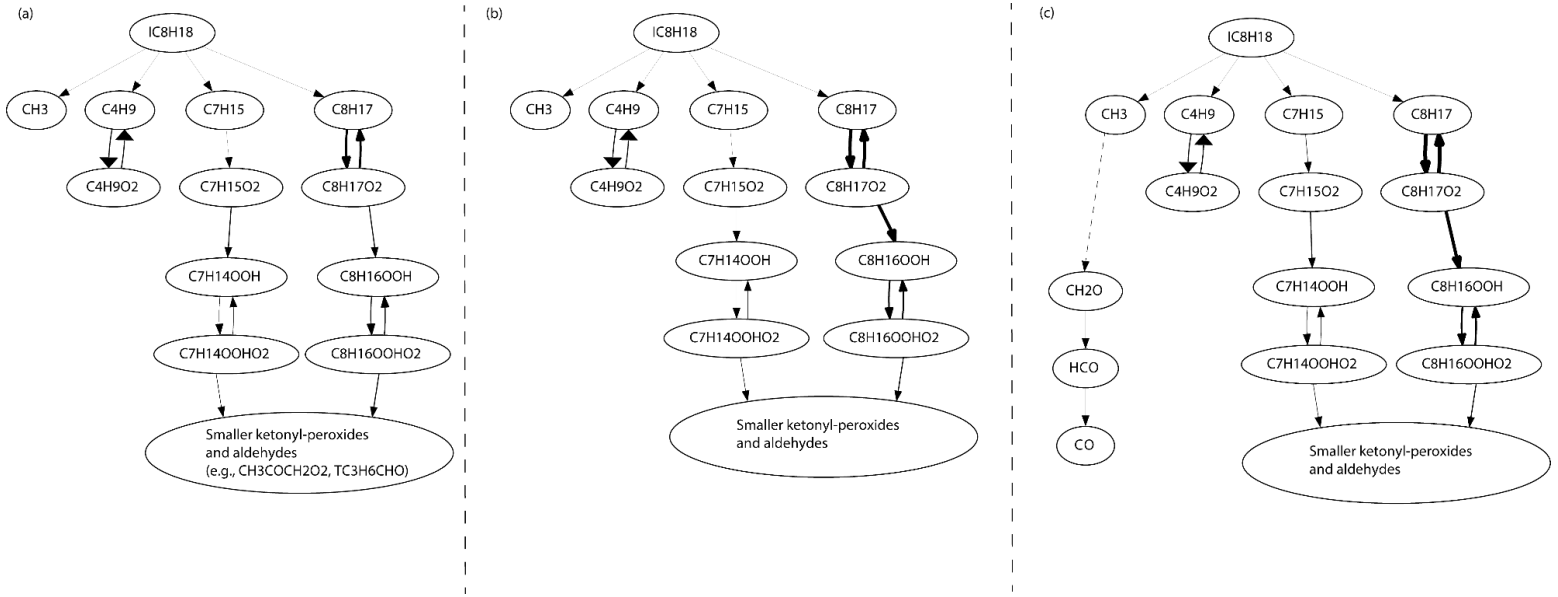

Figure 37. Major reaction pathways of stoichiometric iso-octane oxidation process in 750 K, 30 bar condition by degree of heat capacity modulation, in which (a) original heat capacity of nitrogen maintained, (b) tripled, and (c) quintupled

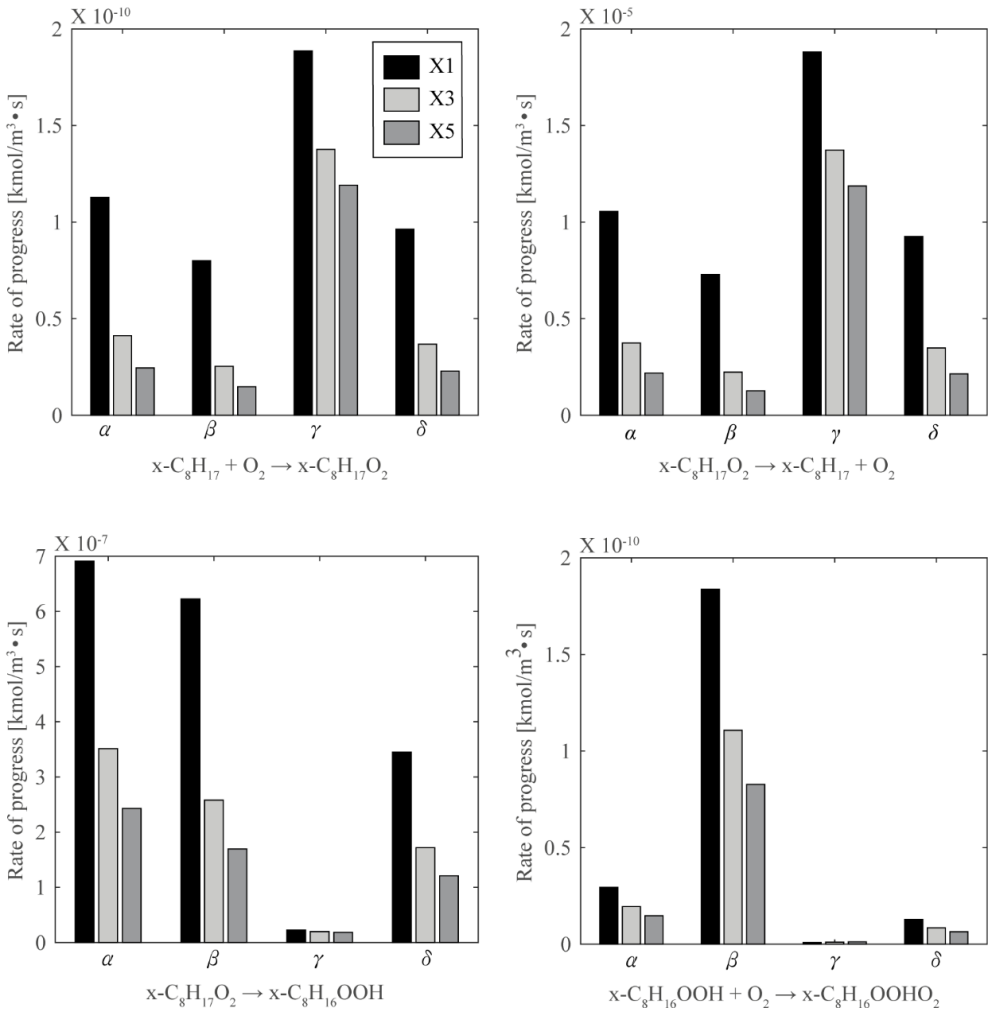

Figure 38. Rate of progress of selected elementary reactions from the major reaction pathway shown in Fig. 37 at 750 K, 30 bar condition

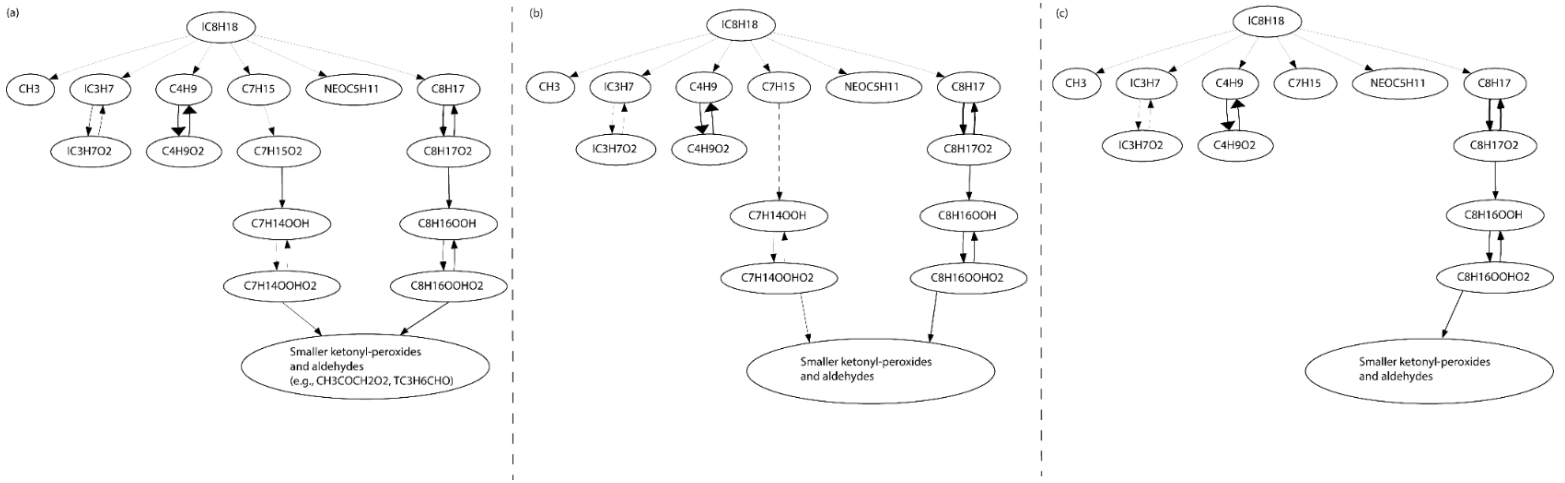

Figure 39. Major reaction pathways of stoichiometric iso-octane oxidation process in 800 K, 41 bar condition by degree of heat capacity modulation, in which (a) original heat capacity of nitrogen maintained, (b) tripled, and (c) quintupled

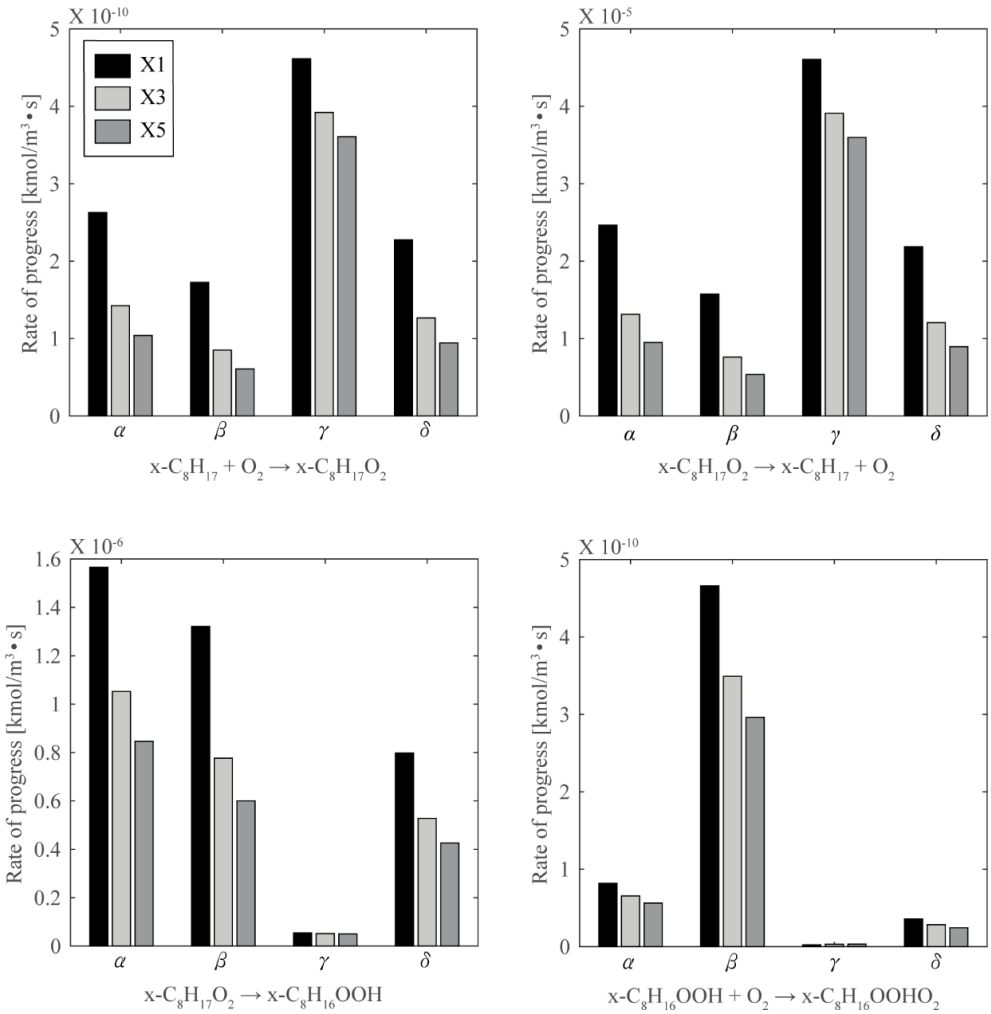

Figure 40. Rate of progress of selected elementary reactions from the major reaction pathway shown in Fig. 39 at 800 K, 41 bar condition

4.3 Cool flame elimination by empirical correlation

In this part, cool-flame eliminated ignition delay is empirically derived from the simulation results which assumes the Livengood-Wu integration output of 1 being reached at the autoignition point. Number of thermodynamic histories of reacting mixture must be provided in order to derive correlation factors by statistical approach, hence an RCM is selected to model the dynamic situation—in-cylinder gas pressure and temperature continuously increasing by the compressing motion of piston—of same iso-octane-air mixture which passes through the NTC region without cool flame appearance until autoignition point. Thermodynamic behavior of test gas from the initial state to the autoignition point shows some similarity to that of an engine unburned gas with continuously increasing temperature and pressure history.

4.3.1 RCM modeling details

RCM is a well-known test device which measures the ignition delay of reactant under high temperature and pressure conditions induced from fast compressing motion of the piston. Usually, it takes about 10–50 ms of time for the compression stroke to reach the “target” condition, i.e. temperature and pressure at the end of compression, and from that point the system is considered a constant volume reactor until autoignition and ignition delay is measured.

In this study, the test chamber is in cylindrical shape with bore and stroke of 63 and 90 mm each, and the reactant state is considered homogeneous and adiabatic within the chamber as of constant volume reactor model in Chapter 2.2. Compressing piston

moves on constant speed from initial to final location for 30 ms. Figure 41 provides the brief test procedure of RCM experiments.

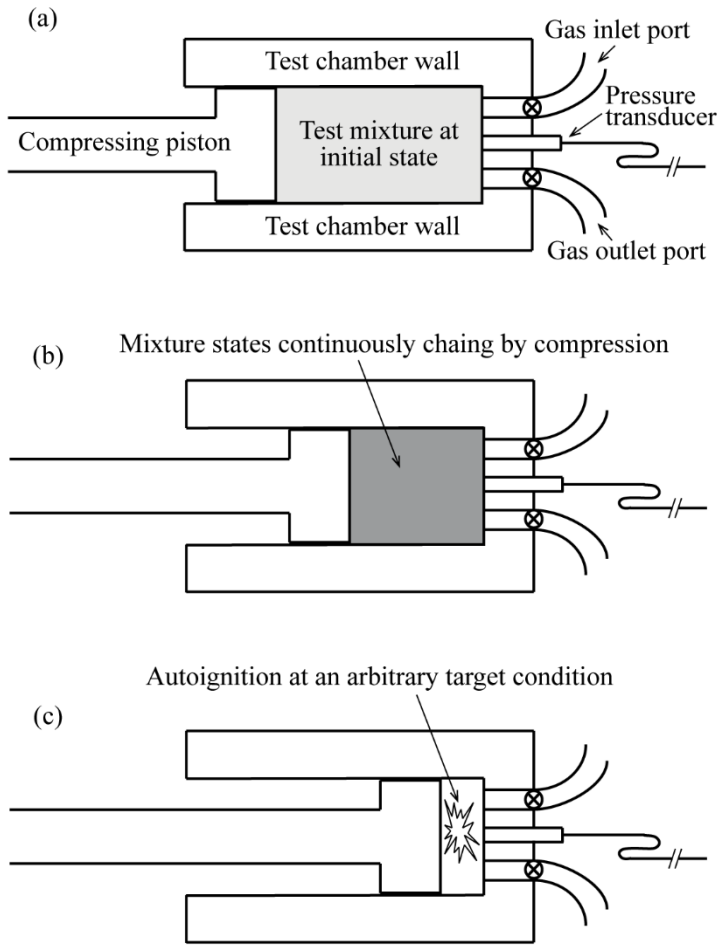

Figure 41. Examples of RCM test procedure. (a) Start of compression at initial state, (b) test mixture being compressed by piston motion, and (c) autoignition at an arbitrary condition

4.3.2 Thermodynamic history of reactant in RCM

The compression history of RCM test is usually neglected when evaluating the ignition delay at the target condition in most cases, since its contribution in advancing the autoignition phase is comparably small, especially within the NTC region as shown in Figs. 21 and 22 for example. However, the integrated chemistry along with the compression history can't be neglected anymore if the target condition is well beyond the NTC-affected region to self-ignite by single stage ignition behavior. Fig. 21 depicts the difference between original and integrated delay growth in high temperature region, implying that adequate evaluation of the integration effect must be considered.

In addition to that, autoignition could take place even before the end of compression stroke, provided that reaction chemistry is sufficiently progressed to change the reactant mixture composition as well as the temperature and pressure condition reaches the critical state during the RCM compression period. In this case ignition delay cannot be measured or evaluated, nevertheless the thermodynamic history of reactant mixture until autoignition point is interpreted to predict autoignition. From this point, it is expected that the Livengood-Wu-based integration value reaches unity for all RCM simulation results with autoignition prior to the end of compression stroke, thus an empirical correlation of ignition delay is derived while cool flame is eliminated and not observed during the NTC region of thermodynamic history of reactant mixture.

Figure 42 shows number of pressure-temperature histories obtained from the RCM simulation whose autoignition point is ahead of the end of piston compression stroke. These histories are closely located to the engine unburned gas profiles which are expected in turbocharged SI engine situation from the engine simulation, in order to

evaluate the empirical coefficients to the correlation formula for cool-flame eliminated ignition delay, which will be discussed in next subsection.

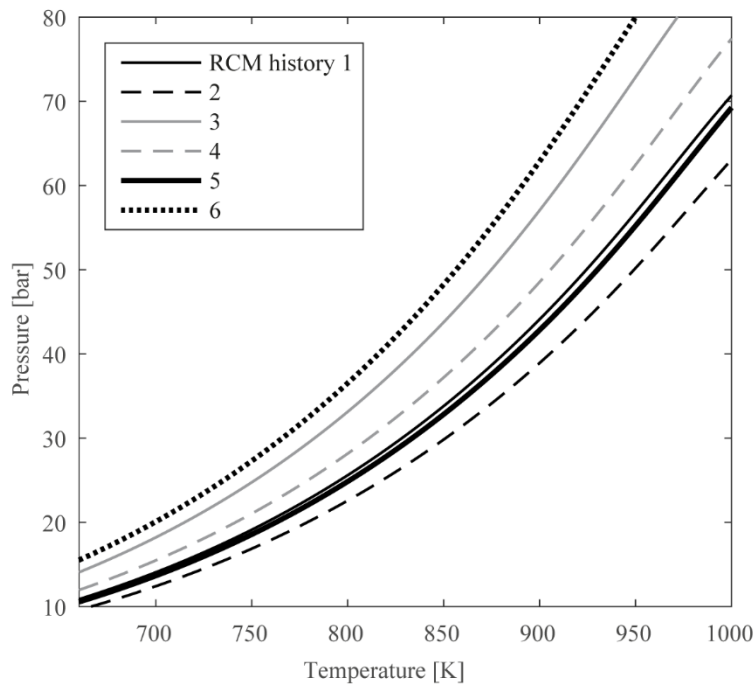

Figure 42. Pressure-temperature histories from the RCM simulation

4.3.3 Empirical correlation by Livengood-Wu integration

Empirical correlation of cool-flame eliminated ignition delay is expressed in similar form as Eq. 3.2, in detail

$$\tau_{cor} = A_{cor} \cdot p^{-n_{cor}} \cdot \exp\left(\frac{B_{cor}}{T}\right) \qquad \text{(Eq. 4.1)}$$

with coverage of all temperature and pressure region relevant to the engine unburned gas history as plotted in Figs. 9 and 31. Here, pressure and temperature history of reactant mixture is acquired from model computation results in Chapter 4.2.2, thus all three coefficients—A_{cor}, n_{cor}, and B_{cor}—need to be determined.

Integration of reciprocals of the ignition delay is transformed into a discrete summation equation for calculation. First of all, it is clear that the definite integral is approximated as

$$\int_{t_i}^{t_e} \frac{1}{\tau} dt = \sum_{i=1}^{m} \frac{1}{\tau} \Delta t \qquad \text{(Eq. 4.2)}$$

if the finite time step Δt is small enough and the integrand is discretized into sufficient number of elements. The right side of Eq. 4.2 is called Riemann sum after the German mathematician Bernhard Riemann. If we adopt the assumption of Livengood-Wu integral and inserting Eq. 4.1 into Eq. 4.2 it becomes

$$\sum_{i=1}^{m} \frac{1}{\tau} \Delta t = \sum_{i=1}^{m} \left(\frac{1}{A_{cor}} \cdot p_i^{n_{cor}} \cdot \exp\left(-\frac{B_{cor}}{T_i}\right) \right) \Delta t = 1 \qquad \text{(Eq. 4.3)}$$

and with some manipulation, it gives

$$\sum_{i=1}^{m} \left(p_i^{n_{cor}} \cdot \exp\left(-\frac{B_{cor}}{T_i}\right) \right) \Delta t = A_{cor} \qquad \text{(Eq. 4.4)}$$

Hence, with the pressure and temperature history from the initial state to the autoignition point along with the known simulation time step of 1 μs, A_{cor} is obtained and dependent on pressure and temperature coefficients n_{cor} and B_{cor}, respectively. Sweeping both coefficients from zero to a reasonable upper limit for N number of different thermodynamic histories of the reactant mixture leads to different A_{cor} calculated for each history. Now, the set of (n_{cor}, B_{cor}) must be determined to maintain the standard deviation of A_{cor} within acceptable error boundary, which is computed by

$$S_c = \sqrt{\frac{1}{N-1}\left(\sum_{i=1}^{N}\left(\frac{A_{cor,i}}{\bar{A}_{cor}} - 1\right)^2\right)} \qquad \text{(Eq. 4.5)}$$

where S_c is the corrected sample standard deviation of this N tests, where N-1 is used instead of N to cancel out the bias in the variance.

Contour lines of iso-S_c is drawn on n_{cor} and B_{cor} axes to search for the smallest value as presented in Fig. 43, and the coefficient set is found to be $n_{cor} = 1.2$ and $B_{cor} = 15400$ while maintaining $S_c \leq 0.02$, hence Livengood-Wu integration of those thermodynamic profiles from RCM simulation results are 1±0.02 in most cases and not bigger than 0.03 for few outliers.

Figures 44 depicts the cool-flame eliminated ignition delay contours by empirical correlation for same temperature and pressure range of the heat capacity modulated case for comparison. Along with that, Fig. 45 shows the difference between cool-flame affected original ignition delay and correlated delay with cool-flame eliminated case. Their overall trend looks quite similar to that of Fig. 33, which was for the kinetics-based cool-flame eliminated ignition delays.

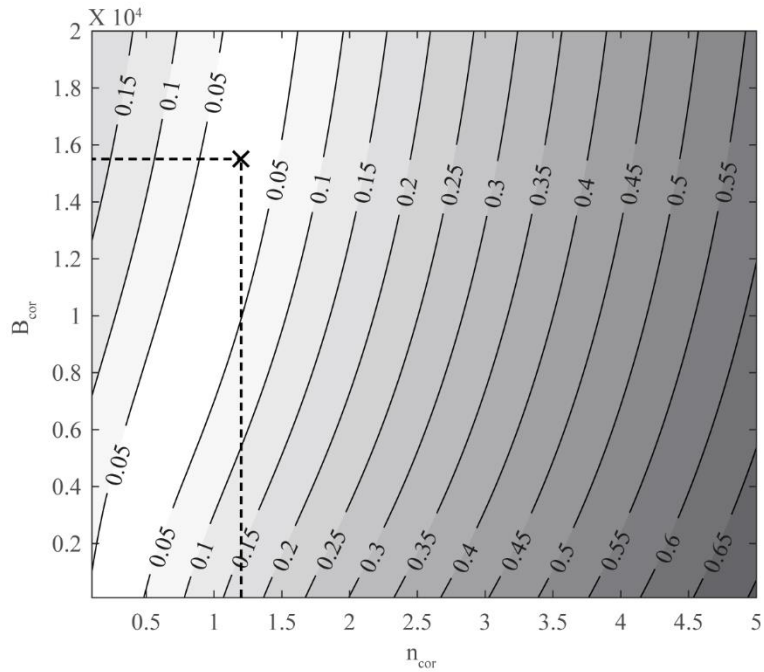

Figure 43. Contour lines of corrected sample standard deviation of RCM simulation histories for pressure and temperature empirical coefficients, assuming Livengood-Wu integration of 1 at the autoignition point

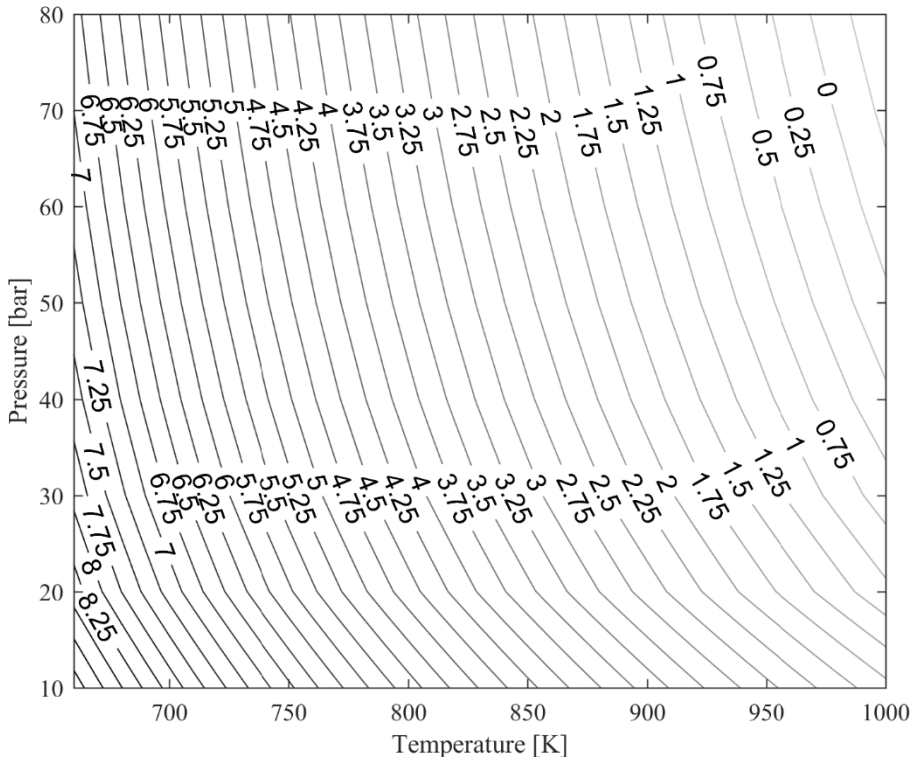

Figure 44. Cool-flame eliminated ignition delay contours by empirical correlation

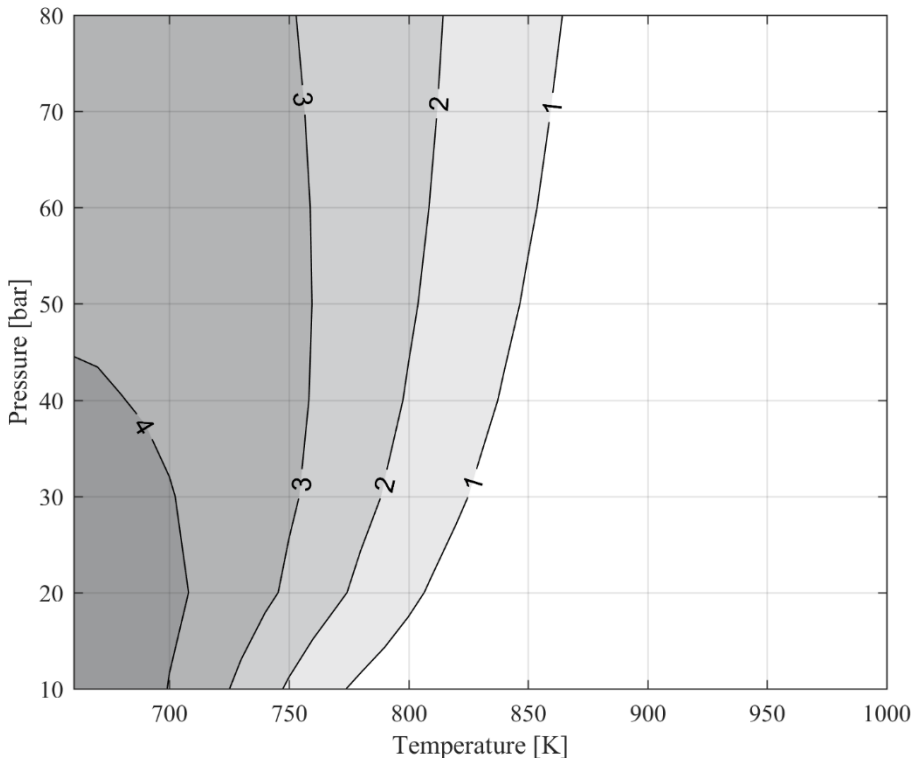

Figure 45. Difference between original and empirically correlated, cool-flame eliminated ignition delays

4.4 Comparison of kinetics-based and correlated ignition delays

4.4.1 Traditional ignition delay curves

From Chapters 4.1 and 4.3, two respective cool-flame eliminated ignition delays are obtained with each method, and their results are presented together with cool-flame affected original ignition delay curves in Fig. 46 for selected pressure conditions. Generally, the trend of both cool-flame eliminated ignition delay on every pressure condition look similar in their slope (i.e., activation energy) as well as absolute numbers within the lower temperature NTC region. However, there is some difference in ignition delays over the temperature and pressure range, however not larger than an order of magnitude, especially where the kinetics-based curves merge into the original ignition delay near the intermediate-to-high temperature region while NTC behavior diminishes. This is due to some questionable points of extrapolation near the NTC boundary where the cool-flame exothermicity and the second-stage delay are almost indistinguishable by explicit approach, thus it deteriorates robustness of extrapolated outputs.

It is previously mentioned that the difference between cool-flame eliminated ignition delays and original cool-flame affected delay, both for the kinetics-based and correlated situation, respectively, are similar to each other. Hence, it is worth plotting the contours of difference between two independent cool-flame eliminated ignition delay for direct comparison, which are presented in Fig. 47. The outputs of these two approach are almost identical in most of the temperature-pressure field, where the variance tends to become larger than an order of magnitude for only limited region. Therefore, cool-flame eliminated ignition delay by any of both methods deserves its role to predict autoignition of NTC-exhibiting fuels without cool-flame exothermicity revelation during their thermodynamic history.

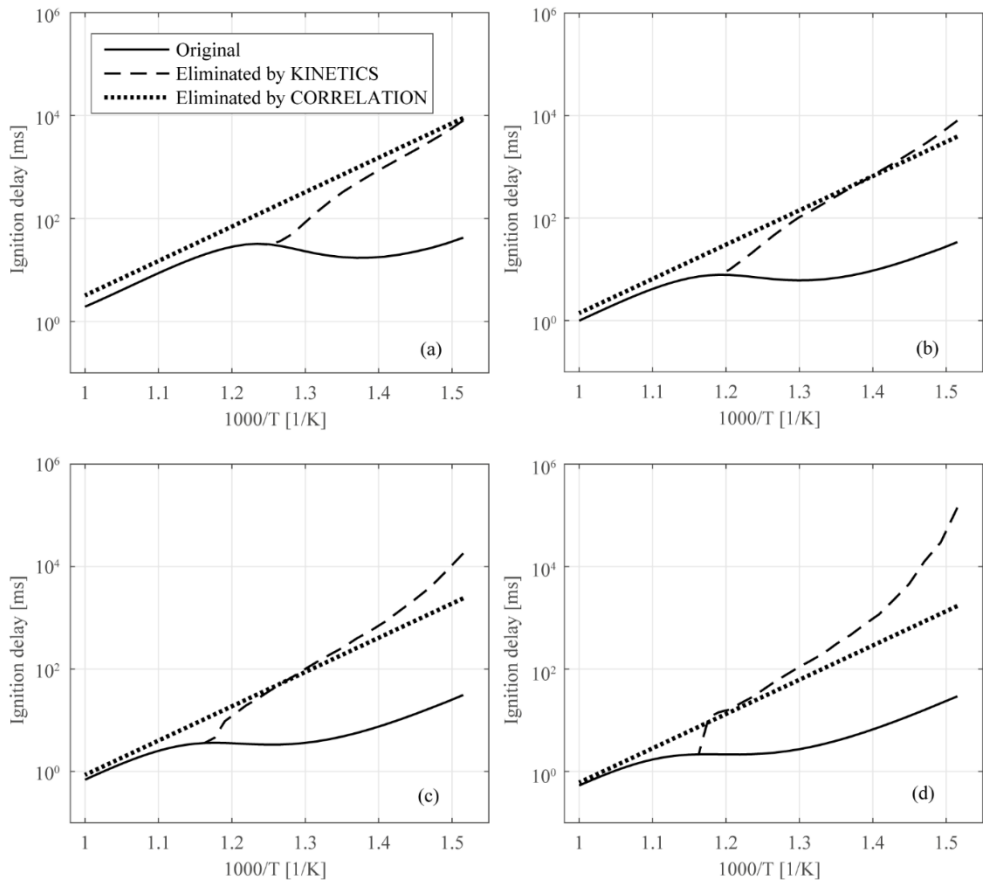

Figure 46. Cool-flame affected original ignition delays and their elimination by kinetics-based, heat capacity modulated ones and empirically correlated values for (a) 20 bar, (b) 40 bar, (c) 60 bar, and (d) 80 bar constant pressure conditions

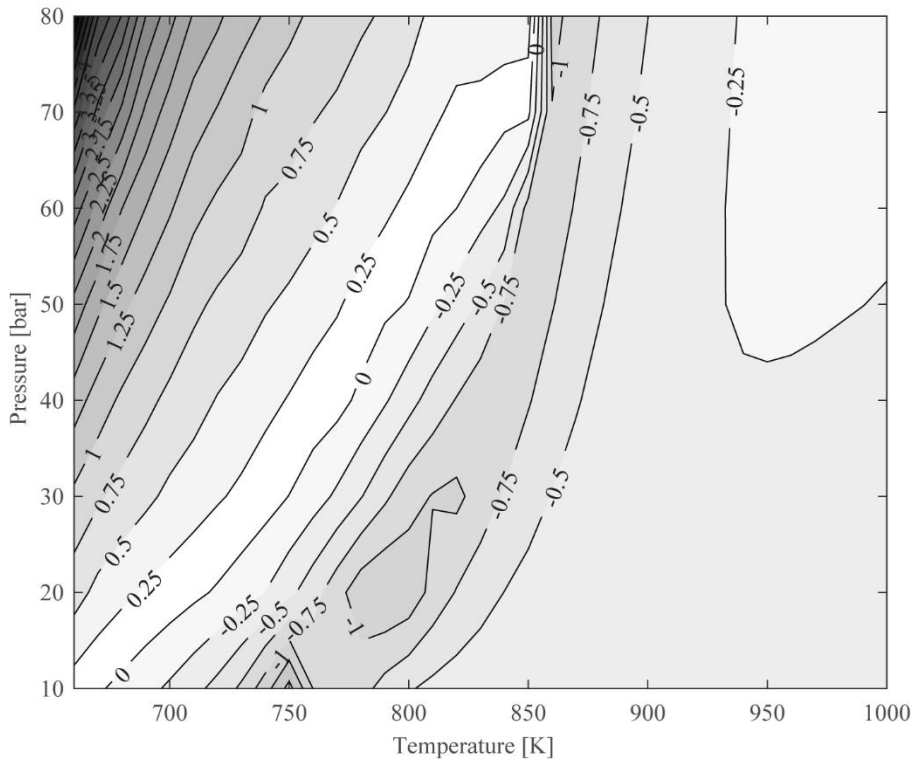

Figure 47. Difference of cool-flame eliminated ignition delays by two independent methods

4.4.2 Livengood-Wu integration by each ignition delay

In Chapter 3.4.3, improvements to the Livengood-Wu prediction of autoignition point was presented by replacing the cool-flame affected original delays with the cool-flame eliminated delays by heat capacity modulation while the unburned gas history is overlapped on the NTC region of fuel, and fairly acceptable predictability was reached. Along with that, derivation of cool-flame eliminated ignition delay by empirical correlation of RCM simulation profiles is proposed and their outputs are compared to the kinetics-based, heat capacity modulated delays in previous section and showed good agreement.

However, certain degree of difference between them are also observed over the NTC-exhibiting conditions, especially at the "transition region" where the cool-flame eliminated ignition delays merge into the original, single stage ignition curves, nevertheless their discrepancy limited to an order of magnitude. Hence, it is interesting to discover the contribution of this discordance in the autoignition predictability by Livengood-Wu integration.

Figure 48 depicts the autoignition prediction of Livengood-Wu integration with cool-flame eliminated ignition delays by heat capacity modulation in which the values are identical to the results from Fig. 26. Linear regression R^2 is also calculated and noted in the figure, showing good agreement. Along with that, the same Livengood-Wu integration with cool-flame eliminated ignition delays, but this time with empirically correlated values derived from the RCM simulation results and their Arrhenius coefficients in Chapter 4.3.3, are plotted in Fig. 49. It is clearly shown that the accuracy of autoignition prediction in the engine simulation results is also excellent with empirically correlated ignition delays, while the base thermodynamic histories for correlation are not from the engine simulation results. In addition to that, the

discrepancy between two separately derived ignition delays seem to affect only little to the prediction results from the Livengood-Wu integration perspective, since their reciprocals within the NTC region are too small to reveal any meaningful difference.

Putting all these investigations together, it suggests that the well-designed computation and experiments with other facilities than the engine itself, e.g. an RCM, can be helpful to draw a universal surface of ignition delay for knock prediction of two-stage ignition fuels without cool-flame appearance during their thermodynamic history.

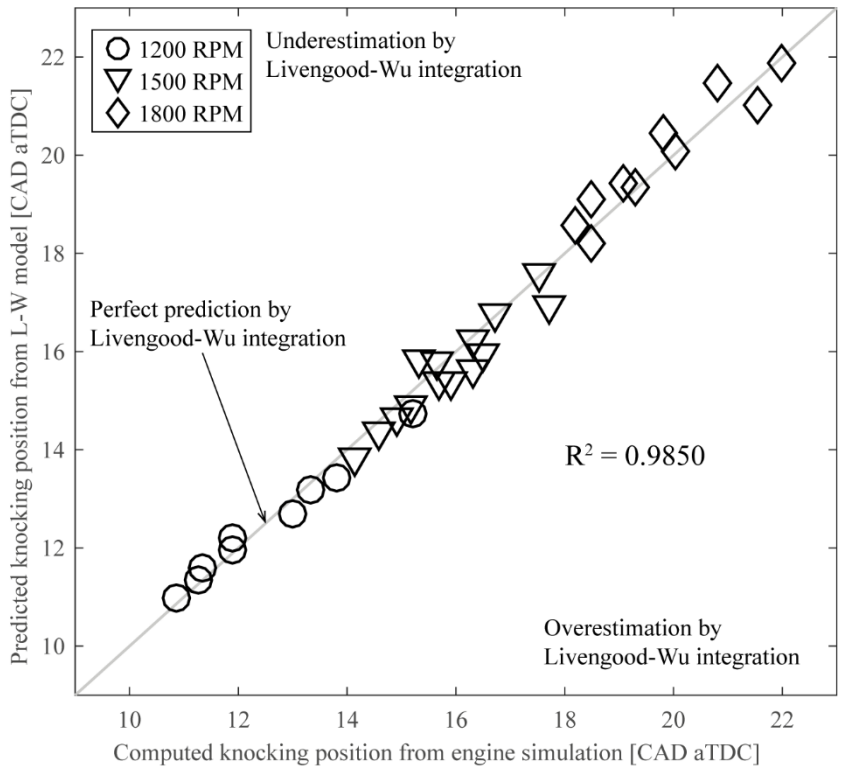

Figure 48. Autoignition point prediction with cool-flame eliminated ignition delays computed by heat capacity modulation

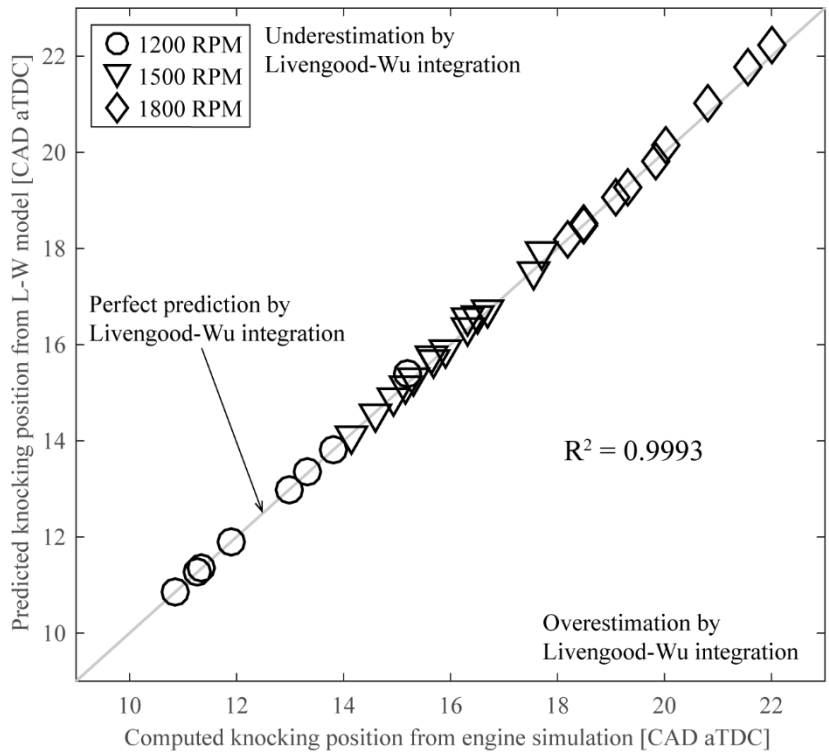

Figure 49. Autoignition prediction with cool-flame eliminated ignition delays derived from empirical correlation

Chapter 5. Experimental validation

5.1 Designing appropriate experiment for validation

Until now, it has been discussed and proved that the thermodynamic history of the unburned gas in an arbitrary SI engine would affect the autoignition phenomena by integrating its instantaneous chemical reactivity without the thermal contribution of cool flame along that corresponding history, when the fuel has two-stage ignition characteristics but relevant cool-flame exothermicity didn't occur until the autoignition point. In addition to that, a correlated ignition delay surface based on RCM simulation is also derived and applied to the engine simulation results to show that this cool-flame eliminated ignition delay is more appropriate to predict the autoignition point in aforementioned cases. Therefore, experiments can be designed to show the applicability of cool-flame eliminated ignition delay in autoignition point prediction.

Thermodynamic history of test mixture in an RCM is similar to that of an engine unburned gas in that the time span along the NTC region of fuels in their respective thermodynamic history is usually within 4–5 ms in knock-prone operating condition, thus it is not likely to observe any cool-flame relevant exothermicity during the compression stroke of an RCM test as well as in engine situations within the extent. Considering this similarity, RCM experiments are conducted to reproduce certain unburned gas history from an engine and the results are interpreted.

5.2 RCM characteristics

5.2.1 Test procedure

A schematic diagram of hydraulically-driven RCM operation is previously depicted in Chapter 4.3.1 with Fig. 41 whose detailed test procedure is as follows:

(a) A separate, cylindrical pre-mixing chamber whose volume is 12.3 L is utilized to prepare the test mixture. First, the chamber is evenly heated on the wall side by an electrical heater until the temperature of in-cylinder residual reaches 60℃, followed by evacuating with a vacuum pump. In-cylinder state is 60±3℃ and less than 0.003 bar at its steady state.

(b) Test mixture is prepared according to partial pressure measurement of every substance, e.g. nitrogen, oxygen, and iso-octane which is feasible with the help of absolute pressure sensor. Usually iso-octane is in liquid phase at room temperature, thus the amount of liquid iso-octane is decided by assuming gas phase iso-octane at 60ºC and converting with equation of state. Using its density value as well as temperature, so the pressure of the gas phase iso-octane is derived. Then the decided amount of iso-octane, which should not exceed its vapor pressure at 60 ºC, is injected into the heated and evacuated chamber by a thread-connection laboratory syringe to secure vacuum during injection, followed by nitrogen and oxygen feeding. After all substances are provided, then the stirring fan is turned on and let the mixture stay at least 15 minutes and be well-mixed before conducting experiment to insure homogeneity of the test gas.

(c) The test chamber is preheated by electric wall heaters surrounding the chamber and submerged within the chamber walls. Due to the experimental

restrictions, there is no thermocouple or similar sensor equipped to measure the in-cylinder temperature directly, however if adiabatic core assumption is accepted, the initial temperature at the beginning of the compression stroke is only necessary for evaluating the temperature history during the compression. Therefore, the correlation between the wall heater temperature and the in-cylinder temperature is calibrated to characterize the temperature distribution inside the chamber, and by measuring five different points in the chamber it is found that the maximum temperature variance is also a function of wall heater temperature and not exceeding 4 K when preheated up to 120ºC. Calibration curve is provided in Fig. 50 while error bars indicate the maximum temperature difference by location in the test chamber. It leads to the maximum post-compression temperature difference of 7 K in experimented temperature range.

(d) Working fluid is pressurized by a centrifugal pump and charged into a main accumulator until the fluid pressure reaches 80 kgf/cm^2, followed by charging the other side of the driving piston at 110 kgf/cm^2 in order to pull the piston back to the "loaded" position in which the piston is located at the farthest from the fully compressed position.

(e) Piston is held at position while the inside of the test chamber is also evacuated before filling with the test gas. Absolute pressure measurement makes it possible to determine the amount of test mixture to be charged as an "initial condition," along with the preheated temperature of the test chamber and known volume at the loaded position of the piston as well. Both intake and exhaust ports are connected to a valve driven by pneumatic force, and after charging is complete then the valve is closed to let the in-cylinder become a closed system.

(f) Hydraulic components, e.g. solenoid valves, check valves, and hoses, are designed to connect between one another in a such way that sudden hydraulic pressure unbalance is intended by discharging the opposite side of the hydraulic piston, which is at 110 kgf/cm^2 as described in procedure (d), by opening the circuit to an atmospheric pressure all of a sudden. This induces the "pushing force" from the accumulator at 80 kgf/cm^2 so that the hydraulic piston is accelerated and travels forward until designated stroke ends, and collides with remaining hydraulic oil in opposite side of the piston to a sudden stop. Hydraulic circuit diagram is presented in Fig. 51. Compressing speed is adjustable between 15 to 40 ms by gradually blocking the fluid passage between the accumulator and the driving piston. Compared to the engine time scale, this compressing speed range is approximately equivalent to 700–2000 RPM of contemporary SI engines.

A full systematic diagram is also shown in Fig. 52 for clarity.

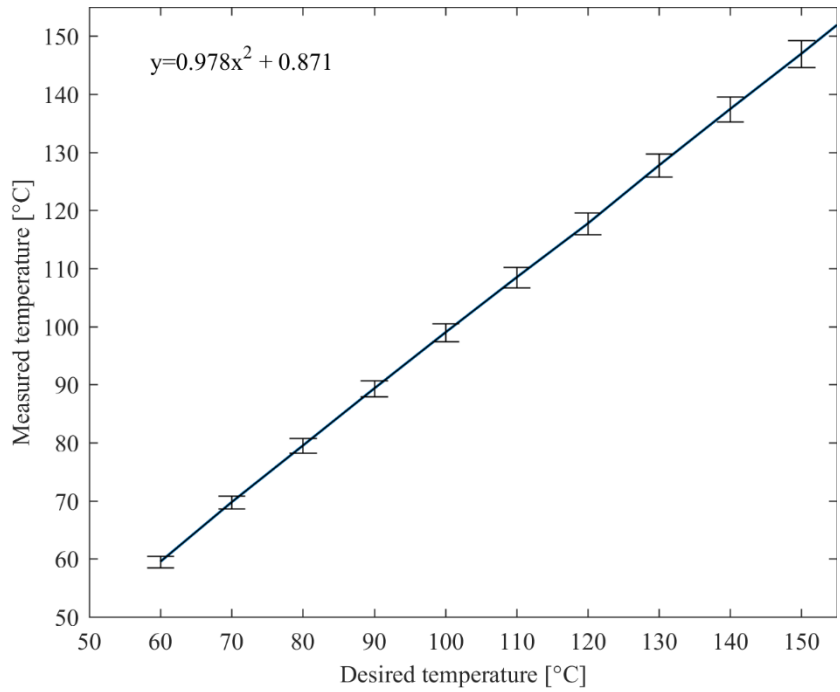

Figure 50. Temperature calibration curve between the desired and measured values.

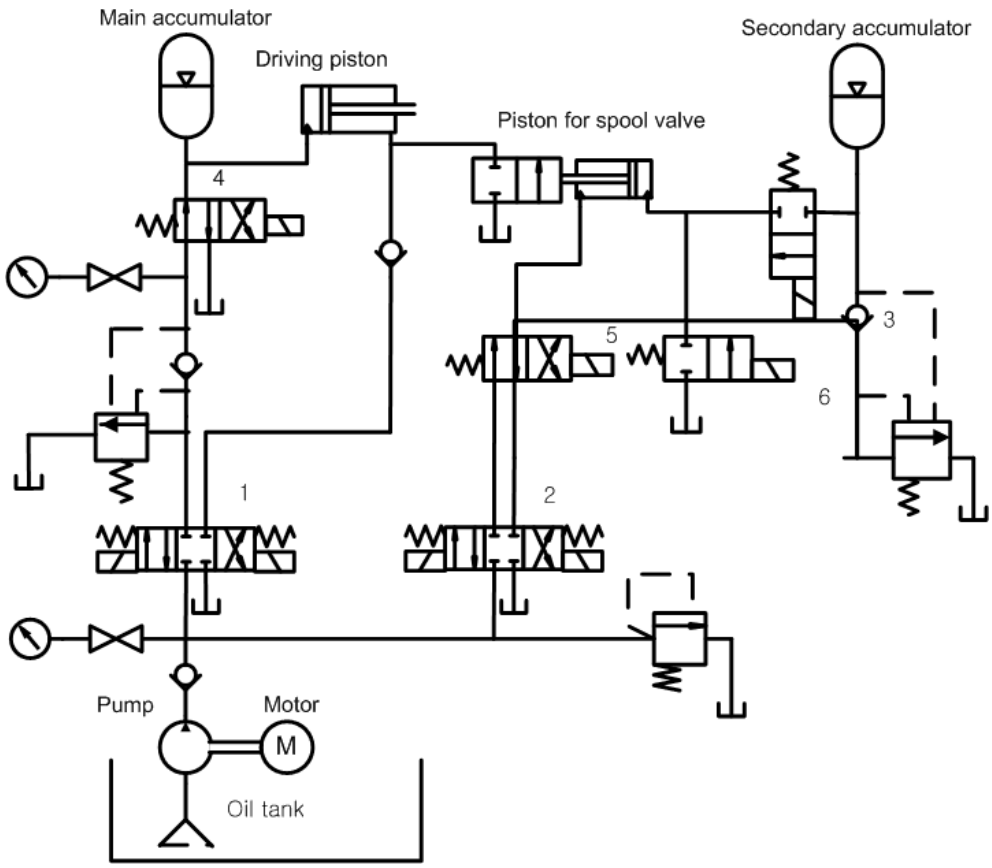

Figure 51. Hydraulic circuit diagram of RCM [48]

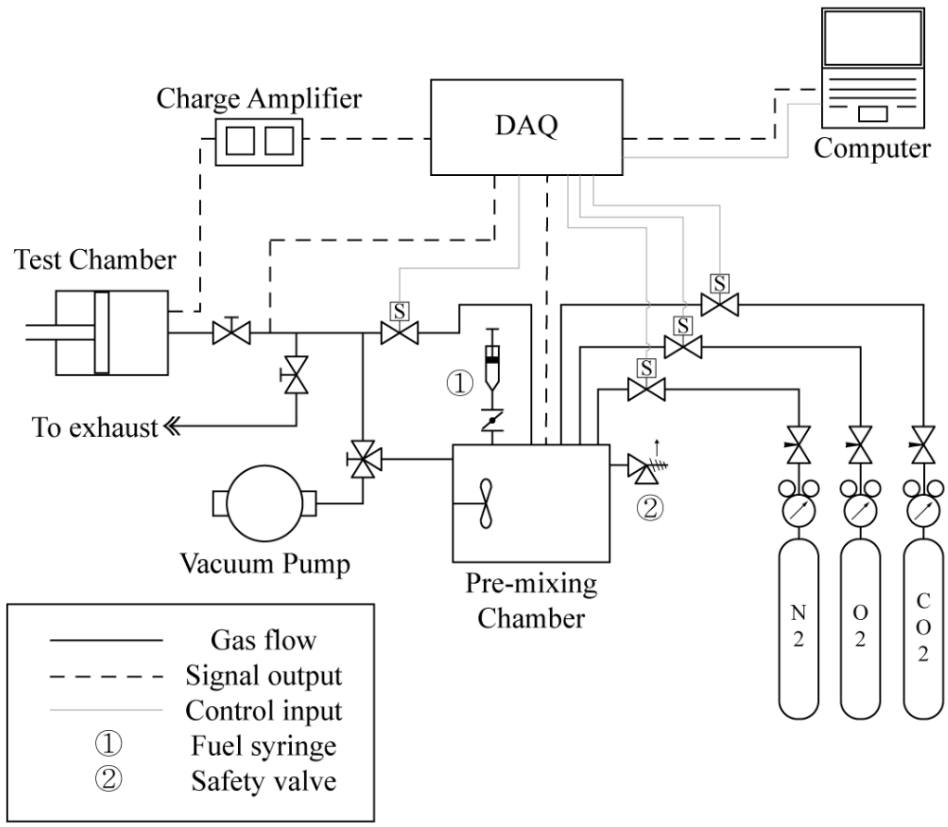

Figure 52. A full systematic diagram

5.2.2 Data processing

In-cylinder pressure history during the experiment is logged by Kistler type 6052C31 piezoelectric pressure transducer and a charge amplifier, then transmitted to National Instruments NI-USB6218 data acquisition unit as a voltage input signal. Data is recorded at a frequency of 10 kHz, i.e. the time resolution is 0.1 ms.

Temperature history is also evaluated by assuming adiabatic core behavior which has been preferably adopted by numerous studies [49–51] where the creviced piston design [52, 53] is used to inhibit corner vortices and relevant non-uniformity of temperature field during the compression stroke. From basic thermodynamics, it is obvious that the relationship between pressure and temperature of the isentropic process is

$$\int_{T_0}^{T_c} \frac{1}{\gamma - 1} d(lnT) = \ln\left(\frac{V_c}{V_o}\right) \qquad \text{(Eq. 5.1)}$$

$$\int_{T_0}^{T_c} \frac{\gamma}{\gamma - 1} d(lnT) = \ln\left(\frac{P_c}{P_0}\right) \qquad \text{(Eq. 5.2)}$$

where Greek letter γ stands for the ratio of constant volume and constant pressure specific heats, c_p/c_v of a mixture without composition change. It can be therefore computed by knowing the specific heat ratio, nevertheless it should be noted that the specific heat ratio is a function of temperature in real situation. That means, from the initial state and following every time step, exact specific heat ratio at corresponding temperature is needed in order to evaluate temperature history properly. This has been done by assuming that over a narrow temperature range, specific heat ratio can be approximated to a constant value, thus it is useful when preparing a lookup table of specific heat ratio of the mixture by Cantera toolbox depending on temperature

and applying them to update the next temperature consistently at every time step, which is expressed as

$$T_{i+1} = T_i\left(\frac{P_{i+1}}{P_i}\right)^{\frac{\gamma(T_i)-1}{\gamma(T_i)}} \quad \text{(Eq. 5.3)}$$

For example, specific heat ratio of stoichiometric iso-octane/air mixture along with temperature is depicted in Fig. 53. Hence, pressure-temperature profile during the RCM experiment is acquired with every test. Uncertainties in temperature history are expected from small non-uniformity of temperature near the test chamber walls or differences in specific heat ratio by composition change due to reaction chemistry progress, however the degree of composition change shall be relatively negligible if cool flame exothermicity were not observed until the autoignition point.

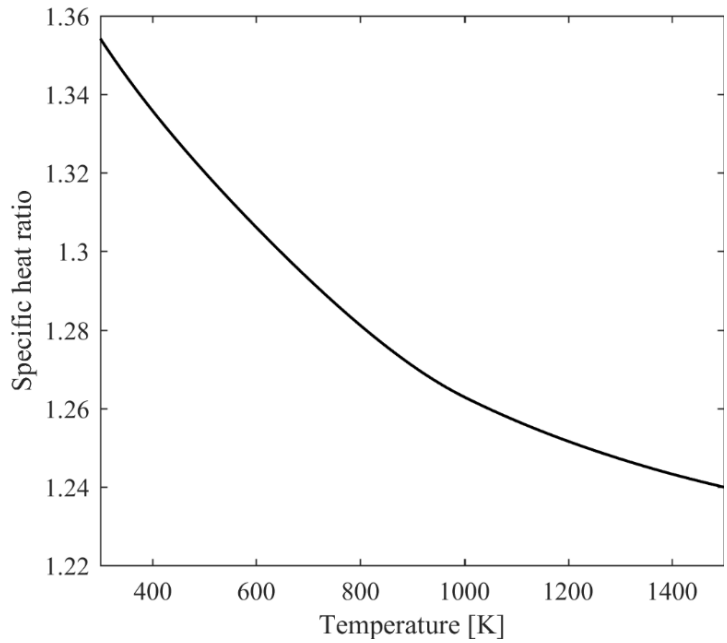

Figure 53. Specific heat ratio curve of stoichiometric iso-octane/air mixture

5.3 Experimental results and analysis

5.3.1 Target test conditions along with the purpose of this study

Computational results from Chapter 4.3.2 concluded that the thermodynamic history of reactant from RCM experiment could be similar if initial conditions and compressing time are correctly controlled. Basic thought throughout this idea is that, if thermodynamic state of reactant is changing towards severer direction as that of the engine unburned gas, autoignition could take place prior to the end of compression stroke of an RCM test. Therefore, experimental conditions are appropriately designed in order to induce autoignition before the compression stroke ends, but there are some limitations.

First of all, preheated temperature and corresponding initial temperature of the mixture thereof cannot exceed ca. 120℃ because of permanent materials damage to the O-rings which are placed in between metal-to-metal surfaces such as test chamber and chamber head, and valve seat and valve. In addition to that, expected mixture pressure at any point during the compression stroke must be kept lower than the hydraulic driving pressure, i.e. 80 kgf/cm^2, to secure the one-way motion of the piston. Also, peak pressure at autoignition is directly related to the safety issue as well as pressure transducer reliability, hence compression ratio should be adjusted properly not to allow too small volume at the autoignition point.

Considering all above experimental limitations, the ultimate target condition at which autoignition occurs is at most 950 K and not exceeding 80 bar. Computational results from an ideal constant volume reactor tells that the “original” ignition delay at this condition would be 1.16 ms, however what we obtain from an RCM experiment is actually an “integrated” one. In other words, measured ignition delay at this condition shall be reduced than the original value and it is likely that we won’t

possibly measure that small value of ignition delay at the harsh target condition. Instead, autoignition would occur at almost right after this condition has reached or even before the end of compression, if compressing speed was slower and more time was allowed for chemistry integration.

Repeated test results from RCM experiment are depicted by symbols on Fig. 54 covering the wide range of temperature and pressure. Thermodynamic histories with diamond symbols indicate that the operating condition is closer to the naturally aspirated situation, i.e. wide open throttle without intake charge boost, while circles stand for boosted engine run where the major regime shifts to a lower temperature and higher pressure domain. From the results it is concluded that RCM experiment is an effective way to validate the cool-flame elimination model as the thermodynamic history is also overlapped on part of the NTC region of iso-octane, including boosted conditions.

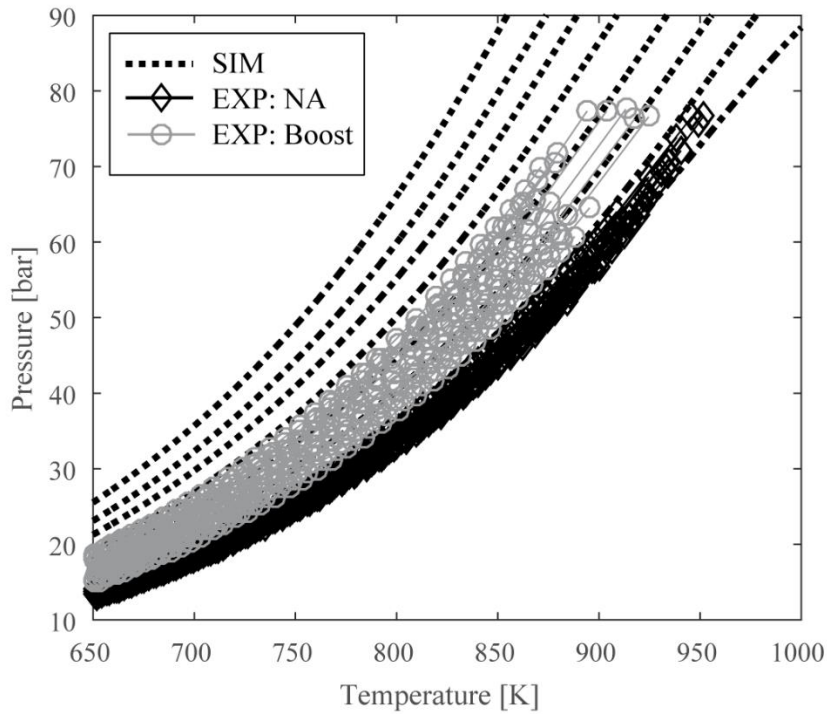

Figure 54. Temperature-pressure history from RCM experiments.

5.3.2 Result from repeated experiments and deriving correlation

Experimental results plotted in Fig. 54 are analyzed with the same methodology as described in Chapter 4.3.3 to derive an empirical correlation of ignition delay by plotting a contour surface of corrected standard deviation and determining two coefficients, i.e. pressure coefficient n_{cor} and temperature coefficient B_{cor}, respectively. Figure 55 depicts the minimum value of standard deviation to be 0.029 when both empirical coefficients are 1.6 and 1500, however it is suggested here to pick the temperature coefficient as large as possible within the acceptable standard deviation range. Since the temperature coefficient B_{cor} is in close relationship with the activation energy term of reaction rate expression, and considering that the chemistry progress within the NTC region before cool-flame revelation is found to be comparably small, this corresponds better to Livengood-Wu model by accounting for the appropriate contribution of higher temperature, single stage ignition region to the autoignition phenomena as well as limiting the thermal effect of cool-flame not to be included in autoignition prediction of two-stage ignition fuels. Well-known ignition delay correlation of Douaud and Eyzat [25] allowed ±0.06 of standard deviation in their discussion, thus same value is also accepted here for data processing and suggested coefficients are found to be 0.7 for pressure and 6500 for temperature, respectively. Cool-flame eliminated ignition delay by experimental evaluation is provided in Fig. 56.

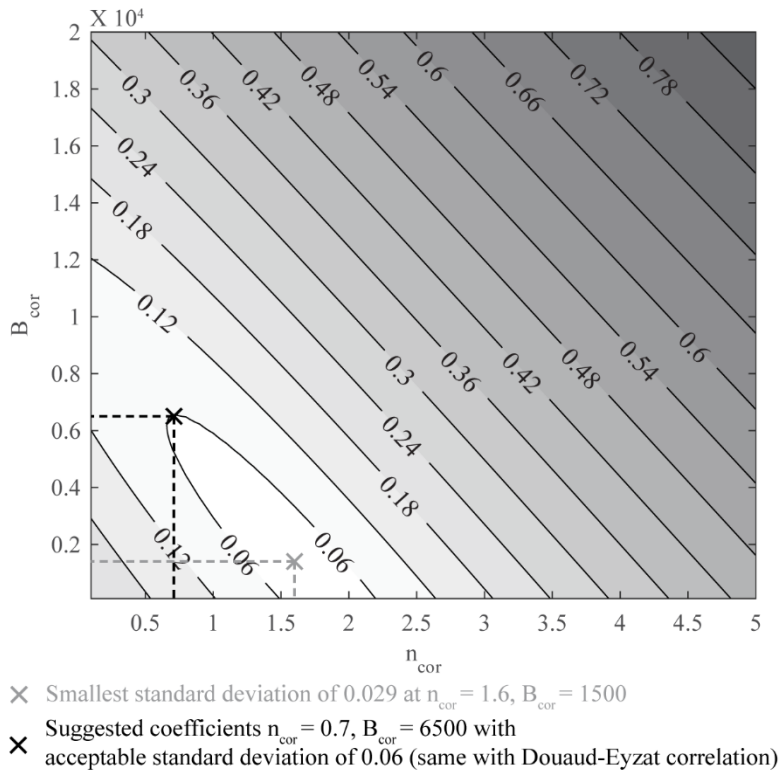

Figure 55. Contour lines of corrected sample standard deviation of RCM experimental results with empirical coefficients as both axes, assuming Livengood-Wu integration output of 1 at autoignition point

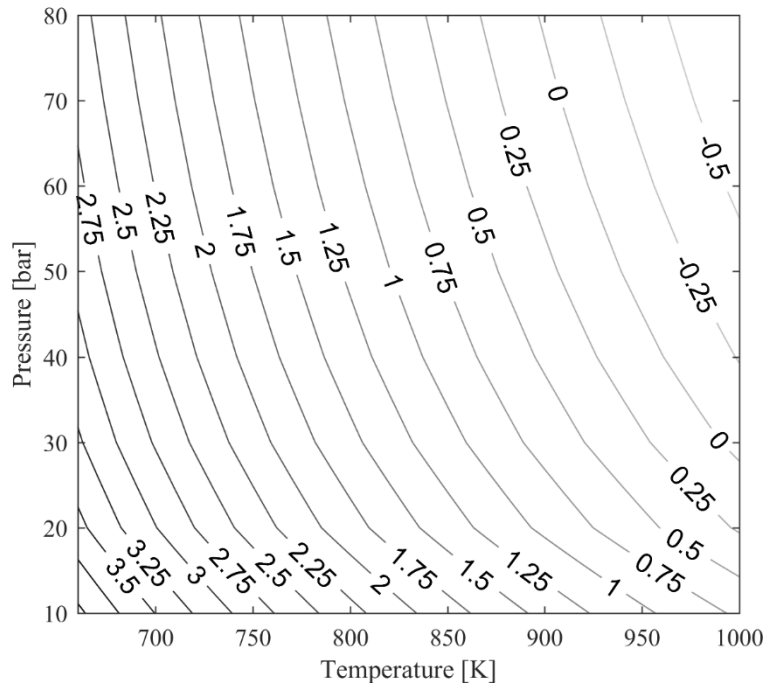

Figure 56. Cool-flame eliminated ignition delay contours evaluated from RCM experimental results

5.3.3 Comparison with other experimental correlation

Newly derived correlation from RCM experiment is compared with other ignition delay expression of iso-octane for validation i.e., Douaud-Eyzat correlation which was suggested in 1978 from CFR engine test for various fuels. The correlation formula covers PRF blend ratio 80–100 for a surrogate gasoline, in detail it is expressed as

$$\tau_{ign,PRF} = 0.01869\left(\frac{ON}{100}\right)^{3.4017} \cdot p^{-1.7} \cdot \exp\left(\frac{3800}{T}\right) \ [s] \qquad \text{(Eq. 5.4)}$$

where pressure and temperature units are bar and K, respectively. In this dissertation study, only iso-octane is of interest and thus the octane number term is disregarded.

Aforementioned in Chapter 1, Douaud-Eyzat correlation is based on octane rating standard test methods with comparably slower engine speed and lower pressure region, which doesn't cover the operating region of low temperature and high pressure conditions of contemporary downsized SI engines. For clarity, unburned gas histories expected from octane rating tests and boosted downsizing SI engines are compared on a temperature-pressure domain in Fig. 57 along with the RCM experiment profiles. From these profiles, it is obvious that Douaud-Eyzat correlation is inappropriate to predict knock outbreak of modern SI engines.

Both ignition delay curves, one from the correlation based on RCM test and the other adopting Douaud-Eyzat suggested coefficients, are plotted in Fig. 58. Interestingly, they have quite different activation energy in their slopes, nevertheless ignition delays tend to be close to each other in low temperature, low pressure and high temperature, high pressure range. On the other hand, big difference between two correlations is mainly in the low temperature, high pressure domain where modern SI engines' operating range is projected. Therefore, using Douaud-Eyzat correlation

for knock prediction in boosted SI engines may result in increased error as it overestimates ignition delay value in low temperature, high pressure conditions. For example, Livengood-Wu integration is conducted to locate autoignition point of SI engine simulation results using Douaud-Eyzat ignition delay correlation and outputs are shown in Fig. 59, and strong overestimating trend is observed as expected. This strongly suggests the necessity of new ignition delay correlation that covers the operating region of modern SI engines.

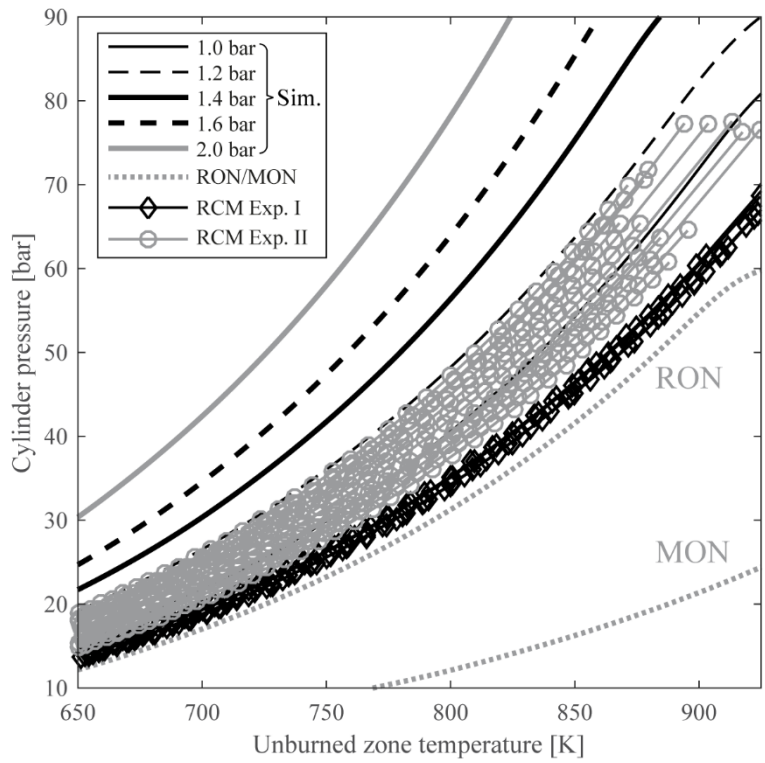

Figure 57. Unburned gas histories from SI engine simulation, RON/MON test (estimated), and RCM experiment under various conditions.

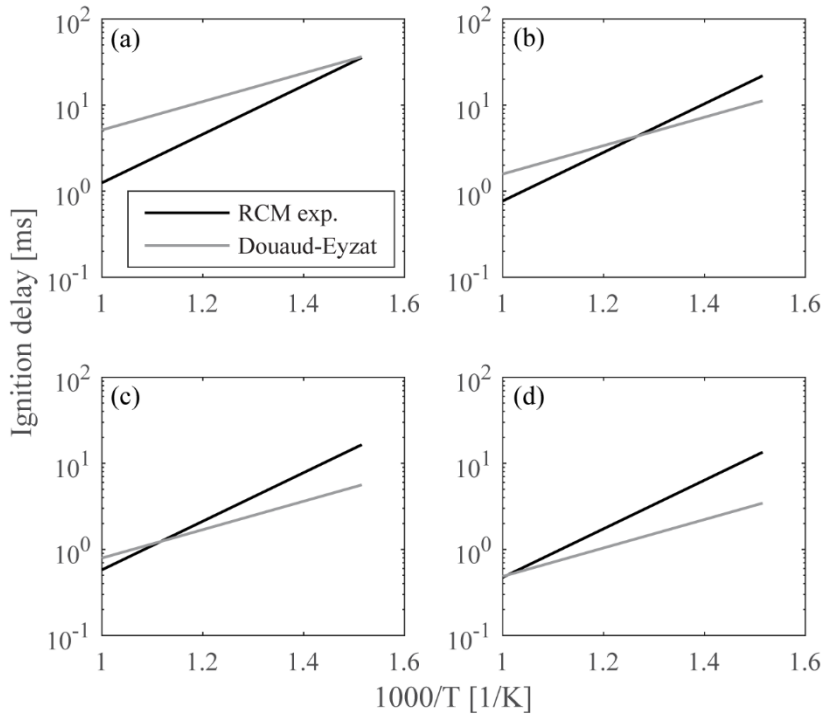

Figure 58. Ignition delay correlations derived from RCM experiment and Douaud-Eyzat coefficients. (a) 20 bar, (b) 40 bar, (c) 60 bar, and (d) 80 bar pressure conditions.

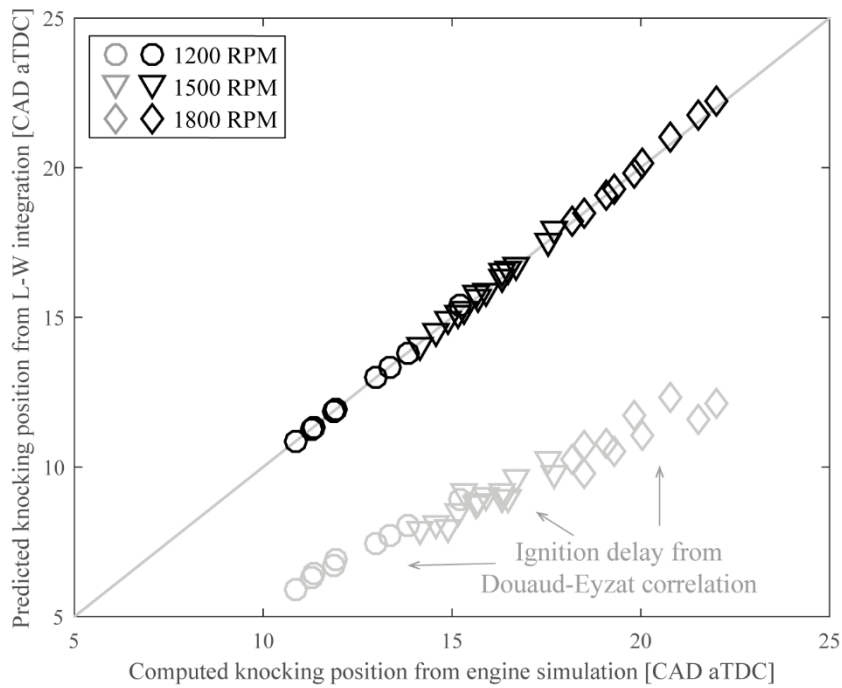

Figure 59. Livengood-Wu prediction by two independent ignition delay correlations. Empirical correlation from RCM simulation (black) and Douaud-Eyzat expression (gray)

Chapter 6. Conclusions

Improvements to the current Livengood-Wu autoignition prediction model is achieved by applying cool-flame elimination method which is more appropriate to the operating characteristics of a contemporary SI engine with aggressive boosting strategy. Previous studies showed that the predictability of integration model with traditional ignition delay deteriorates in many cases with two-stage ignition fuels.

6.1 Modeling results

Modeling and computational studies are first performed to discuss current issue and a new prediction model is applied to the SI engine simulation result to present favorable predictability.

First, a zero-dimensional two-zone SI engine model is constructed and operating parameters are selected to reflect the knock-prone condition in modern engines, e.g. low speed combined with boosted intake pressure. Results showed that the cool-flame and relevant two-stage ignition behavior is unlikely to be revealed within the engine unburned gas under most situation when fueled with NTC-exhibiting substances. Livengood-Wu integration is conducted with cool-flame affected, two-stage ignition delays to predict the onset of autoignition for aforementioned cases, however the predictability deteriorates due to a conflict with the engine simulation results where two-stage ignition behavior is not likely to exist in most cases.

Cool flame phenomenon of two-stage ignition fuel leads to shortened overall ignition delay with decreasing initial temperature under certain temperature-pressure range and causes NTC characteristics. It is found that the thermal contribution from the

cool flame accelerates overall chemistry during the ignition delay period, nevertheless this does not correspond to the specific situation of the engine unburned gas when the two-stage ignition behavior is not found. By accepting the basic idea of Livengood-Wu integration which only considers the chemistry progress of a system, it is concluded that the thermal contribution of a cool flame must be excluded to comply with the integration model idea.

The degree of cool-flame temperature rise is modulated by increasing the heat capacity of inert gas, in this study nitrogen, within the initial fuel-air mixture set for computation. With this approach cool-flame exothermicity gradually decreased as the heat capacity increased and finally extrapolated to zero to fully eliminate the thermal contribution of cool flame. Chemical kinetic analysis also concluded that cool-flame eliminated ignition delays are proper representatives of instantaneous mixture reactivity within the NTC region if no cool flame appeared in engine unburned gas history.

The outputs from the cool-flame elimination method above replaced the cool-flame affected ignition delays within the NTC region. This also leads to an almost perfect prediction of onset of autoignition of the engine unburned gas in computational results. Furthermore, an empirical correlation of ignition delay is also proposed which combines the cool-flame eliminated value within the NTC region and the high-temperature single stage ignition delay in the post-NTC regime to cover the estimated temperature-pressure domain of modern SI engines. Livengood-Wu integration also performed very well with these newly derived ignition delay correlation.

6.2 Experimental results

Experimental validation of this idea is conducted with an RCM which is suitable for investigating the unburned gas behavior leading to autoignition and corresponding knock in an SI engine from a fuel chemistry perspective, rather than in a real engine where lots of uncertainties are potential obstacles to the analysis.

Results showed that regardless of experimental limitations, especially when handling with extreme thermodynamic conditions, it is useful to derive an empirical correlation of ignition delay from RCM experimental results which can be directly applied to similar thermodynamic history from an engine test to predict knock. Along with that, building up an ignition delay database of specific fuel with RCM or other test facilities could be also helpful to predict and avoid knock in an engine when run with that specific fuel.

Newly derived empirical correlation of ignition delay is compared with a Douaud-Eyzat expression and found to be more suitable for contemporary SI engines with boosted downsizing trend.

6.3 Future works

Future works include further investigation with different combustion phasing in an engine simulation, in detail the Wiebe coefficients may be altered to induce various unburned gas histories. Furthermore, it would be meaningful to check the consistency of outputs from this work if other SI engine model is introduced.

Major purpose of this study is to propose a new concept of cool-flame eliminated ignition delay for improved autoignition prediction in a boosted SI engine with NTC-

exhibiting fuels. Only the pure iso-octane is tested with this methodology in this work, but other substances relevant to next-generation petroleum fuels could also be studied and it may be interesting to see if the results comply with the findings from this study.

References

1. Code of Federal Regulations, “Passenger Automobile Average Fuel Economy Standards,” Title 49, Part 531, 213.
2. Regulation of the European Parliament and of the Council, ‘Setting Emission Performance Standards for New Passenger Cars as Part of the Community’s Integrated Approach to Reduce CO2 Emissions from Light-duty Vehicles,” EC No. 443/2009, April 2009.
3. Heywood, J.B., Internal Combustion Engine Fundamentals, McGraw-Hill, New York, 1988.
4. Sivaram, V. and Levi, M.A., Automobile Fuel Economy Standards in a Lower-Oil-Price World, Nov. 2015.
5. The International Council on Clean Transportation Annual Report, Sep. 2015.
6. Pulkrabek, W.W., Engineering Fundamentals of the Internal Combustion Engine, 2nd ed. Pearson Prentice-Hall, 2004.
7. Kukkadapu, G., Kumar, K., Sung, C-J., Mehl. M., Pitz, W.J., “Autoignition of gasoline and its surrogates in a rapid compression machine,” Proceedings of the Combustion Institute 34(1):345–352, 2013.
8. Machrafi, H., Cavadias, S., “Three-stage autoignition of gasoline in an HCCI engine: An experimental and chemical kinetics modeling investigation,” Combustion and Flame 155:557–570, 2008.
9. Bieleveld, T., Frassoldati, A., Cuoci, A., Faravelli, T., Ranzi, E., Niemann, U., Seshadri, K., “Experimental and kinetic modeling study of combustion of gasoline, its surrogates and components in laminar non-premixed flows,” Proceedings of the Combustion Institute 32:493–500, 2009.

10. Mehl, M., Curran, H.J., Pitz, W.J., Westbrook, C.K., “Chemical Kinetics Modeling of Component Mixtures Relevant to Gasoline,” Proceedings of the 4th European Combustion Meeting, 2009.

11. Scott Goldsborough, S., “A chemical kinetically based ignition delay correlation for iso-octane covering a wide range of conditions including the NTC region,” Combustion and Flame 156(6):1248–1262, 2009.

12. Ranzi, E., Faravelli, T., Gaffuri, P., Sogaro, A., “A wide-range modeling study of iso-octane oxidation,” Combustion and Flame 108(1–2):24–42, 1997.

13. Curran, H.J., Gaffuri, P., Pitz, W.J., Westbrook, C.K., “A comprehensive modeling study of n-heptane oxidation,” Combustion and Flame 114(1–2):149–177, 1998.

14. Sahetchian, K.A., Heiss, A., Rigny, R., Ben-Aïm, R.I., “Determination of the Gas-Phase Decomposition Rate Constants of Heptyl-1 and Heptyl-2 Hydroperoxides C7H15OOH,” International Journal of Chemical Kinetics 14:1325–1337, 1982.

15. Westbrook, C.K., Pitz, W.J., Boercker, J.E., Curran. H.J., Griffiths, J.F., Mohamed, C., Ribaucour, M., “Detailed Chemical Kinetic Reaction Mechanisms for Autoignition of Isomers of Heptane under Rapid Compression,” Proceedings of the Combustion Institute 29(1):1311–1318, 2002.

16. Lee, K., Kim. Y., Min, K., “Development of a reduced chemical kinetic mechanism for a gasoline surrogate for gasoline HCCI combustion,” Combustion Theory and Modeling 15(1):107–124, 2010.

17. Fikri, M., Herzler, J. Starke, R., Schulz, C., Roth, P., Kalghatgi, G.T., “Autoignition of gasoline surrogate mixtures at intermediate temperatures and high pressures,” Combustion and Flame 152(1–2):276–281, 2008.

18. Andrae, J.C.G., “Development of a detailed kinetic model for gasoline surrogate fuels,” Fuel 87(10–11):2013–2022,2008.

19. Curran, H.J., Gaffuri, P., Pitz, W.J., Westbrook, C.K., “A comprehensive modeling study of iso-octane oxidation,” Combustion and Flame 129(3):253–280, 2002.

20. Smith, G.P., Golden, D.M., Frenklach, M., Moriarty, N.W., Eiteneer, B., Goldenberg, M., Bowman, C.T., Hanson, R.K., Song, S., Gardiner Jr., W.C., Lissianski, V.V., Qin, Z., GRI-MECH 3.0, http://www.me.berkeley.edu/gri_mech/

21. Livengood, J.C, Wu, P.C., “Correlation of autoignition phenomena in internal combustion engines and rapid compression machines,” 5th Symposium (International) on Combustion 20(1):347–356, 1955.

22. Hernández, J.J., Lapuerta, M., Sanz-Argent, J., “Autoignition prediction capability of the Livengood-Wu correlation applied to fuels of commercial interest,” International Journal of Engine Research 15(7):817–829, 2014.

23. Wagnon, S.W., Wooldridge, M.S., “Effects of buffer gas composition on autoignition,” Combustion and Flame 161(4):898–907, 2014.

24. Di, H., He, X., Zhang, P., Wang, Z., Wooldridge, M.S., Law, C.K., Wang, C., Shuai, S., Wang, J., “Effects of buffer gas composition on low temperature ignition of iso-octane and n-heptane,” Combustion and Flame 161(10):2531–2538, 2014.

25. Douaud, A.M., Eyzat, P., “Four-Octane-Number Method for Predicting the Anti-Knock Behavior of Fuels and Engines,” SAE Technical Paper 780080, 1978.

26. Chen, L., Li, T., Yin, T., Zheng, B., “A predictive model for knock onset in spark-ignition engines with cooled EGR,” Energy Conversion and Management 87:946–955, 2014.

27. Pan, J., Zhao, P., Law, C.K., Wei, H., “A predictive Livengood-Wu correlation for two-stage ignition,” International Journal of Engine Research 17(8):825–835, 2016.

28. DelVescovo, D., Kokjohn, S., Reitz, R., “The Development of an Ignition Delay Correlation for PRF Fuel Blends from PRF0 (n-heptane) to PRF100 (iso-Octane),” SAE International Journal of Engines 9(1):2016, SAE 2016-01-0551, 2016.

29. Beccari, S., Pipitone, E., Genchi, G., “Knock onset prediction of propane, gasoline and their mixtures in spark ignition engines,” Journal of the Energy Institute 89:101–114, 2016.

30. Yates, A., Bell, A., Swarts, A., “Insights relating to the autoignition characteristics of alcohol fuels,” Fuel 89(1):83–92, 2010.

31. Kalghatgi, G., Morganti, K., Algunaibet, I., Sarathy, M., Dibble, R., “Knock Prediction Using a Simple Model for Ignition Delay,” SAE Technical Paper 2016-01-0702, 2016.

32. Lumley, J.L., Engines: an introduction, 210–218, Cambridge University Press, New York, 1999.

33. ASTM International, “Standard Test Method for Research Octane Number of Spark-Ignition Engine Fuel,” ASTM D2699-15a, Rev. Oct. 2015.

34. ASTM International, “Standard Test Method for Motor Octane Number of Spark-Ignition Engine Fuel,” ASTM D2700-16, Rev. Jan. 2016.

35. Yeliana, Y., Cooney, C., Worm, J., Michalek, D., Naber, D., “Wiebe function parameter determination for mass fraction burn calculation in an ethanol-gasoline fuelled SI engine,” Journal of KONES Powertrain and Transport 15(3):567–574, 2008.

36. Woschni, G., “Universally applicable equation for the instantaneous heat transfer coefficient in the internal combustion engine,” SAE Technical Paper 670931, 1967.

37. Mehl, M., Pitz, W.J., Sjöberg, M., Dec, J.E., “Detailed kinetic modeling of low-temperature heat release for PRF fuels in an HCCI engine,” SAE Technical Paper 2009-01-1806, 2009.

38. Mehl, M., Faravelli, T., Giavazzi, F., Ranzi, E., Scorletti, P., Tardani, A., Terna, D., "Detailed chemistry promotes understanding of octane numbers and gasoline sensitivity," Energy and Fuels 20(6):2391–2398, 2006.

39. Tanoue, K., Jimoto, T., Kimura, T., Yanamoto, M., Hashimoto, J., "Effect of initial temperature and fuel properties on knock characteristics in a rapid compression and expansion machine," Proceedings of the Combustion Institute, in press, 2016.

40. Perumal, M., Floweday, G., "An Investigation of Cascading Autoignition and Octane Number using a Multi-zone Model of the CFR Engine," SAE Technical Paper 2011-01-0850, 2011.

41. Kee, R.J., Rupley, F.M., Miller, J.A., "The Chemkin thermodynamic data base," 1990.

42. Zhao, P., Law, C.K., "The role of global and detailed kinetics in the first-stage ignition delay in NTC-affected phenomena," Combustion and Flame 160(11):2352–2358, 2013.

43. Davidson, D.F., Gauthier, B.M., Hanson, R.K., "Shock tube ignition measurements of iso-octane/air and toluene/air at high pressures," Proceedings of the Combustion Institute 30(1):1175–1182, 2005.

44. Kasseris, E., Heywood, J., "Charge Cooling Effects on Knock Limits in SI DI Engines Using Gasoline/Ethanol Blends: Part 1 – Quantifying Charge Cooling," SAE Technical Paper 2012-01-1275, 2012.

45. Kasseris, E., Heywood, J., "Charge Cooling Effects on Knock Limits in SI DI Engines Using Gasoline/Ethanol Blends: Part 2 – Effective Octane Numbers," SAE Technical Paper 2012-01-1284, 2012.

46. Turanyi, T., Tomlin, A.S., Analysis of Kinetic Reaction Mechanisms, Springer, 2014.

47. Androulakis, I.P., Grenda, J.M., Bozzelli, J.W., “Time-integrated pointers for enabling the analysis of detailed reaction mechanisms,” AIChE Journal 50(11):2956–2970, 2004.

48. Kim, Y., “A Study on the CAI Combustion Characteristics Using a Reduced Chemical Kinetic Mechanism,” Ph.D. Thesis, Seoul National University, 2007.

49. Minetti, R., Carlier, M., Ribaucour, M., Therssen, E., Sochet, L.R., “A Rapid Compression Machine Investigation of Oxidation and Auto-Ignition of n-Heptane: Measurements and Modeling,” Combustion and Flame 102:298–309, 1995.

50. Griffiths, J.F., Halford-Maw, P.A., Rose, D.J., “Fundamental Features of Hydrocarbon Autoignition in a Rapid Compression Machine,” Combustion and Flame 95:291–306, 1993.

51. Mittal, G., “A Rapid Compression Machine – Design, Characterization, and Autoignition Investigations,” Ph.D. Thesis, Case Western Reserve University, 2006.

52. Lee, D., Hochgreb, S., “Rapid Compression Machines: Heat Transfer and Suppression of Corner Vortex,” Combustion and Flame 114(3):531–545, 1998.

53. Mittal, G., Sung, C-J., “Aerodynamics inside a rapid compression machine,” Combustion and Flame 145:160–180, 2006.

요 약

Livengood-Wu 점화지연 적분 모델은 불꽃점화 엔진의 노킹 시점을 예측함에 있어서 매우 간결하면서도 상당히 높은 예측 정확성을 갖는 방법으로 지난 수십 년간 널리 사용되어왔다. 이 모델의 기저에는 임의의 열역학적 상태에 대하여 연료의 화학적 반응성은 그 때에 얻어지는 점화지연의 역수로써 대표할 수 있다는 생각이 내재되어 있다. 그러나 최근 들어 특정한 반응 경향을 나타내는 연료의 경우 Livengood-Wu 모델의 예측 정확성이 크게 떨어진다는 사실이 알려지고 있다. 이는 대부분 온도 범위에 따라 서로 다른 화학적 반응 경로를 갖는 연료가 2 단점화 양상 및 그에 의한 negative temperature coefficient (NTC) 특성이 있는 경우임이 밝혀지고 있는데, 이 모델의 예측 정확성을 떨어뜨리는 주요한 원인 중 하나로서 냉염이 발생하는 1 차점화 구간에서 냉염에 의한 발열 및 이에 따른 온도상승이 지목되었다. 따라서 이와 같은 냉염의 온도상승 효과를 가능한 한 억제한 상황에서 구해진 새로운 점화지연의 개념을 정립하고 이를 냉염 배제법이라 명명하였다.

본 학위논문에서는, 최근의 다운사이징 과급운전 경향을 반영한 불꽃점화 엔진 시뮬레이션을 활용하여 엔진 미연소 혼합기의 자발화에 의한 노킹 발생에 대해 분석하였다. 이 때 연료로 이소옥탄을 사용하였으며, 여기에서 이소옥탄은 가솔린 모사 연료의 주요한 구성성분 중 하나이며 동시에 엔진 운전조건과 깊이 관련된 열역학적 상태에서 NTC 특성이 잘 나타나는 연료이다. 그리고 냉염효과가 그대로 반영된 점화지연 값들을 사용한 경우와 냉염배제법에 의한

새로운 점화지연 값을 사용한 Livengood-Wu 적분 결과를 비교 제시하였다. 그 결과 냉염의 온도상승 효과를 배제한 경우에 노킹 시점 예측성능이 크게 개선되는 것을 확인하였으며 냉염 배제법의 타당성을 화학반응론적 분석기법을 사용하여 검증하였다. 그와 더불어, 냉염효과가 배제된 새로운 점화지연의 관계식을 구하는 방법론을 제시하고 계산적 방법과 실험적 검증을 동시에 진행하였다. 이 때 실험은 엔진 미연소 혼합기의 상태변화를 모사할 수 있는 급속압축장치(rapid compression machine)를 사용하였다. 여기에서 구한 새로운 관계식을 기존에 널리 알려진 다른 관계식과 비교해 본 결과, 기존의 실험 조건이 현대적인 엔진의 다운사이징 및 과급운전 경향을 효과적으로 재현하기 어렵다는 점이 확인되었다. 따라서, 최신 엔진 운전조건을 반영할 뿐 아니라 연료의 화학적 반응성 특성도 함께 고려한 새로운 점화지연의 관계식을 사용하는 것이 보다 향상된 노킹 예측 성능을 나타낼 수 있다는 점에 주목할 필요가 있다.

주요어: 노킹, 자발화, Livengood-Wu 모델, 냉염, 이소옥탄, 급속압축장치, 화학반응론

학 번: 2013-30201